# Engineering cytochrome $P450_{BM3}$ for oxidation and silicon–carbon bond cleavage of volatile methylsiloxanes

Thesis by

Nicholas Singh Sarai

In Partial Fulfillment of the Requirements for

the degree of

Doctor of Philosophy


CALIFORNIA INSTITUTE OF TECHNOLOGY

Pasadena, California

2023

(Defended May 5, 2023)

Nicholas Singh Sarai
ORCID: 0000-0002-4655-0038

# ACKNOWLEDGEMENTS

In my final few months at Caltech, I have often found myself reflecting on my experience at this singular and storied institution. My time at Caltech has shaped my scientific interests and cemented my confidence that society thrives when rooted in scientific truth. I will miss Caltech dearly. My thesis research has required me to be simultaneously more focused and more creative than I ever have been. Through it all, my greatest privilege in life is to have remarkable people in my corner, and I hope to thank some of them here.

To my advisor, Professor Frances Arnold. Thank you for enabling me to embark on the most rewarding—and simultaneously most challenging—project of my life. The highlight of my career has been working with you to build a new reality for how enzymes can interact with and even remodel man-made compounds. Throughout my graduate work, you gave me the freedom to explore an untrodden area of science while ensuring that I remained focused on the goal. You also served as a constant inspiration, showing me how to ask the right questions, how to convene others, and how to utilize science for the common good. Beyond our shared scientific interests, I will carry forward our common love of humanity and Nature.

To my thesis committee: Professors Dianne Newman, Jonas Peters, and Harry Gray. Thank you for your energy and guidance throughout my PhD. Dianne, your enthusiasm for the diversity of microbes and their catalytic arsenals grounded my research in the natural world. Jonas, you constantly encouraged me to tackle the hard things first and lent important perspective on catalysis. Harry, your enthusiasm for novel P450 chemistry and encyclopedic knowledge inspired me to explore new directions.

To the members of the Arnold Group past and present. My rotation mentors, David Romney and Markus Dick, entrusted a young graduate student with their projects and showed me what I was capable of. As I progressed through my PhD, I found myself surrounded by incredible teammates: Tyler Fulton, Ryen O'Meara, Kadina Johnston, Sabine Brinkmann-Chen, and Susanne Baehr. Tyler and Ryen, I can only dream of having teammates and friends like you in the future. I often felt like we were unstoppable! Tyler, I immediately noticed your unshakable work ethic, unparalleled understanding of chemistry, and ability to quickly find the right course of action. Ryen, your skill and focus are enviable. I am so proud of what you have done in what is just the start of your PhD and I am excited to see what you do next. Kadina, working with you is always easy; you are incisive, kind, and driven. Sabine, you pushed me to think about what matters as a scientist and honed my writing and presentation skills. Susanne, you brought me into the world of organosilicon chemistry. It would be impossible to name everyone who had an influence on me in the Arnold Lab; suffice it to say I feel honored to have worked with each and every one of you. I thank my colleagues from The Dow Chemical Company, John Roberts, Dimitris Katsoulis, Ryan Maar, Ron Tecklenburg, and Jordan Reddel for lending their support and expertise throughout my PhD.

My journey to the Arnold Lab began long before I ever stepped onto Caltech's campus. Mr. Gleich, my high school chemistry teacher, opened my eyes to the world of chemistry and advised my high school senior thesis on advanced biofuels. My mentors at NREL, Yannick

Bomble, Michael Himmel, and Daehwan Chung shaped me into a young scientist. Yannick, you gave me freedom to explore many horizons of science as a freshly minted college graduate. It was during my time at NREL that I became a student of enzyme engineering. I distinctly remember the day in 2016 that I read a paper from the Arnold Lab on an enzyme that could forge bonds between carbon and silicon atoms, a feat unknown in the natural world. At that moment I knew I wanted to study directed evolution. What a twist of fate that my PhD ended up focusing on engineering enzymes to break a bond between the same elements.

Throughout my PhD, my friends and family supported me and filled these five years with joy. I can't possibly do justice to all my friends at Caltech. I shared great times with everyone from the Arnold lab. Patrick, our adventures in both science and the mountains were a constant source of happiness; your drive and talent are singular. William, you were one of my first mentors at Caltech; your passion for science and the mountains are unmatched. Matthieu, you always ask the right questions about science and life. I can only try to match your ability to analyze the world around you. One of the trials of academic training is that it forces you to live in many different places. Despite that, my friends from St. Louis, Denver, and elsewhere have always been a major source of joy and support.

Most of all, the love and support of my family carried me through this experience. Not a day goes by when I don't think about how lucky I am to have them. My grandparents took great risks to build a better life for their children. My parents, Teresa and Baldev Sarai, continued that legacy. You raised me to care about people and the natural world. I wouldn't be pursuing science if it wasn't for your encouragement, which was both perfectly subtle and urgent. Beyond leading by thought, you also lead by example, and continue to serve as an inspiration for how to live a fulfilling life while raising up those around you. To my sister, Eva (Mimi) Sarai, you inspire me to be a better scientist and person with your unique ability to connect with people and understand complex systems. To Eva's partner, Cúán, your wit, humor, and ability to pan between the smallest detail and the big picture are admirable. I am beyond lucky that my partner's family are equally wonderful. Jim and Cindy, I have felt your excitement and support since high school and throughout my PhD. Your life stories, wisdom, generosity, and work ethic have taught me how to lead an impactful life. Anna, James, and Will, your enthusiasm, humor, and friendship throughout these years has been a major source of motivation. The three of you inspire me with your unique perspectives, analytical abilities, and positivity. I also thank my large extended family for their encouragement.

Finally, to my life partner, best friend, and future wife, Cynthia Coyle. We made it happen! Not a single bit of this would have been possible without you. From the moment we met twelve years ago, we have tackled everything together and you have been my most steadfast supporter. When I came home from lab and wanted to tell you about the joys of a new discovery, you celebrated with me. When that same research was trying, you lifted me up. I have never met anyone with your combination of energy, compassion, and brilliance. I can't wait to see what the rest of our journey has in store.

# ABSTRACT

Directed evolution of enzymes can reveal activities that do not occur in the natural world. While most examples of directed evolution of new-to-nature chemistry have been applied in a synthetic direction, enzymatic biodegradation typically relies on wild-type enzymes. This thesis posits that directed evolution can generate enzymes capable of degrading non-biodegradable anthropogenic compounds, focusing on efforts to break silicon–carbon bonds, which are not known to be cleaved by enzymes in Nature. Chapter I establishes background on how enzymes evolve to catalyze degradation of compounds over long timescales in Nature, highlighting the enzymatic depolymerization of lignocellulosic biomass. This sets the stage for a case study of rapid enzyme evolution in response to anthropogenic molecules such as plastics and agrochemicals. With this background, directed evolution of new-to-nature synthetic activities is presented to demonstrate how new enzymatic activities can be evolved in the laboratory. In Chapter II, the state of the art for biocatalytic reactions involving organosilicon compounds is reviewed, starting with a description of how biology uses silicon and concluding with a perspective on future opportunities in this nascent field. Finally, Chapter III describes the engineering of a novel siloxane oxidase based on a cytochrome P450, which conducts two reaction steps in tandem to cleave silicon–carbon bonds. First, it hydroxylates the C–H bonds of siloxanes—the anthropogenic building blocks of silicone polymers—to yield a carbinol species, an activity reminiscent of the parent enzyme's native hydroxylation of fatty acids. Via a function entirely different than its native activity, the enzyme converts this carbinol to a silanol species. In performing both of these steps, this is the first known enzyme that can cleave Si–C bonds, an activity which is the first step toward enzymatic degradation of these persistent, man-made compounds. In sum, this thesis demonstrates that directed evolution can reveal enzymatic degradation chemistries that are not known in Nature by establishing new-to-nature Si–C cleavage of siloxanes.

# PUBLISHED CONTENT AND CONTRIBUTIONS

1. **N. S. Sarai**, T. J. Fulton, R. L. O'Meara, K. E. Johnston, S. Brinkmann-Chen, R. R. Maar, R. E. Tecklenburg, J. M. Roberts, J. C. T. Reddel, D. E. Katsoulis, F. H. Arnold, Directed evolution of enzymatic silicon–carbon bond cleavage in siloxanes. *Submitted*.

NSS participated in project conception along with most coauthors. NSS, TJF, RLO, KEJ, SBC, RET, and JMR designed and executed research. NSS found initial activity and identified carbinol and silanol products. NSS, TJF, and RLO hypothesized and found that the enzyme is responsible for both reaction steps. NSS, TJF, and RLO drafted the manuscript with input from all coauthors. NSS prepared all figures.

2. **N. S. Sarai**, B. J. Levin, J. M. Roberts, D. E. Katsoulis, F. H. Arnold, Biocatalytic transformations of silicon—the other Group 14 element. *ACS Cent. Sci.* **7**, 944–953 (2021).

NSS developed the idea for the article. NSS prepared the manuscript and all figures with input from all coauthors.

# PUBLISHED CONTENT NOT INCLUDED IN THESIS

3. M. Dick, **N. S. Sarai**, M. W. Martynowycz, T. Gonen, F. H. Arnold, Tailoring tryptophan synthase TrpB for selective quaternary carbon bond formation. *J. Am. Chem. Soc.* **141**, 19817–19822 (2019).

MD and NSS participated in project conception. MD and NSS found initial activity, conducted directed evolution, and profiled the substrate scope of the evolved enzyme. MWM obtained MicroED structures of enzymatic quaternary carbon products. MD and NSS drafted the manuscript with input from all coauthors.

4. D. K. Romney, **N. S. Sarai**, F. H. Arnold, Nitroalkanes as versatile nucleophiles for enzymatic synthesis of noncanonical amino acids. *ACS Catal.* **9**, 8726–8730 (2019).

DKR participated in project conception. DKR and NSS designed and conducted research.

# TABLE OF CONTENTS

*Acknowledgements* ... iii
*Abstract* ... v
*Published content and contributions* ... vi
*Table of contents* ... viii
*List of figures and tables* ... x
*Abbreviations* ... xiii
*Chapter I: Directed Evolution as a Tool to Access Novel Degradation Activities* ... 1
Abstract ... 2
1.1 Evolution of Catabolic Enzyme Activities ... 3
1.1.1 Enzymatic Lignocellulose Degradation ... 4
1.2 Evolution of New Activities on Anthropogenic Compounds ... 6
1.2.1 Enzymatic Plastic Degradation ... 7
1.2.2 Enzymatic Degradation of Agrochemicals ... 12
1.3 Outlook: Harnessing Directed Evolution to Develop Novel Degradation Activities 13
Bibliography for Chapter I ... 15
*Chapter II: Biocatalytic Transformations of Silicon—the Other Group 14 Element* ... 20
Abstract ... 21
2.1 Introduction ... 22
2.2 Biotransformation of Silicon ... 26
2.2.1 Biosilicification — Siliceous Marine Microorganisms and Plants ... 26
2.2.2 Enzymes that Transform Silicon Species ... 29
2.3 Engineering Enzymes for Non-Natural Silicon Biocatalysis ... 30
2.4 Opportunities for Biocatalysis to Impact Organosilicon Chemistry ... 35
2.4.1 Using Silicon as a Bioisostere of Carbon in Bioactive Compounds ... 36
2.4.2 Silicon-Containing Amino Acids (SiAAs) ... 37
2.4.3 Chiral Silicon Centers ... 40
2.4.4 Enzymatic Synthesis of Hypervalent Silicon Species ... 42
2.4.5 Silicon–Carbon Bond Construction ... 43
2.4.6 Biologically Templated Inorganic Materials ... 45
2.5 Summary and Outlook ... 46
Bibliography for Chapter II ... 46

*Chapter III: Directed Evolution of Enzymatic Silicon–Carbon Bond Cleavage in Siloxanes* ..... 55
Abstract ..... 56
3.1 Introduction ..... 57
3.2 Discovery of Siloxane C–H Hydroxylation Activity ..... 59
3.3 Investigation of Product Hydrolysis and Enzymatic Si–C Cleavage ..... 61
3.4 Directed Evolution on Cyclic and Linear Siloxane Substrates ..... 62
3.5 Unlocking New-to-Nature Degradation Activities in the Laboratory ..... 65
Bibliography for Chapter III ..... 66
*Supplementary Information for Chapter III* ..... 70
A.1 Materials and Methods ..... 71
A.1.1 General ..... 71
A.1.2 Cloning, Mutagenesis, and Plasmid Isolation ..... 72
A.1.3 Small-Scale Enzymatic Reactions to Identify Improved Variants ..... 77
A.1.4 Determination of Hemeprotein Concentration ..... 79
A.1.5 Protein Purification ..... 79
A.1.6 Small-Scale Enzymatic Reactions for Lineage Validation ..... 80
A.1.7 Enzymatic Reactions with Lyophilized Enzymes ..... 82
A.1.8 Enzymatic Reactions Relevant to Figure 3-2B and Figure 3-2C ..... 83
A.2 GC/MS Analytical Methods ..... 86
A.2.1 Analysis of Hexamethyldisiloxane (1) Biocatalytic Reactions ..... 87
A.2.2 Analysis of Octamethyltrisiloxane (2) Biocatalytic Reactions ..... 90
A.2.3 Analysis of Octamethylcyclotetrasiloxane (3) Biocatalytic Reactions ..... 96
A.3 Experimental Data Relevant to Figures ..... 98
A.4 DNA Sequences of Engineered Enzymes ..... 105
A.5 Materials and Methods for Analytical Standard Preparations ..... 111
A.6 NMR Spectra ..... 123
A.7 Bibliography for Appendix A ..... 143

# LIST OF FIGURES AND TABLES

***Table Number*** ***Page***

A-1 Thermocycler conditions for SSM protocol ..... 73
A-2 Primers used for PCR mutagenesis and amplification ..... 73
A-3 Thermocycler conditions for insert PCR ..... 75
A-4 Thermocycler conditions for BB1/BB2 ..... 75
A-5 Thermocycler conditions for recombination of PCR products ..... 76
A-6 Thermocycler conditions for amplification of StEP insert ..... 76
A-7 GC/MS oven parameters ..... 87
A-8 Mass spectrometer parameters (scan mode) ..... 87
A-9 Summary of analytes ..... 87
A-10 GC/MS oven parameters ..... 90
A-11 Mass spectrometer parameters (scan mode) ..... 90
A-12 Summary of analytes ..... 90
A-13 GC/MS oven parameters ..... 96
A-14 Mass spectrometer parameters (scan mode) ..... 96
A-15 Summary of analytes ..... 96
A-16 Summary of enzyme lineage for hexamethyldisiloxane (1) ..... 98
A-17 Experimental data relevant to Figure 3-2A ..... 99
A-18 Experimental data relevant to Figure 3-2B ..... 100
A-19 Experimental data relevant to Figure 3-2C ..... 101
A-20 Summary of enzyme lineage for octamethyltrisiloxane (2) ..... 102
A-21 Experimental data relevant to Figure 3-3A ..... 102
A-22 Summary of enzyme lineage for octamethylcyclotetrasiloxane (3) ..... 103
A-23 Experimental data relevant to Figure 3-3C ..... 104

***Figure Number*** ***Page***

1-1 Structures of some of the most common plastics ..... 9
1-2 Degradation of PET by Ideonella sakaiensis PETase and MHETase ..... 11
1-3 Enzymatic degradation of atrazine ..... 13

2-1 The group 14 elements silicon and carbon form molecules with different properties ..... 23

2-2 Biosynthesis of siliceous cell walls ..... 26

2-3 Silica polymerization is catalyzed by silicatein enzymes ..... 28

2-4 New-to-nature enzymatic Si–C bond formation ..... 32

2-5 Repurposing cytochrome $P450_{BM3}$ to oxidize Si–H bonds ..... 34

2-6 Some opportunities for biocatalysis in organosilicon chemistry ..... 40

3-1 Siloxanes have diverse molecular structures and are prone to complex interconversion reactions ..... 58

3-2 Engineered variants catalyze both hydroxylation and [1,2]-Brook-like rearrangement steps of Si–C cleavage ..... 62

3-3 Directed evolution with octamethyltrisiloxane (2) and octamethylcyclotetrasiloxane (3) as substrates ..... 64

A-1 Representative gas chromatogram and EI mass spectrum of a 0.482 mM sample of carbinol 4 with 5 mM 1,3,5-trimethoxybenzene ..... 88

A-2 Calibration curve for carbinol 4 ..... 89

A-3 Representative gas chromatogram and EI mass spectrum of a 0.341 mM sample of silanol 5 with 5 mM 1,3,5-trimethoxybenzene ..... 89

A-4 Calibration curve for silanol 5 ..... 90

A-5 Representative gas chromatogram and EI mass spectrum of a 0.328 mM sample of carbinol 9 with 5 mM 1,3,5-trimethoxybenzene ..... 91

A-6 Calibration curve for carbinol 9 ..... 91

A-7 Representative gas chromatogram and EI mass spectrum of a 0.436 mM sample of silanol 10 with 5 mM 1,3,5-trimethoxybenzene ..... 92

A-8 Calibration curve for silanol 10 ..... 92

A-9 Representative gas chromatogram and EI mass spectrum of carbinol 11 ..... 93

A-10 Calibration curve for carbinol 11 ..... 93

A-11 Representative gas chromatogram and EI mass spectrum of a 0.394 mM sample of silanol 12 with 1,3,5-trimethoxybenzene ..... 94

A-12 Calibration curve for silanol 12 ..... 94

A-13 Representative gas chromatogram and EI mass spectrum of a 0.341 mM sample of silanol 5 with 5 mM 1,3,5-trimethoxybenzene ..... 95

A-14 Calibration curve for silanol 5 ..... 95

A-15 Representative gas chromatogram and EI mass spectrum of a 0.320 mM sample of carbinol 13 with 5 mM 1,3,5-trimethoxybenzene ..... 96

A-16 Calibration curve for carbinol 13 ..... 97

A-17 Representative gas chromatogram and EI mass spectrum of a 0.362 mM sample of silanol 14 with 5 mM 1,3,5-trimethoxybenzene ..... 97

A-18 Calibration curve for silanol 14..... 98

A-19 Representative example of trace carbinol 5 detected in a biocatalytic reaction with 2.5 mM LSilOx4 (purified) with ions 147.0, 135.0, 118.8, and 162.9..... 99

A-20 Representative example of trace carbinol 9 detected in a biocatalytic reaction with LSilOx7 with ions 192.9 and 221.0 ..... 103

A-21 Representative example of trace silanol 5 detected in a biocatalytic reaction with LSilOx4 with ions 149.0 and 132.9 ..... 103

A-22 Representative example of trace carbinol 13 detected with CSilOx2 with ions 281.1, 252.9, and 265.1..... 105

# ABBREVIATIONS

| | |
|---|---|
| 1,3,5-TMB | 1,3,5-trimethoxybenzene |
| ALA | 5-aminolevulinic acid |
| Bz | benzoyl |
| DNA | deoxyribonucleic acid |
| dSSM | double site-saturation mutagenesis |
| epPCR | error-prone polymerase chain reaction |
| equiv | equivalents |
| FI | field ionization |
| G6P | D-glucose-6-phosphate |
| G6PD | glucose-6-phosphate dehydrogenase |
| GC | gas chromatography |
| GC/MS | gas chromatography couple mass spectrometry |
| IPTG | isopropyl β-D-1-thiogalactopyranoside |
| $KP_i$ | potassium phosphate buffer |
| LBcarb | Luria–Bertani medium with 100 μg/mL carbenicillin |
| MeCN | acetonitrile |
| $MnCl_2$ | manganese chloride |
| $NADP^+/H$ | nicotinamide adenine dinucleotide phosphate |
| NEB | New England Biolabs |
| NMR | nuclear magnetic resonance |
| PCR | polymerase chain reaction |
| PLP | pyridoxal phosphate |
| SOC | super optimal broth with catabolite repression |
| SSM | site-saturation mutagenesis |
| StEP | staggered extension processes *in vitro* recombination |
| TBcarb | terrific broth medium with 100 μg/mL carbenicillin |
| THF | tetrahydrofuran |
| TLC | thin-layer chromatography |
| Tris | tris(hydroxymethyl)aminomethane buffer |
| UV | ultraviolet |

Chapter I

# DIRECTED EVOLUTION AS A TOOL TO ACCESS NOVEL DEGRADATION ACTIVITIES

# ABSTRACT

Enzymes, the catalysts of the living world, empower organisms to access a diversity of nutrient sources in their environment. Over time, as new nutrient sources are introduced, new enzymatic activities evolve to expand the catabolic repertoire of an organism. For example, cellulose and lignin in plant biomass were not enzymatically accessible millions of years ago and instead accumulated into what are now fossil fuel deposits. In the intervening eons, organisms have evolved a myriad of enzymes capable of depolymerizing plant biomass to its constituent monomers. On a more human timescale, megatons (Mt) of plastics have been introduced to the environment each year since the middle of the 20$^{th}$ century. These petrochemical-derived polymers are difficult to degrade enzymatically but represent a highly concentrated and carbon-rich substrate. Unsurprisingly, organisms have evolved enzymatic activities that are beginning to allow them to access the carbon locked in recalcitrant plastic polymers. Enzymatic evolution in the laboratory—directed evolution—has analogously enabled access to enzymatic activities that have never been observed in the natural world. By accelerating the evolution of new enzymatic activities, directed evolution can uncover enzymes capable of degrading molecules that are non-biodegradable in the natural world.

## 1.1 Evolution of Catabolic Enzyme Activities

Biological systems are a complex symphony of chemical reactions that are mediated by catalytic biomolecules, enzymes. Enzymes accelerate reactions throughout organismal biology—polymerases stitch together DNA, proteases break proteins down into amino acids, and nitrogenases cleave the dinitrogen triple bond to fix nitrogen into usable forms. Among these important functions, one of the foundational roles of enzymes is to access the energy and nutrients from a variety of substrates—together known as food. Heterotrophic organisms prefer to use organic substrates as sources of energy and have an arsenal of enzymes that can cleave bonds in these substrates. The diversity in enzymes is mirrored by the diversity in food substrates, which harbor a vast trove of chemical linkages. When confronted with a new type of substrate that has energetic or nutritional value, it is often the case that organisms do not possess the degradative machinery to access the nutrients or calories in that substrate. However, if an organism can gain benefit to breaking down the substrate, it is often that case they will eventually evolve catalytic machinery that can unlock the value in these substrates. This adaptation occurs via evolution. By acting on enzymes that exhibit promiscuity—the ability to act on substrates beyond the native substrate—evolution can unlock new functions from existing enzymes.

This chapter will describe how evolution engenders enzymes with novel activities both in Nature and in the laboratory. The appearance of lignocellulose-degrading enzymes in response to the proliferation of plant biomass will introduce important concepts in enzyme evolution. This background will set the stage for a discussion of enzymes that have evolved on human timescales to degrade anthropogenic compounds that pose a benefit to the

organism when degraded, such as unlocking carbon from plastic or reducing the toxicity of a new agrochemical. This background will set the stage for a perspective on how directed evolution of enzymes can unlock degradation chemistries unknown to biology, an ever-important direction given the numerical and volumetric proliferation of man-made chemicals.

### 1.1.1 Enzymatic Lignocellulose Degradation

Heterotrophic organisms make a living by consuming organic compounds, mostly originating from primary producers such as plants. Despite the abundance of organic material on Earth, not all naturally occurring organic compounds are facile to degrade enzymatically. To illustrate this, let us take a step back in time to discuss the formation of fossil fuels. Fossil fuel deposits form when organic carbon is buried and fossilizes. The rate of burial is intrinsically linked to the rate of organic carbon degradation pre-burial such that lower extents of degradation lead to more carbon burial and thus greater quantities of fossil carbon.

Unprecedented carbon burial rates during the Carboniferous (359 Mya to 299 Mya) and Permian (299 Mya to 252 Mya) periods led to the accumulation of enormous coal deposits. The primary biopolymer that fossilizes as coal is lignin, which evolved prior to these periods and enhanced the structural integrity of plants (*1*). Lignin is recalcitrant—difficult to degrade—due to its heterogenous structure, high molecular weight, and insolubility (*2*). However, lignin presents a reservoir of carbon and nitrogen if an enzyme could be evolved to decompose it. On the basis of fossil and phylogenetic evidence, it has been hypothesized that biological lignin degradation evolved in white rot fungi in the middle of the Permian period (*2*, *3*). Proliferation of these organisms (and their enzyme arsenals) is hypothesized to

be behind the sharp decline in coal burial rates at the end of the Permian period (*2*, *3*). That the evolution of lignin-degrading enzymes seems to have taken hundreds of millions of years may have to do with tradeoff between the difficulty of depolymerizing lignin and the relatively low nutrient value obtained for doing so (lignin contains few nutrients beyond its carbon content) (*2*).

Fast forward to the modern day—organisms have evolved numerous strategies for depolymerizing lignin and other plant polymers, namely cellulose and hemicelluloses. An illustrative figure is that only 3% of lignin that is biosynthesized is buried; the rest is subject to degradation (*2*). The universe of enzymes used to deconstruct plant biomass is vast and encompasses many modes of action and mechanisms. For example, cellulose and hemicellulose are degraded by fungal and bacterial glycoside hydrolases. Cellulolytic organisms often express a battery of glycoside hydrolases with complementary activities, such as exo- and endo-glucanase activity, to degrade polysaccharides more effectively. These enzyme 'cassettes' often exhibit more activity per active site than enzymes in isolation due to synergies between different activities (*4–7*). Microorganisms have also evolved multidomain cellulases that colocalize glycoside hydrolases of different specificities in a single polypeptide chain (*8*, *9*) and cellulosomes, megadalton-scale complexes harboring dozens of glycoside hydrolases (*10–14*). These hydrolases are accompanied by oxidative enzymes, including lytic polysaccharide monooxygenases, that utilize copper centers and molecular oxygen to directly oxidize carbohydrate chains (*7*, *15*). Lignin degradation in the modern day relies on enzymes with a diversity of activities, including peroxidases and

laccases with activities toward different linkages, the diversity of which is essential to decomposing the heterogenous structure of lignin (*6*, *16*, *17*).

The variety of strategies and mechanisms of enzymatic lignocellulose degradation demonstrates the power of enzyme evolution over millions of years at a planetary scale. Just as the development of plant cells structured around lignin presented a challenge for microorganisms of a different eon to adapt to, the introduction of anthropogenic molecules to the biosphere presents another opportunity for evolution to diversify the catalytic repertoire of life. Examples of natural evolution on anthropogenic molecules, albeit on much shorter timescales than described above, will be illustrated in the next section.

### 1.2 Evolution of New Activities on Anthropogenic Compounds

One of the pillars of modern society is composed of the application of synthetic chemical compounds throughout the economy. The diversity of these chemicals enables a myriad of applications. Perhaps most familiar due to their visible applications and high production volumes are plastic polymers, which are used to construct lightweight building materials, prevent food spoilage, and assemble performance clothing (*18*). Similarly, silicone polymers and oligomers, which will be discussed in much greater detail in **Chapter II**, are used as lubricants, sealants, and in personal care products (*19*). The green revolution has been driven in part by agrochemicals, which are used to prevent invasive species, improve crop yields, and reduce infestation by pests (*20*). Pharmaceutical compounds display vast structural and functional diversity that allows them to function on disparate targets in a wide variety of disease contexts.

These examples only scratch the surface of the diversity trove of chemicals used in modern society. There are an estimated 100,000-300,000 chemicals that are commercially manufactured and sold (*21–23*), and this number grows each year. This figure only accounts for chemicals that have been registered and does not account for the many compounds that result from their speciation and degradation (*22*). To satisfy worldwide demand for chemicals, in 2013 the chemical sector transformed hundreds of Mt of fossil fuel and refinery feedstocks into an estimated 820.3 Mt of products (*23*).

In addition to allowing the innumerable applications introduced above, the structural diversity and production volumes of anthropogenic chemicals are also cause for concern as these new substances can exert a variety of effects when released into the environment. Chemicals not previously present in the Earth system are known as 'novel entities' under the planetary boundaries framework (*21*) and may present risks to the Earth system when they exhibit persistence, long-range transport and widespread geographical distribution, and potential impacts on biological or geological processes (*21*, *22*, *24*). Upon introduction of a novel entity into the environment, they can pose an opportunity—as a new source of food or nutrients—or a threat—as a toxin—to organisms. This section will discuss how organisms can evolve enzymatic activities capable of harnessing the opportunities or neutralizing the threats presented by anthropogenic chemicals.

### 1.2.1 Enzymatic Plastic Degradation

Plastics were first manufactured at scale in the mid-20$^{th}$ century, with a production volume of 2 Mt in 1950. In the intervening decades, these man-made polymers have come to hold vast importance in global commerce and society, so much so that 381 Mt of plastic was

produced in 2015 (HuID 97241) (*25*, *26*). The annual production of plastics exceeds that of all man-made materials except concrete and steel (*25*, *26*). Plastic production is estimated to reach 700 Mt in 2030 (*27*). Driven by the ever-expanding applications of plastics, humanity's appetite for plastic is so large that a cumulative 8.3 Gt of plastic was produced by 2015 (*26*). Of this quantity, 6.3 Gt of plastic has been discarded, with the vast majority–79%–of this being directed to landfill or mismanaged and directed to natural environments (*26*).

This mass of plastics is composed of a variety of different polymer types, mostly derived from monomers synthesized via derivatization of fossil hydrocarbon feedstocks. These polymers harbor a diversity of different linkages that must be broken for degradation to occur. The structures of the four plastic categories with the largest market sizes—polyethylene, polypropylene, poly(ethylene terephthalate), and polyvinyl chloride—illustrate this diversity (**Figure 1-1**). Most of these linkages (and those in other plastics) present a new chemical challenge to microorganisms in the environment, and most plastics are not readily biodegradable, exhibiting environmental decomposition half-lives ranging from years to thousands of years (*28*). However, the vast quantity of carbon locked in plastic polymers represents an attractive potential energy source for heterotrophs (*29*), a selective pressure which has driven evolution of enzymatic activities that can break some of the linkages illustrated in **Figure 1-1**.

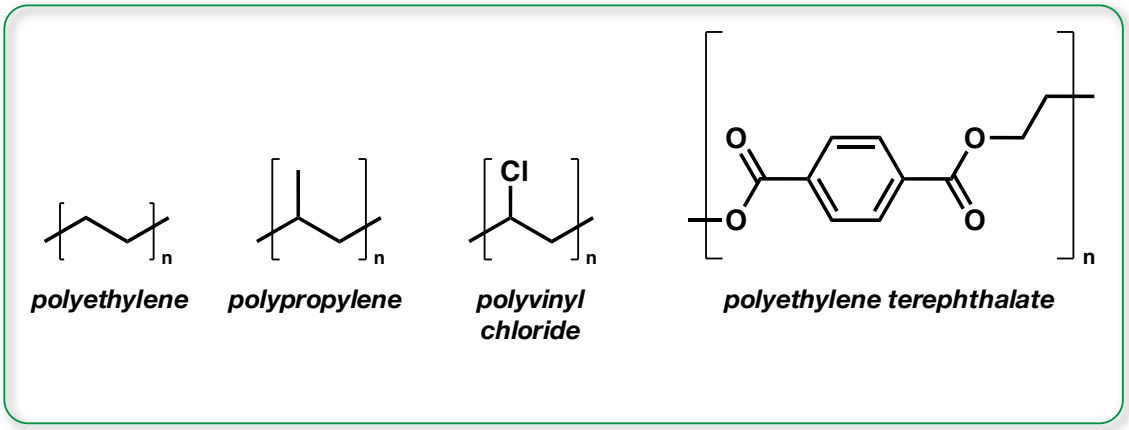


**Figure 1-1. Structures of some of the most common plastics.** Some of the most produced plastics exhibit diverse chemical structures which enable them to be used in different applications. Polyethylenes (102.9 Mt/yr) are used in films and containers, polypropylenes (50.4 Mt/yr) are utilized for myriad structural and home applications, polyvinyl chloride (PVC, 50.5 Mt/yr) is used extensively in building materials and furniture, and poly(ethylene terephthalate) (PET, 65.4 Mt/yr) is used in textiles and packaging (*18*, *30*).

Poly(ethylene terephthalate) (PET) is a plastic familiar to most people on earth (even if not in name) due to its use in synthetic clothing (where it is referred to generically as polyester) and in the ubiquitous plastic water bottle, which was patented in 1973 (*18*, *27*, *31*). Large quantities of PET have been introduced to the environment since, resulting in its widespread distribution throughout the planet's ecosystems. PET consists of aromatic ester linkages and was thought to be entirely non-biodegradable. Early reports of aliphatic polyester degradation (*32*) and a report that a *Thermobifida fusca* cutinase could partially degrade amorphous PET in a weeks-long incubation at elevated temperature (*33*) suggested that it could be possible to cleave the aromatic ester linkages in PET enzymatically. Despite these advances, microorganisms capable of growing on PET or enzymes capable of degrading it rapidly had not yet been discovered. In 2016, researchers collected environmental samples contaminated with PET from a recycling plant, representing a man-made ecosystem highly

enriched in PET. A novel species, *Ideonella sakaiensis*, that can grow on PET was isolated from these samples (*34*).

This ability to grow on PET is conferred by a set of enzymes, one that can convert PET to mono(2-hydroxyethyl)terephthalic acid (MHET), and another that can convert MHET to the PET monomer terephthalic acid (TPA) which can then be funneled into central carbon metabolism by extant enzymes (**Figure 1-2**). The PETase exhibits only 51% sequence identity to the *T. fusca* cutinase. Interestingly, the enzyme outperforms several other PET hydrolases on PET by 5.5 to 120-fold while preferring to hydrolyze PET over aliphatic ester substrates relative to the other enzymes (*34*). How did these novel enzymes arise in this bacterium isolated from this PET-rich environment? Upon searching genome databases, the researchers were unable to find any organisms beyond *I. sakainesis* that possess the requisite arsenal of genes encoding PET-degrading enzymes. However, several organisms were identified with genes encoding MHETase homologs and the downstream metabolic genes required for TPA metabolism (*34*). The authors suggest that living in a PET-enriched environment set the stage for selection of a bacterium possessing a PETase-encoding gene that had been acquired through lateral gene transfer or mutation of a gene encoding a cutinase with promiscuous activity for PET hydrolysis (*31*, *34*).

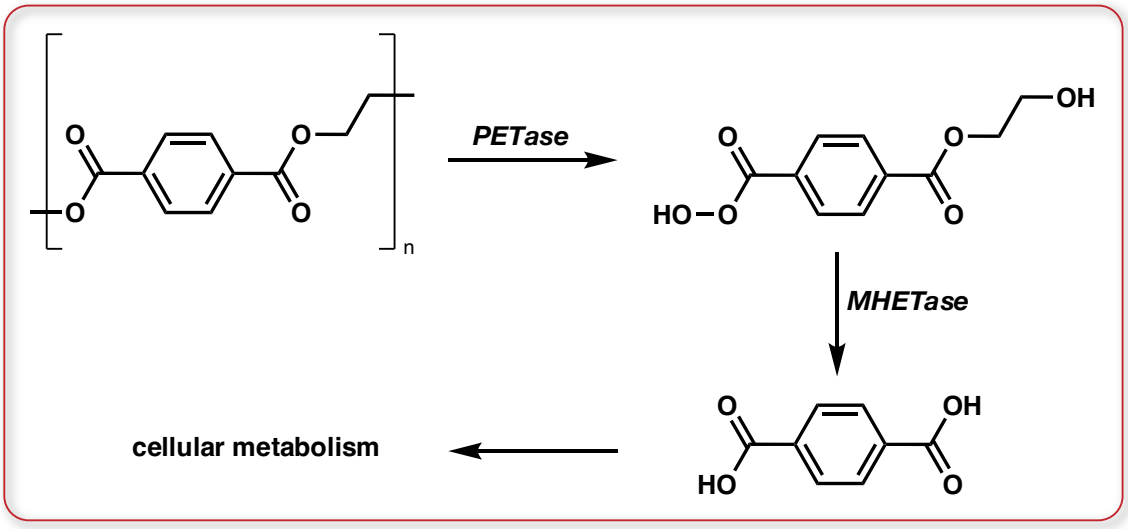


**Figure 1-2. Degradation of PET by *Ideonella sakaiensis* PETase and MHETase.** PETase acts on PET to yield MHET which is then converted into the monomer of PET, TPA. TPA can be funneled into central metabolism by enzymes that already exist in many microorganisms.

Although it is the most prominent example of enzymatic plastic degradation, PET is not the only plastic polymer for which enzymatic activity has been demonstrated (*27*, *30*). The rapid evolution of enzymatic PET hydrolysis as well as examples on other polymers demonstrate that Nature's catalog of enzymatic activities can be expanded to encompass novel activities on decadal timescales under certain conditions, including sufficient substrate concentration, substrate persistence, and presence of an enzyme exhibiting promiscuous activity. Highlighting the presence of plastic pollution as a key driver of evolution is the increased incidence of plastic-degrading enzymes in metagenomes obtained from environments enriched in plastics (*35*). In addition to these factors, for a novel degradative activity to evolve, an organism must gain some selective benefit from degrading the substrate.

### 1.2.2 Enzymatic Degradation of Agrochemicals

Along with plastics, agrochemicals constitute the primary contributions of man-made chemicals to the biosphere by mass. Agrochemicals including synthetic fertilizers, herbicides, and insecticides are largely responsible for improved agricultural yields and efficiencies, yet they also pose substantial environmental and toxicological risk to ecosystems and human communities. The massive quantities of these chemicals that are applied to agricultural soils throughout the globe and their resulting high concentrations presents another challenge and opportunity for evolution of novel enzymatic degradation activities.

Atrazine was first patented in 1958 and used to reduce weeds among corn, sugarcane, and other major crops. Atrazine is one of the most commonly used herbicides in the world, and it fits the definition of a 'novel entity' in all regards. It is highly persistent, can be transported hundreds or thousands of kilometers via rainfall, and is a potent endocrine disruptor in ppb quantities (*20*, *36*). Atrazine biodegradation in the first decades of its use was slow, when it exhibited a half-life of two months to one year (*37*, *38*). After decades of use, atrazine was observed to undergo dealkylation via a nonspecific cytochrome P450 (**Figure 1-3**) (*38*). However, this reaction resulted in a species that was still chlorinated and could present potential ecotoxicological issues. After decades of exposure to atrazine, an enzyme atrazine chlorohydrolase (AtzA) that is effective at dechlorinating atrazine was discovered (**Figure 1-3**) (*37*, *39*). AtzA shares 98% sequence identity with a melamine deaminase from the same organism, yet the substrate specificities of these two enzymes diverge dramatically (*38*, *39*). In addition to this remarkable sequence similarity, only nine mutations were required for the

enzyme to adapt from its native deaminase function into the AtzA chlorohydrolase, which displays no deaminase activity. (*38*, *39*). Further studies revealed that only two of these nine mutations are responsible for the bulk of the divergence in activity between these two enzymes (*40*).

Beyond atrazine, organisms have evolved enzymes capable of deactivating numerous other agrochemicals (*41*), and other toxic compounds such as nitroaromatics (*42–44*). The rapid evolution of atrazine chlorohydrolase and other enzymes that detoxify agrochemicals and other toxic novel entities sets the stage for evolution of new-to-nature activities with only a handful of mutations.

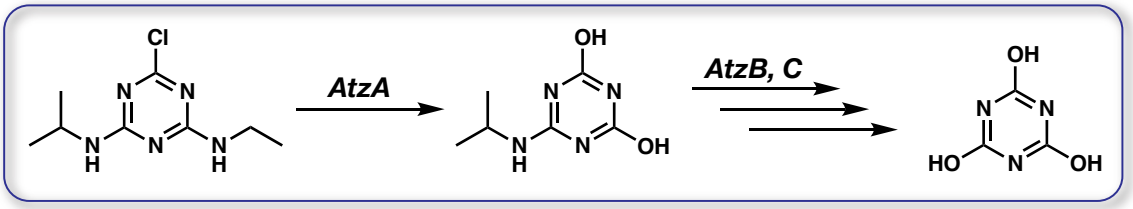


**Figure 1-3. Enzymatic degradation of atrazine.** Atrazine chlorohydrolase (AtzA) dechlorinates atrazine. Other enzymes, AtzB and AtzC exhaustively hydroxylate the intermediate compound.

### 1.3 Outlook: Harnessing Directed Evolution to Develop Novel Degradation Activities

Evolution is beautiful in its simplicity; mutations give rise to new or altered functions that are selected for or against by environmental conditions. Evolution of biomolecules in the laboratory, directed evolution, follows this elegant algorithm. By imparting mutations to the genes encoding enzymes, functional diversity is generated. This functional diversity can then be evaluated by testing the encoded enzymes for their function, any function. The best mutant is selected and mutated again, and the cycle repeats. Directed evolution has proven to be a

powerful tool for generation of enzymes with improved function, and recently has extended its repertoire to encompass the generation of *new* functions (*45–47*).

The proliferation of anthropogenic chemicals and their release to the environment presents biological systems with a challenge and an opportunity. Through evolution, organisms may be able to adapt to break down these compounds provided that there is a benefit to doing so. However, some anthropogenic chemicals do not challenge organisms via toxicity, nor do they tempt them via the nutrients dictated by their elemental composition. Thus, they pose little benefit to an enterprising organism that can degrade them. In these cases, it is unlikely that an enzyme for degrading these compounds will evolve in the natural world, unless the compound of interest so closely resembles existing compounds that promiscuous activity alone is sufficient to degrade the compound. In the cases where the compound presents a truly novel challenge and the selective pressures are insufficient to drive rapid evolution, directed evolution in the laboratory presents a route around these obstacles. By allowing artificial selective pressures to be imposed upon the genes encoding enzymes and allowing the use of precursors not found in the natural world, directed evolution can unlock these new activities.

Chapter II introduces the reader to organosilicon compounds and goes on to describe their interaction with enzymes. It bears noting that the first enzyme capable of forging a silicon–carbon bond was engineered via directed evolution. Chapter III establishes a critical proof point that directed evolution can unlock new-to-nature degradation activities, in this case the first known enzyme capable of deconstructing silicon–carbon bonds.

**Chapter I Bibliography**


1. J. M. Robinson, Atmospheric bulk chemistry and evolutionary megasymbiosis. *Chemosphere*. **33**, 1641–1653 (1996).

2. J. M. Robinson, Lignin, land plants, and fungi: Biological evolution affecting Phanerozoic oxygen balance. *Geology*. **18**, 607–610 (1990).

3. D. Floudas, M. Binder, R. Riley, K. Barry, R. A. Blanchette, B. Henrissat, A. T. Martínez, R. Otillar, J. W. Spatafora, J. S. Yadav, A. Aerts, I. Benoit, A. Boyd, A. Carlson, A. Copeland, P. M. Coutinho, R. P. de Vries, P. Ferreira, K. Findley, B. Foster, J. Gaskell, D. Glotzer, P. Górecki, J. Heitman, C. Hesse, C. Hori, K. Igarashi, J. A. Jurgens, N. Kallen, P. Kersten, A. Kohler, U. Kües, T. K. A. Kumar, A. Kuo, K. LaButti, L. F. Larrondo, E. Lindquist, A. Ling, V. Lombard, S. Lucas, T. Lundell, R. Martin, D. J. McLaughlin, I. Morgenstern, E. Morin, C. Murat, L. G. Nagy, M. Nolan, R. A. Ohm, A. Patyshakuliyeva, A. Rokas, F. J. Ruiz-Dueñas, G. Sabat, A. Salamov, M. Samejima, J. Schmutz, J. C. Slot, F. St. John, J. Stenlid, H. Sun, S. Sun, K. Syed, A. Tsang, A. Wiebenga, D. Young, A. Pisabarro, D. C. Eastwood, F. Martin, D. Cullen, I. V. Grigoriev, D. S. Hibbett, The paleozoic origin of enzymatic lignin decomposition reconstructed from 31 fungal genomes. *Science*. **336**, 1715–1719 (2012).

4. R. Brunecky, D. Chung, N. S. Sarai, N. Hengge, J. F. Russell, J. Young, A. Mittal, P. Pason, T. Vander Wall, W. Michener, T. Shollenberger, J. Westpheling, M. E. Himmel, Y. J. Bomble, High activity CAZyme cassette for improving biomass degradation in thermophiles. *Biotechnol. Biofuels*. **11**, 22 (2018).

5. M. Andlar, T. Rezić, N. Marđetko, D. Kracher, R. Ludwig, B. Šantek, Lignocellulose degradation: An overview of fungi and fungal enzymes involved in lignocellulose degradation. *Eng. Life Sci.* **18**, 768–778 (2018).

6. S. M. Cragg, G. T. Beckham, N. C. Bruce, T. D. Bugg, D. L. Distel, P. Dupree, A. G. Etxabe, B. S. Goodell, J. Jellison, J. E. McGeehan, S. J. McQueen-Mason, K. Schnorr, P. H. Walton, J. E. Watts, M. Zimmer, Lignocellulose degradation mechanisms across the Tree of Life. *Curr. Opin. Chem. Biol.* **29**, 108–119 (2015).

7. Y. J. Bomble, C.-Y. Lin, A. Amore, H. Wei, E. K. Holwerda, P. N. Ciesielski, B. S. Donohoe, S. R. Decker, L. R. Lynd, M. E. Himmel, Lignocellulose deconstruction in the biosphere. *Curr. Opin. Chem. Biol.* **41**, 61–70 (2017).

8. D. Chung, N. S. Sarai, B. C. Knott, N. Hengge, J. F. Russell, J. M. Yarbrough, R. Brunecky, J. Young, N. Supekar, T. Vander Wall, D. W. Sammond, M. F. Crowley, C. M. Szymanski, L. Wells, P. Azadi, J. Westpheling, M. E. Himmel, Y. J. Bomble, Glycosylation is vital for industrial performance of hyperactive cellulases. *ACS Sustain. Chem. Eng.* **7**, 4792–4800 (2019).

9. N. S. Sarai, A. Kahn, E. A. Bayer, M. E. Himmel, Y. J. Bomble, "3.02 - Fundamentals and Industrial Applicability of Multifunctional CAZyme Systems" in *Comprehensive Biotechnology (Third Edition)*, M. Moo-Young, Ed. (Pergamon, ed. 3, 2019), vol. 3, pp. 14–23.

10. L. Artzi, E. A. Bayer, S. Moraïs, Cellulosomes: Bacterial nanomachines for dismantling plant polysaccharides. *Nat. Rev. Microbiol.* **15**, 83–95 (2017).

11. K. Hirano, M. Kurosaki, S. Nihei, H. Hasegawa, S. Shinoda, M. Haruki, N. Hirano, Enzymatic diversity of the *Clostridium thermocellum* cellulosome is crucial for the degradation of crystalline cellulose and plant biomass. *Sci. Rep.* **6**, 35709 (2016).

12. Q. Xu, M. G. Resch, K. Podkaminer, S. Yang, J. O. Baker, B. S. Donohoe, C. Wilson, D. M. Klingeman, D. G. Olson, S. R. Decker, R. J. Giannone, R. L. Hettich, S. D. Brown, L. R. Lynd, E. A. Bayer, M. E. Himmel, Y. J. Bomble, Dramatic performance of *Clostridium thermocellum* explained by its wide range of cellulase modalities. *Sci. Adv.* **2**, e1501254 (2016).

13. A. Kahn, S. Moraïs, A. P. Galanopoulou, D. Chung, N. S. Sarai, N. Hengge, D. G. Hatzinikolaou, M. E. Himmel, Y. J. Bomble, E. A. Bayer, Creation of a functional hyperthermostable designer cellulosome. *Biotechnol. Biofuels*. **12**, 44 (2019).

14. A. Kahn, S. Moraïs, D. Chung, N. S. Sarai, N. N. Hengge, A. Kahn, M. E. Himmel, E. A. Bayer, Y. J. Bomble, Glycosylation of hyperthermostable designer cellulosome components yields enhanced stability and cellulose hydrolysis. *FEBS J.* **287**, 4370–4388 (2020).

15. P. Chylenski, B. Bissaro, M. Sørlie, Å. K. Røhr, A. Várnai, S. J. Horn, V. G. H. Eijsink, Lytic polysaccharide monooxygenases in enzymatic processing of lignocellulosic biomass. *ACS Catal.* **9**, 4970–4991 (2019).

16. G. de Gonzalo, D. I. Colpa, M. H. M. Habib, M. W. Fraaije, Bacterial enzymes involved in lignin degradation. *J. Biotechnol.* **236**, 110–119 (2016).

17. G. Janusz, A. Pawlik, J. Sulej, U. Świderska-Burek, A. Jarosz-Wilkołazka, A. Paszczyński, Lignin degradation: microorganisms, enzymes involved, genomes analysis and evolution. *FEMS Microbiol. Rev.* **41**, 941–962 (2017).

18. A. L. Andrady, M. A. Neal, Applications and societal benefits of plastics. *Philos. Trans. R. Soc. B*. **364**, 1977–1984 (2009).

19. C. Rücker, K. Kümmerer, Environmental chemistry of organosiloxanes. *Chem. Rev.* **115**, 466–524 (2015).

20. P. I. Devi, M. Manjula, R. V. Bhavani, Agrochemicals, environment, and human health. *Annu. Rev. Environ. Resour.* **47**, 399–421 (2022).

21. W. Steffen, K. Richardson, J. Rockstrom, S. E. Cornell, I. Fetzer, E. M. Bennett, R. Biggs, S. R. Carpenter, W. de Vries, C. A. de Wit, C. Folke, D. Gerten, J. Heinke, G. M. Mace, L. M. Persson, V. Ramanathan, B. Reyers, S. Sorlin, Planetary boundaries: Guiding human development on a changing planet. *Science*. **347**, 1259855 (2015).

22. L. Persson, B. M. Carney Almroth, C. D. Collins, S. Cornell, C. A. de Wit, M. L. Diamond, P. Fantke, M. Hassellöv, M. MacLeod, M. W. Ryberg, P. Søgaard Jørgensen, P. Villarrubia-Gómez, Z. Wang, M. Z. Hauschild, Outside the safe operating space of the planetary boundary for novel entities. *Environ. Sci. Technol.* **56**, 1510–1521 (2022).

23. P. G. Levi, J. M. Cullen, Mapping global flows of chemicals: From fossil fuel feedstocks to chemical products. *Environ. Sci. Technol.* **52**, 1725–1734 (2018).

24. W. Steffen, K. Richardson, J. Rockström, H. J. Schellnhuber, O. P. Dube, S. Dutreuil, T. M. Lenton, J. Lubchenco, The emergence and evolution of Earth System Science. *Nat. Rev. Earth Environ.* **1**, 54–63 (2020).

25. G. Chure, R. A. Banks, A. I. Flamholz, N. S. Sarai, M. Kamb, I. Lopez-Gomez, Y. Bar-On, R. Milo, R. Phillips, Anthroponumbers.org: A quantitative database of human impacts on Planet Earth. *Patterns*. **3**, 100552 (2022).

26. R. Geyer, J. R. Jambeck, K. L. Law, Production, use, and fate of all plastics ever made. *Sci. Adv.* **3**, e1700782 (2017).

27. V. Tournier, S. Duquesne, F. Guillamot, H. Cramail, D. Taton, A. Marty, I. André, Enzymes' power for plastics degradation. *Chem. Rev.* (2023), doi:10.1021/acs.chemrev.2c00644.

28. A. Chamas, H. Moon, J. Zheng, Y. Qiu, T. Tabassum, J. H. Jang, M. Abu-Omar, S. L. Scott, S. Suh, Degradation rates of plastics in the environment. *ACS Sustain. Chem. Eng.* **8**, 3494–3511 (2020).

29. A. Stubbins, K. L. Law, S. E. Muñoz, T. S. Bianchi, L. Zhu, Plastics in the Earth system. *Science*. **373**, 51–55 (2021).

30. L. D. Ellis, N. A. Rorrer, K. P. Sullivan, M. Otto, J. E. McGeehan, Y. Román-Leshkov, N. Wierckx, G. T. Beckham, Chemical and biological catalysis for plastics recycling and upcycling. *Nat. Catal.* **4**, 539–556 (2021).

31. I. Taniguchi, S. Yoshida, K. Hiraga, K. Miyamoto, Y. Kimura, K. Oda, Biodegradation of PET: Current status and application aspects. *ACS Catal.* **9**, 4089–4105 (2019).

32. Y. Tokiwa, T. Suzuki, Hydrolysis of polyesters by lipases. *Nature*. **270**, 76–78 (1977).

33. R.-J. Müller, H. Schrader, J. Profe, K. Dresler, W.-D. Deckwer, Enzymatic degradation of poly(ethylene terephthalate): Rapid hydrolyse using a hydrolase from *T. fusca*. *Macromol. Rapid Commun.* **26**, 1400–1405 (2005).

34. S. Yoshida, K. Hiraga, T. Takehana, I. Taniguchi, H. Yamaji, Y. Maeda, K. Toyohara, K. Miyamoto, Y. Kimura, K. Oda, A bacterium that degrades and assimilates poly(ethylene terephthalate). *Science*. **351**, 1196–1199 (2016).

35. J. Zrimec, M. Kokina, S. Jonasson, F. Zorrilla, A. Zelezniak, Plastic-degrading potential across the global microbiome correlates with recent pollution trends. *mBio*. **12**, e02155-21 (2021).

36. T. B. Hayes, V. Khoury, A. Narayan, M. Nazir, A. Park, T. Brown, L. Adame, E. Chan, D. Buchholz, T. Stueve, S. Gallipeau, Atrazine induces complete feminization and chemical castration in male African clawed frogs (Xenopus laevis). *Proc. Natl. Acad. Sci. U.S.A.* **107**, 4612–4617 (2010).

37. N. Udiković-Kolić, C. Scott, F. Martin-Laurent, Evolution of atrazine-degrading capabilities in the environment. *Appl. Microbiol. Biotechnol.* **96**, 1175–1189 (2012).

38. J. L. Seffernick, L. P. Wackett, Rapid evolution of bacterial catabolic enzymes: A case study with atrazine chlorohydrolase. *Biochemistry*. **40**, 12747–12753 (2001).

39. C. Scott, C. J. Jackson, C. W. Coppin, R. G. Mourant, M. E. Hilton, T. D. Sutherland, R. J. Russell, J. G. Oakeshott, Catalytic improvement and evolution of atrazine chlorohydrolase. *Appl. Environ. Microbiol.* **75**, 2184–2191 (2009).

40. S. Raillard, A. Krebber, Y. Chen, J. E. Ness, E. Bermudez, R. Trinidad, R. Fullem, C. Davis, M. Welch, J. Seffernick, L. P. Wackett, W. P. C. Stemmer, J. Minshull, Novel enzyme activities and functional plasticity revealed by recombining highly homologous enzymes. *Chem. Biol.* **8**, 891–898 (2001).

41. Z. Arbeli, C. L. Fuentes, Accelerated biodegradation of pesticides: An overview of the phenomenon, its basis and possible solutions; and a discussion on the tropical dimension. *Crop Prot.* **26**, 1733–1746 (2007).

42. M. D. Roldán, E. Pérez-Reinado, F. Castillo, C. Moreno-Vivián, Reduction of polynitroaromatic compounds: The bacterial nitroreductases. *FEMS Microbiol. Rev.* **32**, 474–500 (2008).

43. M. Kivisaar, Evolution of catabolic pathways and their regulatory systems in synthetic nitroaromatic compounds degrading bacteria. *Mol. Microbiol.* **82**, 265–268 (2011).

44. Shapir N., Mongodin E. F., Sadowsky M. J., Daugherty S. C., Nelson K. E., Wackett L. P., Evolution of catabolic pathways: Genomic insights into microbial s-triazine metabolism. *J. Bacteriol.* **189**, 674–682 (2007).

45. F. H. Arnold, Directed evolution: Bringing new chemistry to life. *Angew. Chem. Int. Ed.* **57**, 4143–4148 (2018).

46. N. P. Dunham, F. H. Arnold, Nature's machinery, repurposed: Expanding the repertoire of iron-dependent oxygenases. *ACS Catal.* **10**, 12239–12255 (2020).

47. H. Renata, Z. J. Wang, F. H. Arnold, Expanding the enzyme universe: Accessing non-natural reactions by mechanism-guided directed evolution. *Angew. Chem. Int. Ed.* **54**, 3351–3367 (2015).

Chapter II

# BIOCATALYTIC TRANSFORMATIONS OF SILICON—THE OTHER GROUP 14 ELEMENT

Material from this chapter appears in: **N. S. Sarai**, B. J. Levin, J. M. Roberts, D. E. Katsoulis, F. H. Arnold, Biocatalytic transformations of silicon—the other Group 14 element. *ACS Cent. Sci.* **7**, 944–953 (2021).

# ABSTRACT

Significant inroads have been made using biocatalysts to perform new-to-nature reactions with high selectivity and efficiency. Meanwhile, advances in organosilicon chemistry have led to rich sets of reactions holding great synthetic value. Merging biocatalysis and silicon chemistry could yield new methods for the preparation of valuable organosilicon molecules as well as the degradation and valorization of undesired ones. Despite silicon's importance in the biosphere for its role in plant and diatom construction, it is not known to be incorporated into any primary or secondary metabolites. Enzymes have been found that act on silicon-containing molecules, but only a few are known to act directly on silicon centers. Protein engineering and evolution has and could continue to enable enzymes to catalyze useful organosilicon transformations, complementing and expanding upon current synthetic methods. The role of silicon in biology and the enzymes that act on silicon-containing molecules are reviewed to set the stage for a discussion of where biocatalysis and organosilicon chemistry may intersect.

## 2.1 Introduction

Silicon is found in copious amounts on Earth, where it comprises ~28% of the lithosphere, is the second most abundant element after oxygen, and is present in teramole quantities in the oceans (*1*, *2*). It also holds a privileged position as one of the key elements of human enterprise. Humans have harnessed the unique properties of silicon for centuries, using silica to make structural materials including concrete, brick, and glass. More recent applications have propelled society to capabilities unimaginable a century ago. Leveraging of its electronic properties has laid the foundation for our modern society and innumerable resultant innovations (*3*). Simultaneously, organosilicon compounds are deployed on the scale of megatons / year for use in sealants and adjuvants for construction, agriculture, cosmetic, automotive, and high-performance aerospace applications (*4*).

Silicon is also important in the biosphere where its role is dictated by its chemical properties and the scope of reactions it undergoes in the environment. Silicon appears just below carbon in group 14 of the periodic table and shares some similarities with the element that takes center stage throughout the tree of life, but they differ in important ways (*5*, *6*). Silicon has a larger covalent radius and a lower Pauling electronegativity than carbon (**Figure 2-1**). This leads to Si–E bonds being more polar in general than corresponding C–E bonds (*7*). Like carbon, silicon generally has a valency of four, but lacks carbon's ability to form double or triple bonds under mild conditions (*8*). Silicon can also form hypervalent species, bonding to five—or even six—other atoms. Perhaps the most important difference between carbon and silicon is the ease with which the former forms long chains of the same element, known as catenation. Carbon, as is evident from the most rudimentary inspection

of organic molecules, is highly adept at catenation. The predominant forms of silicon in nature contain Si–O bonds, which are substantially more stable than Si–Si bonds and explain the dearth of natural silicon catenation species (**Figure 2-1**) (*9*). Polysilanes can be accessed synthetically (*10*) but only under conditions that are wholly inaccessible biologically.

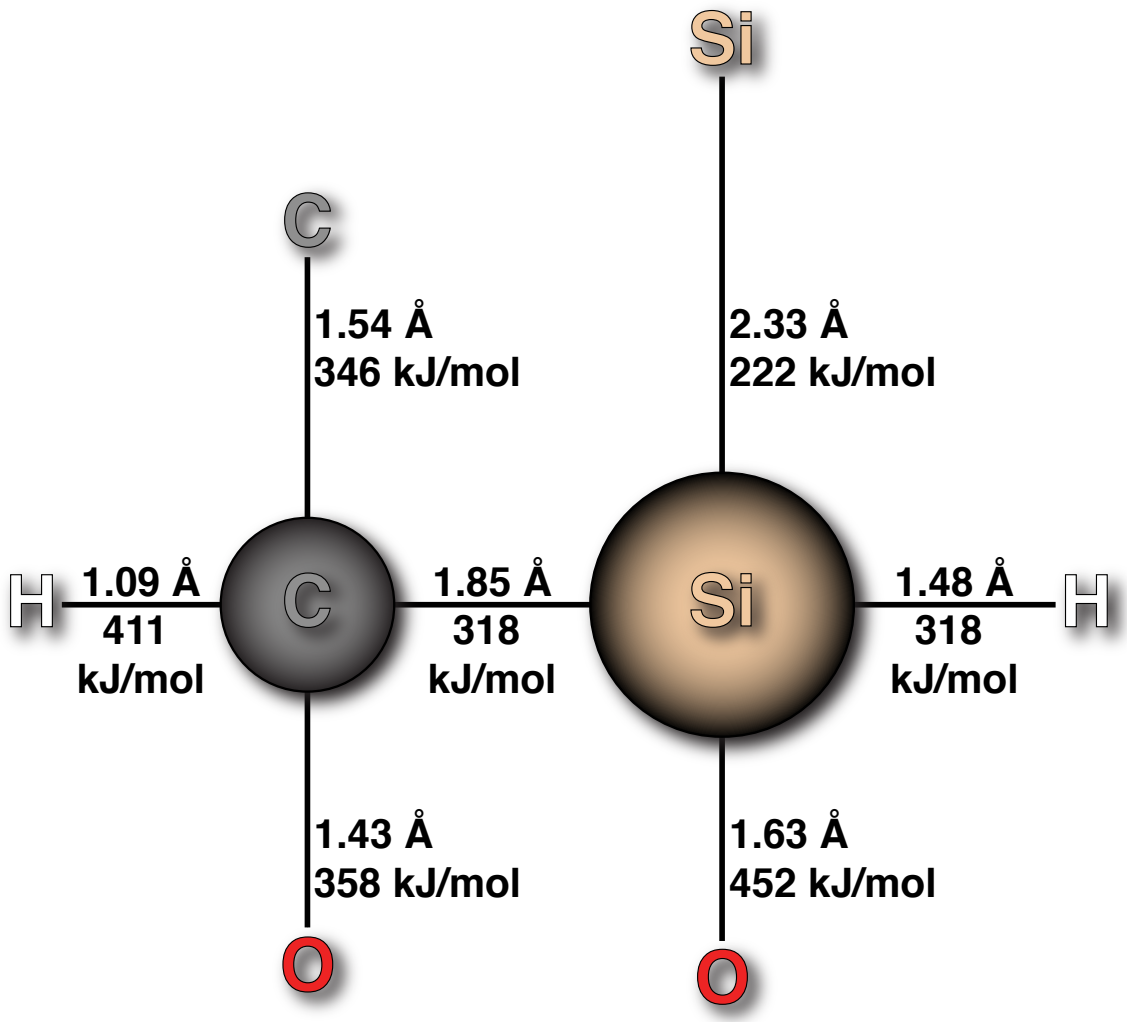


**Figure 2-1. The group 14 elements silicon and carbon form molecules with different geometries.** Diagram of the typical bond lengths and bond energies of carbon and silicon (*11*). Silicon (covalent radius = 1.17 Å) can coordinate up to six atoms, while carbon (covalent radius = 0.77 Å) is maximally tetravalent.

That is not to say that silicon is absent in biochemistry. Silicon is an important structural building block for the skeletons of marine organisms such as diatoms, sponges, and radiolarians, which take up silicic acid ($H_4SiO_4$) and polymerize it to form a variety of intricate cell wall structures (*2*). In addition to modulating the flux of silicon in marine environments (*12*), these organisms play a key role in the carbon cycle via the "biological pump" through which photosynthetically fixed carbon from the surface ocean is transferred to the deep ocean, where it either remains sequestered or is eventually remineralized to $CO_2$ (*13*).

In addition to its role in the cell walls of marine microbes, silicon plays important structural roles in plants. Silicon is widespread in soil in crystalline forms, and in the form of silicic acid, it is taken up by plants that then precipitate it to silicate species. This pathway has been demonstrated to alleviate biotic and abiotic stresses on plants, partly by structurally stabilizing the plant cell wall (*14*). Highlighting the importance of silicon for plant growth is the low concentration of silicic acid in soil, which limits the availability of silicon for plant growth and has become an agricultural challenge in certain regions (*15*). Besides these structural uses of silicon, this element is elusive in the biochemistry of most organisms (*11*).

Myriad organosilicon compounds have been created in laboratory settings, and silicon and silicates are highly abundant and diverse on Earth, yet no organosilicon species have been found in nature. Organosilicon compounds have many uses in pharmaceuticals (*9*, *16*), asymmetric synthesis (*17*), polymers (*18*, *19*), and materials science (*20*). However,

production of these compounds is often not easily accomplished and more facile synthetic methods are desirable. For example, most organosilicon compounds are produced from methylchlorosilane monomers, necessitating the use of nucleophilic substitution reactions or energy intensive reductions/direct synthesis reactions for production of useful organosilicon compounds (*21*). These reactions are stoichiometric in nature, often rely on harsh conditions, have inefficiencies in product yields and can generate undesired byproducts (*22*, *23*). Biocatalysis has many features that can complement more traditional synthetic approaches (*24*, *25*), and recent advances in directed evolution have led to enzymes capable of non-natural activities including C–Si and C–B bond formation (*26*–*28*). The time is ripe to use enzyme engineering to realize these potential applications and extend the reactivity of enzymes toward organosilicon chemistry.

Since silicon has received relatively little attention in the biocatalysis literature, we begin with a review of the role of silicon in biological systems to give a sense of the possibilities that nature has explored for this element. We then review the enzymes that act on silicon-containing molecules and how biocatalysis has been used to perform organosilicon chemistry, including using reactivities not found in Nature. We close with a perspective on opportunities in the emerging field of silicon biocatalysis with an eye toward a broad scope of applications in organosilicon chemistry, materials, and synthetic biology.

## 2.2 Biotransformation of Silicon

### 2.2.1 Biosilicification—Siliceous Marine Microorganisms and Plants

To understand how and why silicon is used by biological systems, consider the global biogeochemical cycle of silicon. Teramoles of silicon per year are processed by organisms as part of the silicon cycle, which mostly occurs in the world's oceans. Silicon is released from long-term storage in the lithosphere to the oceans by weathering where it dissolves in seawater as silicic acid ($H_4SiO_4$) (*2*). This soluble compound is distributed widely throughout the oceans where it is transferred from the hydrosphere to the biosphere. This process is essential for the life cycle of radiolarians, some flagellates, and diatoms, which use dissolved silicic acid to construct their intricate biosilica cell walls (**Figure 2-2**).

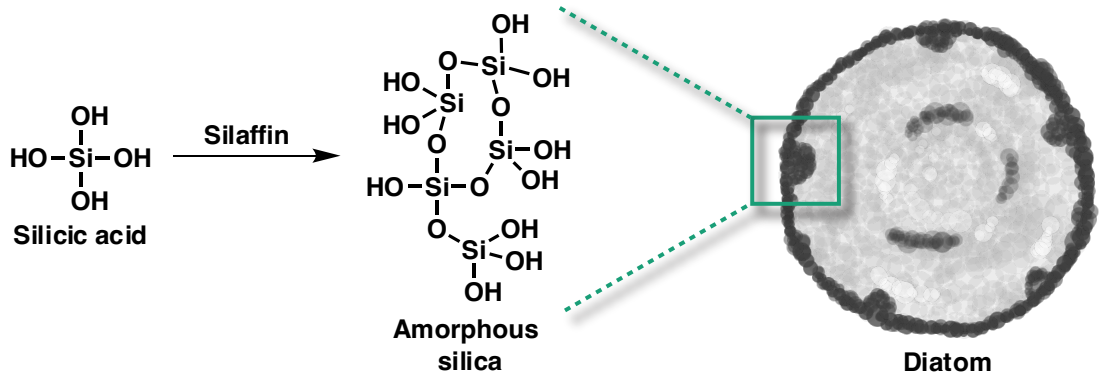


**Figure 2-2. Biosynthesis of siliceous cell walls.** Diatoms and other siliceous microorganisms precipitate dissolved silica to generate cell walls composed of biosilica.

The most abundant siliceous marine microorganisms are the photosynthetic diatoms, which synthesize silicified cell walls to provide mechanical protection against grazing. Global bio- sphere studies have estimated that diatoms conduct as much as 20% of total primary

production—the amount of carbon dioxide fixed via photosynthesis—on Earth (*13*). These quickly growing organisms in turn strongly influence the global silicon and carbon cycles.

Diatoms generate their own inorganic silicified cell walls via a genetically encoded process that results in an array of unique cell wall arrangements. These cell walls are composed of nanopatterned silica with intricately arranged pores. The biosilica mineralization process occurs in silica-deposition vesicles and is directed by polypeptides known as silaffins that are enmeshed in biosilica and precipitate silica. These silaffins generate the regular patterns of silica observed in diatom cell walls (*29*, *30*). In order to form patterns that resemble diatom biosilica, extensive post-translational phosphorylation of silaffins is required (*31*).

The siliceous marine sponge *Tethya aurantia* produces siliceous spicules that comprise some 75% of the organism's dry mass (*32*). Embedded within the spicules are proteinaceous filaments comprised of three "silica proteins" known as silicateins α, *β*, and γ. Silicatein α is the most abundant of these proteins, comprising roughly 70% of the total silicatein mass and having approximately 50% sequence similarity to cathepsin L cysteine proteases (*32*, *33*). Silicatein α is able to hydrolyze the silicic acid surrogate tetraethyl orthosilicate *in vitro* (**Figure 2-3A**) (*33*, *34*). The catalytic triad of silicatein α is composed of histidine and asparagine residues, similar to cathepsin L, while the third residue is not the canonical cysteine but rather a serine, which is the motif found in serine proteases (*35*). To investigate whether silicatein α functions as a catalyst, Morse and colleagues mutated residues Ser26 and His165 to alanine and assayed the variants for hydrolysis of tetraethyl

orthosilicate. Mutation of either active site residue nearly abolishes activity, highlighting the importance of both residues and establishing that silicateins act as enzymes and play a catalytic role in templating biosilica formation in *T. aurantia* spicules (*34*).

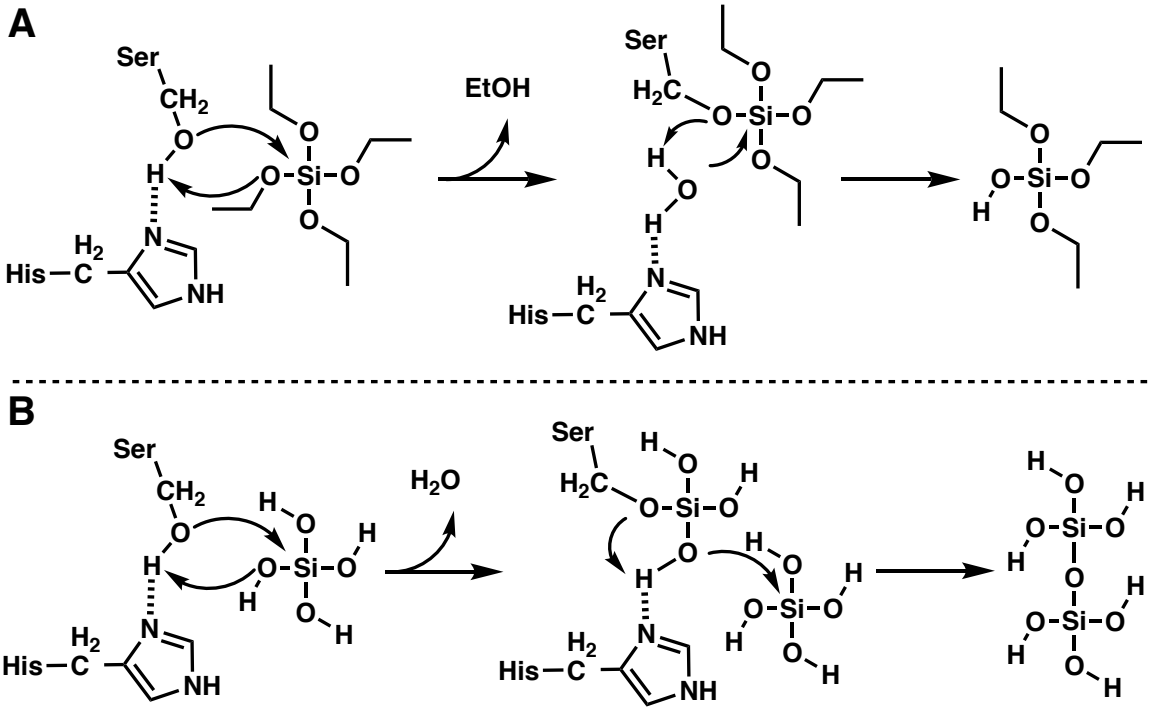


**Figure 2-3. Silica polymerization is catalyzed by silicatein enzymes.** (**A**) Mechanism of tetraethyl orthosilicate hydrolysis by silicatein (*33*, *34*). (**B**) Proposed mechanism of silicic acid hydrolysis and subsequent polymerization by silicatein (*32*, *36*).

Recombinantly produced silicateins were demonstrated to act as enzymes and catalyze Si–O bond hydrolysis and condensation (*37*). The authors demonstrated that these enzymes could catalyze condensation of silanols and alcohols to yield silyl ethers. Silicatein α plays a catalytic role in silica polymerization via a mechanism including nucleophilic attack on the silicon atom, alcohol displacement, and siloxane bond formation (**Figure 2-3B**) (*36*).

Despite the abundance of silicon on Earth and its critical roles in plants and marine microbes, its known biochemistry does not venture far beyond these roles. Highlighting this is the lack of known natural enzymes that form Si–C bonds or perform biological alkylation of silicon (*38*).

### 2.2.2 Enzymes that Transform Silicon Species

Biocatalysis has proven to be a useful platform for addressing challenges in synthetic organic chemistry, yet biocatalytic approaches to the formation of organosilicon compounds, including polymers and small molecules, are rare. Reinhold Tacke and colleagues were among the first to use microorganisms and enzymes to mediate such transformations (*39*, *40*). Most of these reactions were developed for the enantioselective reduction of silicon compounds and have been summarized in detail in excellent reviews by Frampton and Zelisko (*41*, *42*).

A variety of enzymes, including lipases and proteases, have been demonstrated to catalyze the formation and hydrolysis of Si–O bonds (*43–45*). Siloxane bond formation under mild conditions was reported using several lipases and phytases expressed in *Escherichia coli* (*44*). Frampton and Zelisko, along with others, have studied how proteases and lipases hydrolyze alkoxysilanes, form siloxane bonds, and cleave Si–O bonds (*46–51*). Their 2017 review details these efforts, which have expanded the known scope of siloxane chemistry accessible to enzymes (*42*).

Silicones, which are comprised of siloxane units, are generally engineered to be stable under most environmental conditions. This stability means certain species are subject to

long-range transport and persist in aqueous systems for more than a month while experiencing very little degradation (*4*). Thus, they can serve as a model system with which to study the activities of enzymes toward catalyzing transformations of silicon species. As long as organosilicon compounds have been in production, they have been released into various environmental compartments, and certain organisms may have either evolved or possess latent methods to metabolize some of them (*4*, *52–54*). The enzymes that act on these compounds can be used as a case study for what reactivities toward silicon have evolved in nature.

In addition to the enzymes that hydrolyze and condense Si–O bonds *in vitro*, enzymes also likely cleave Si–O bonds in living organisms (*4*). Studies claiming cleavage of Si–C bonds by microorganisms exist, but these have largely not been reproducible or have not unequivocally proven Si–C bond cleavage (*4*, *55*). In contrast, Si–C cleavage has been demonstrated to occur in higher organisms, including rats (*52*, *53*, *56*, *57*) and humans (*58*), but the enzymes responsible for these transformations are unknown. Notably, C–H oxidation followed by the Brook rearrangement (*59*) could be responsible for the Si–C cleavage exhibited in these studies.

### 2.3 Engineering Enzymes for Non-Natural Silicon Biocatalysis

The enzymes described above act on Si–O bonds, not Si–C bonds. No enzyme in nature is known that can form Si–C bonds or natively synthesize organosilicon compounds from available precursors. Biocatalysts have been engineered to conduct a myriad of new-to-nature reactions, which inspired Arnold and colleagues to engineer an enzyme that can construct Si–C bonds via carbene insertion into Si–H bonds (*26*, *60*).

Si–C bond-formation strategies in chemical synthesis can achieve high selectivity, but are limited in scope due to lengthy or energy-intensive routes, use of harsh reagents, and poor catalyst total turnover number (TTN) (*26*). Previous demonstrations that enzymes can selectively catalyze non-natural carbene transfer reactions under aqueous conditions led to the hypothesis that heme enzymes might catalyze carbene insertion into Si–H bonds (*26*, *61*, *62*). Since iron was not known to catalyze Si–H carbene insertion, the authors tested whether free heme could catalyze the reaction between phenyldimethylsilane and ethyl 2-diazopropanoate (Me-EDA) and observed the formation of racemic product in aqueous buffer. A panel of cytochromes P450, cytochromes *c*, and myoglobins catalyzed the reaction with higher turnover number than free heme but generally poor enantioselectivity.

The electron-transfer protein *Rhodothermus marinus* cytochrome *c* (*Rma* cyt *c*), however, catalyzed the reaction with ~40 TTN and 97% *ee*. Three rounds of directed evolution led to variant *Rma* cyt *c* V75T M100D M103E that catalyzed the reaction with >1500 TTN and >99% *ee*. The new enzyme was shown to selectively accept a variety of electronically diverse substituted silanes. It was also highly chemoselective: when challenged with 4-(dimethylsilyl)aniline, a substrate having two possible carbene insertion handles, it catalyzed Si–H insertion preferentially over N–H insertion (**Figure 2-4**). Interestingly, over the course of evolution, each variant showed improved chemoselectivity even though the screen only assessed Si-H insertion activity. When tested in a whole-cell reaction, the final variant furnished the Si–H insertion product with 3410 TTN, 70% yield, and 99% *ee*. These reactions represent the first examples of *in vitro* and *in vivo* enzymatic Si–C bond formation and far outperform existing synthetic routes.

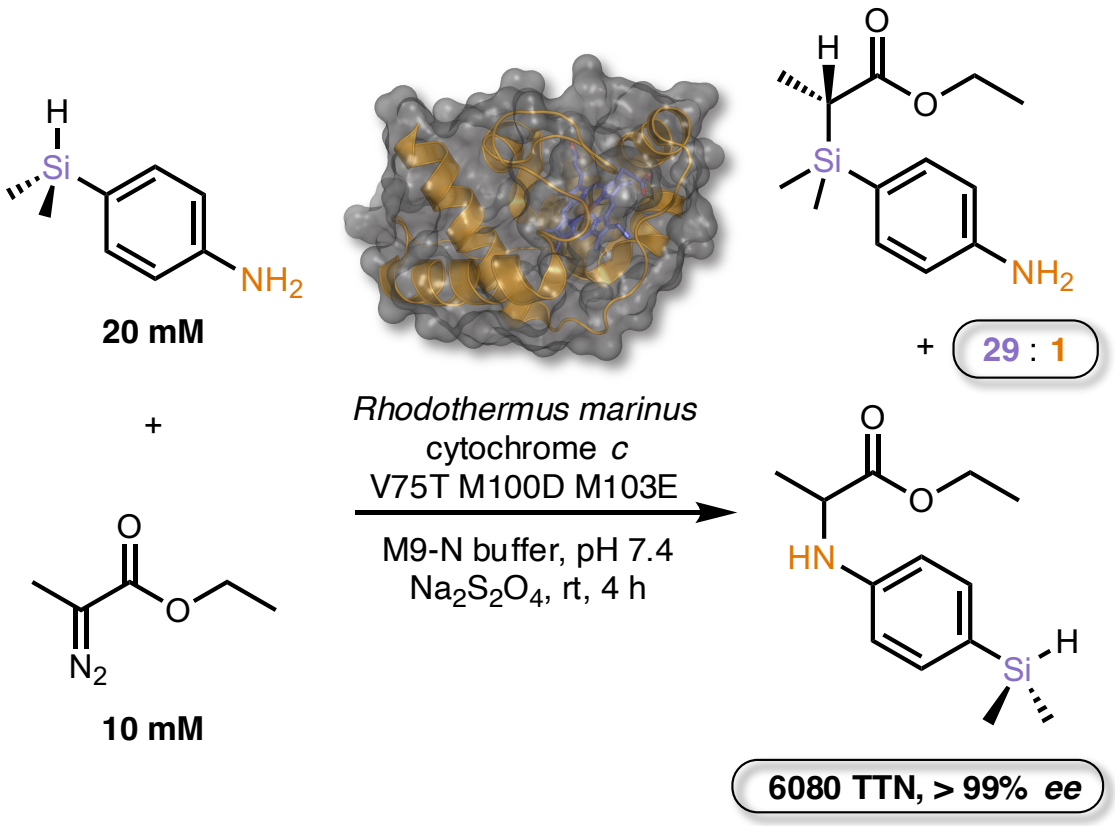


**Figure 2-4. New-to-nature enzymatic Si–C bond formation.** *Rma* cytochrome *c* catalyzes Si–H insertion between 4-(dimethylsilyl)aniline and Me-EDA with 29:1 chemoselectivity over N–H insertion, 6080 TTN, and >99% *ee* (*26*). The same reaction can also proceed in whole *E. coli* cells. TTN = total turnover number.

In a further demonstration that enzymes can be engineered to directly functionalize silicon centers, the Arnold group demonstrated that cytochrome $P450_{BM3}$ variants can hydroxylate silanes to make silanols. Silanols are important compounds for chemical transformations (*63*, *64*), polymer synthesis (*65*), catalysis (*66*), and synthesis (*67*), as functional groups in drugs (*16*), and as antimicrobial agents (*68*). The primary routes for silanol synthesis involve the oxidation of hydridosilanes, which rely on precious metal catalysts or toxic and commercially unavailable oxidation agents (*69–73*). Synthetic methods involving the hydrolysis of chlorosilane or alkoxysilane precursors encounter process challenges that

include the formation of disiloxane byproducts (*74*). For the latter approach, extra care must be taken to select suitable reaction conditions (such as pH) and to control reaction byproducts (such as salts) which can affect product stability (*75–77*).

Aiming to develop a biocatalytic route to selectively synthesize silanols, Bähr and colleagues hypothesized that cytochrome $P450_{BM3}$ could be repurposed to hydroxylate Si–H bonds (*74*). They found that the wild type enzyme accepted dimethylphenylsilane and formed product with 210 TTN (**Figure 2-5A**) in whole-cell reactions. Site-saturation mutagenesis of residue F87—which lies proximal to the heme cofactor and has been demonstrated to control substrate specificity—resulted in the identification of mutation F87G, which improved activity 1.5-fold. Further rounds of mutagenesis and screening identified additional activating mutations A328L, L181D, and A184H.

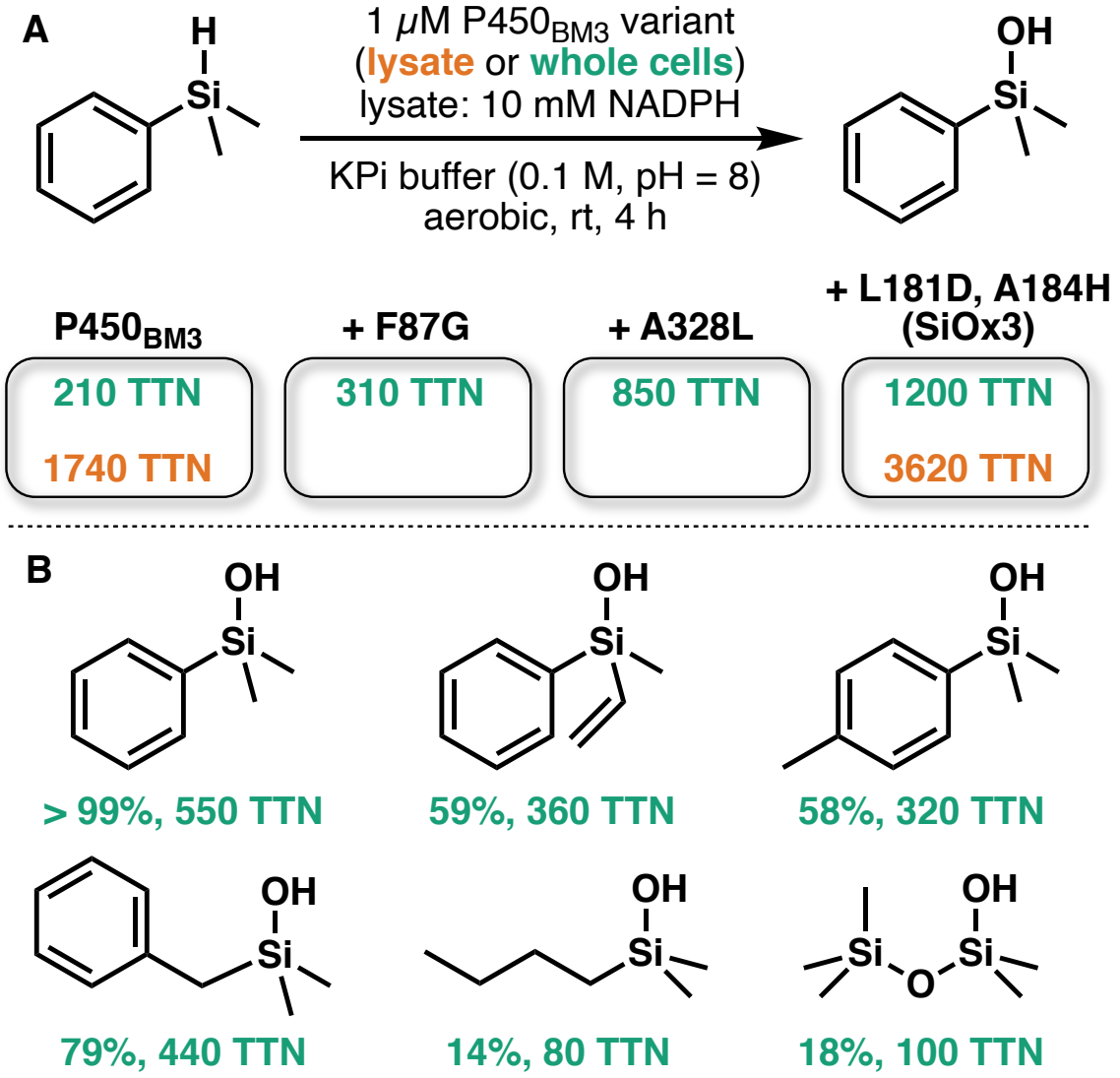


**Figure 2-5. Repurposing cytochrome P450$_{BM3}$ to oxidize Si–H bonds.** (**A**) Cytochrome P450$_{BM3}$ variants can hydroxylate the silicon center of dimethylphenylsilane in whole cells and lysate. (**B**) Variant SiOx3 oxidized dimethylphenylsilane with quantitative yield and can oxidize a variety of substituted, bulky, and aliphatic silanes, as well as one siloxane (*74*). TTN = total turnover number.

The final variant bearing these mutations catalyzes the formation of the silanol product with 1200 TTN. Using the enzyme in lysate boosted the TTN to 3620, an increase attributed to increased availability of NADPH. The authors then modified the reaction conditions to use higher protein concentration (8.1–9.0 μM) and lower substrate concentration (5 mM),

which led to >99% analytical yield and 76% isolated yield of the silanol formed from dimethylphenylsilane (**Figure 2-5B**). Under these reaction conditions, the enzyme hydroxylates a variety of silane Si–H bonds (**Figure 2-5B**). The $P450_{BM3}$ variants developed in this study can oxidize silanes in both cellular and *in vitro* contexts.

These engineering approaches have endowed naturally occurring enzymes with activities that were previously confined to the world of synthetic chemistry; the enzymes provide proof of principle and a platform from which to expand the application of enzymes to organosilicon chemistry. Although the repertoire of enzymes that act on silicon compounds is limited, these few examples suggest the potential for more activities on silicon species to be discovered and optimized by directed evolution.

### 2.4 Opportunities for Biocatalysis to Impact Organosilicon Chemistry

Expanding the ability of enzymes to directly functionalize and transform silicon species may enable more facile syntheses of organosilicon compounds. These molecules are of high value as pharmaceuticals and agrochemicals (*9*, *16*), and biocatalytic approaches to their production would complement existing synthetic methods. Traditional methods to form Si–C bonds in silicones rely on energy-intensive processes or require coinage metal catalysts, often making these molecules more expensive to produce than traditional organic polymers. In addition to being potentially more environmentally friendly and less costly than established methods, biocatalysts are exceptional at promoting reactions with high selectivity (*28*). Engineering proteins to act on organosilicon compounds would lead to new routes to their production and modification, and could even expand the realm of accessible organosilicon compounds, resulting in previously unrealized applications.

### 2.4.1 Using Silicon as a Bioisostere of Carbon in Bioactive Compounds

Although both silicon and carbon often display tetrahedral geometries, the longer Si–C bond length and silicon's lower electronegativity and greater lipophilicity make swapping these elements a powerful way to modulate the properties of molecules (*16*). Silicon's use as a bioisostere for carbon can endow molecules with convenient properties, particularly for use in biological systems (**Figure 2-6A)**. Silicon is not inherently toxic and its increased lipophilicity can improve its potency in pharmaceuticals (*78*). Drugs containing silicon are also metabolized differently than their exclusively carbon analogues, making this substitution an attractive tool to influence pharmacokinetics. For example, the antipsychotic drug haloperidol, a treatment for schizophrenia, is known to form a neurotoxic pyridinium metabolite (*9*, *79*). On the other hand, the silicon analogue sila-haloperidol, which is formed by sila-substitution of the quaternary carbon atom, is processed via an alternative metabolic pathway that does not include formation of the pyridinium metabolite due to the instability of the Si–C bond (*79*).

Biocatalysts that can selectively synthesize Si–C or Si–heteroatom bonds could lead to convenient routes to bioactive silicon compounds. As has been reported previously, a key challenge to using silicon in pharmaceuticals is the synthesis of target molecules (*9*). Entirely different routes are often needed to incorporate Si into druggable small molecules, even in compounds where silicon is used as a simple bioisostere to substitute carbon atoms. The most common route for the formation of Si–C bonds in small molecule synthesis is through the Pt-catalyzed hydrosilylation reaction of hydridosilanes with olefins or through organometallic/Grignard chemistry—two reactions not commonly used in pharmaceutical

synthesis and that may present chemoselectivity issues with the polar functionalities commonly found on drugs (*80*). Additionally, Si is typically limited to being incorporated in place of a quaternary carbon or ketone (as a silane diol). Si–H and other Si–heteroatom bonds are much more reactive than the corresponding C–H or C–heteroatom bonds and thus are not amenable to incorporation into pharmaceuticals (*9*). The availability of protein biocatalysts capable of synthesizing organosilicon compounds (*26*, *74*) would open up new areas of medicinal silicon chemistry.

### 2.4.2 Silicon-Containing Amino Acids (SiAAs)

Noncanonical amino acids have a variety of applications in the life sciences and adjacent industries. In particular, SiAAs are useful for synthesizing bioactive peptides with altered properties (**Figure 2-6A**) (*81*). These peptides are, like other peptides containing noncanonical amino acids, more resistant to proteolysis than natural peptides, but SiAAs can endow them with other beneficial effects as well. For instance, replacing a single Pro with γ-(dimethylsila)proline in Pro-rich cell-penetrating peptides was found to dramatically improve cellular uptake (*82*). β-TMS-Ala has been used as an effective substitute for β-*t*-butyl-alanine as well as phenylalanine. β-TMS-Ala and β-*t*-butyl-alanine are identical except for a single C to Si substitution, while β-TMS-Ala and Phe have similar lipophilicities (*16*). Examples of bioactive silicon-containing peptides are described in a recent review (*81*).

Despite the utility of SiAAs, methods for the enantioselective preparation of SiAAs remain difficult (*81*). Their construction may be facilitated by the exquisite selectivity of enzymes. Indeed, biocatalysts have been used extensively to construct noncanonical amino acids,

with tryptophan synthase being a prominent example (*83*, *84*). Traditional methods to prepare chiral SiAAs require chiral auxiliaries, which could be avoided with a biocatalytic route.

**A**

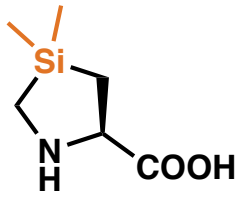


**γ-(dimethylsila)proline**

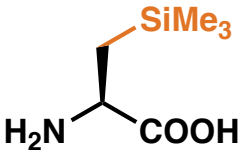


***β*-TMS-Ala**

*Si is a bioisostere for C and can improve properties of therapeutics*

**B**

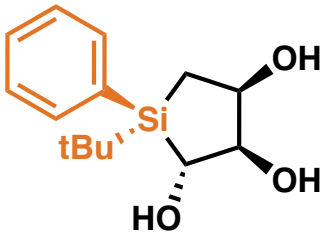


**$S_{Si}$ epimer**
***biologically active***

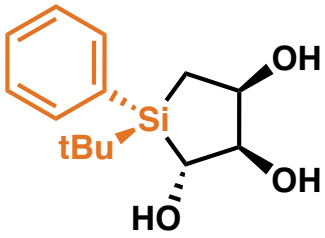


**$R_{Si}$ epimer**

*Syntheses and uses for compounds chiral at Si remain underexplored*

**C**

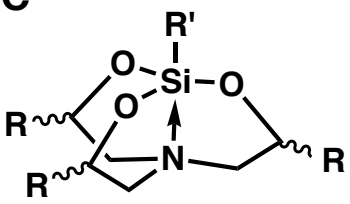


*No asymmetric methods toward hypervalent Si compounds are known*

**D**

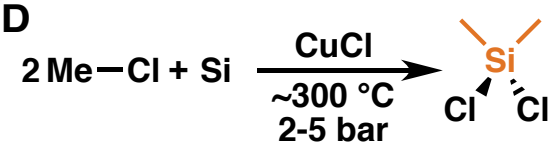


*Direct synthesis of methyl-chlorosilanes requires harsh reaction conditions*

**E**

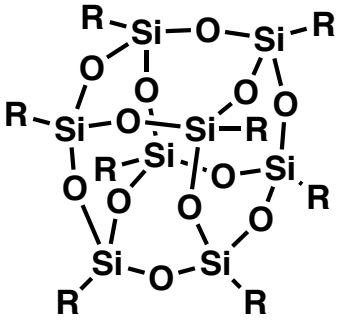


*Selective functionalization of silsesquioxanes can tailor their material properties*

**Figure 2-6. Some opportunities for biocatalysis in organosilicon chemistry.** (**A**) Silicon is a bioisostere for carbon and substituting Si for C can be a powerful strategy for modulating the properties of pharmaceuticals and other molecules. SiAAs are a key example. (**B**) Molecules chiral at Si can have important biological properties but can be difficult to synthesize. The $S_{Si}$ epimer of silacyclopentanetriol binds the serotonin receptor 5-$HT_{2B}$ tightly, while the $R_{Si}$ epimer is inactive (*85*). (**C**) No methods for the asymmetric synthesis of hypervalent Si complexes, like silatranes, are known despite their unique properties. (**D**) Dimethyldichlorosilane, the key feedstock for the silicone industry, relies on energy-intensive synthetic routes (*21*, *22*). Biomethylation of silicon would present an alternative route to methylated feedstocks. (**E**) Silsesquioxane materials have numerous emerging applications. Enzymes may complement existing functionalization strategies.

### 2.4.3 Chiral Silicon Centers

Silicon often adopts a tetrahedral geometry and thus can be a chiral center. The preparation of molecules chiral at silicon has been reviewed extensively (*86*). Critically, asymmetric syntheses of these compounds are particularly challenging because $sp^2$ silicon species are exceptionally labile (*87*, *88*). Unlike carbon, which readily forms double bonds with many other elements, Si–E bonds (E = Si, C, N, P, and others) are highly reactive; these compounds, when they exist at all, typically require low temperatures, large substituents, and air- and water-free conditions to persist. This is due to the π bonds between Si and other atoms being very weak. As a result, desymmetrization of silicon cannot be achieved by going through an $sp^2$ intermediate, unlike with carbon, where desymmetrization of aldehydes, olefins, and other $sp^2$ carbon atoms is a powerful strategy for creating chiral carbon centers. Biocatalytic methods complementing existing synthetic tools would be invaluable for expanding the chemical space available to researchers.

Examples of bioactive chiral silicon molecules are limited, presumably due to difficulties with their construction. One recent example is a silacyclopentanetriol (**Figure 2-6B**). One epimer of this molecule binds tightly to the serotonin receptor 5-$HT_{2B}$ ($IC_{50}$ = 6.4 μM),

while the other epimer does not display significant binding ($IC_{50}$ > 100 μM) (*85*). This example underscores how effective methods to prepare molecules chiral at silicon could open up an underexplored chemical space for pharmaceuticals. There are no known natural molecules exhibiting chirality at silicon, and no natural enzymes are known to be capable of constructing these compounds.

The "sila-substitution" of drugs is not a new strategy (*89*). Silicon has long been used as a bioisostere of carbon, and syntheses of sila-substituted compounds go back over 50 years (*90*). One recent study compared loperamide, an antidiarrheal, with sila-loperamide, a sila-substituted analogue (*91*). A comparison of these compounds' pharmacokinetic and pharmacodynamic properties revealed that, despite major differences in their *in vitro* properties (including clearance and permeability), their *in vivo* pharmacokinetic profiles are nearly identical. Thorough studies like this example underscore how the ability to access sila-substituted compounds can lead to novel molecules with unique pharmaceutical properties. Critically, the vast majority of sila-substituted drug analogues studied have been achiral at silicon (*16*). Methods to access molecules chiral at silicon would enable sila-substitutions at other carbons in pharmaceuticals.

Outside of biology, chiral polysilanes are of interest to polymer chemists (*92*). Polysilanes are polymers containing solely silicon backbones, and this σ-conjugated backbone endows these molecules with unique electronic and optical properties. When their backbone Si atoms are connected to chiral side groups, the resulting chiral polysilanes form helical structures (*93*). These features make polysilanes of potential use in applications that range

from enantioselective separations and molecular recognition to nonlinear optics and chiroptical switches. However, their synthesis from dialkyldichlorosilanes involves a Wurtz reductive coupling and can be challenging to control, limiting the types of chiral polysilanes that can be produced. Methods to construct these molecules more cheaply and with greater selectivity would be invaluable for realizing these applications and more.

### 2.4.4 Enzymatic Synthesis of Hypervalent Silicon Species

Silicon can form hypervalent species with coordination numbers greater than 4 (*9*, *94*). Methods to generate penta- and hexavalent silicon species from silica are well established but often require harsh conditions and a stoichiometric strong base. Even more problematic is that no asymmetric syntheses are known: all chiral hypervalent silicon species have been prepared via resolution (**Figure 2-6C**). Enzymatic catalysis presents a potential tool to construct chiral species in an asymmetric fashion under milder conditions.

Pentavalent silicon species such as silatranes exhibit valuable biological activities, including antimicrobial, antiviral, and anticancer properties (*95*). Asymmetric methods to construct these compounds would not only lower production costs but would enable the production of previously inaccessible chiral compounds. Notably, silatranes are reasonably stable to hydrolysis and can be synthesized under mild conditions with (substituted) triethanolamines and alkoxysilanes. The lack of natural enzymes capable of forming these non-natural compounds should not discourage the biocatalysis community from taking on this challenge.

Hydrolytically stable hexacoordinate silicon complexes have been shown to serve as nontoxic DNA intercalators (*9*, *96*). Silicon is less toxic and costly than transition metals, and thus, there is value in developing biologically active coordination complexes using Si rather than other metals. However, syntheses of hexavalent Si typically rely on intermediates unstable in water (*97*), and new chemical strategies would need to be developed to construct these molecules biocatalytically.

### 2.4.5 Silicon–Carbon Bond Construction

Si–C motifs are of importance to chemical synthesis, pharmaceuticals, and materials. Most methods to prepare these compounds rely on precious metals or start with reduced forms of silicon. Expanding the capability of enzymes to form Si–C motifs may enable more efficient and cost-effective preparations of these compounds (*17*, *98*).

Biological methylation of many metals and metalloids is performed by organisms using methyltransferases. Of the primordial group 14 elements, Si is the only element that is not known to be methylated (or alkylated) in nature (*38*, *99*, *100*). The lack of enzymatically produced alkylsilanes can probably be attributed to silicon's form in the biosphere. Silicon is found largely as silica and silicic acid, which are highly stable and of low toxicity. Organisms have little need to evolve enzymes and expend energy to metabolize these compounds, and such pathways have not been found. Alkylsilanes, however, are tremendously valuable industrially. Methyl groups are the most ubiquitous Si–C motifs and are typically installed via the Rochow-Müller "Direct Process" reaction (*21*, *101*). In this reaction, elemental Si is reacted with methyl chloride at elevated temperatures (300 – 320 ˚C) in the presence of a copper catalyst (**Figure 2-6D**). The production of elemental Si

itself requires an energy-intensive carbothermic reduction of silica at temperatures above 2000 °C. Biomethylation of Si presents a milder, redox-neutral route to Me–Si bonds, and directed evolution of known methyltransferases may be an approach to access these compounds.

Hydridosilanes have been shown to undergo reactions with engineered enzymes to form Si–C bonds. Hydrosilylation, the reaction of an Si–H bond with an unsaturated C–C bond or carbonyl, is typically catalyzed by Pt or other expensive metals (*80*). The reaction is also known with more abundant first-row transition metals but is much less robust. It may be possible to generate enzymes that perform this reaction using more earth-abundant metals and access regio- and chemoselectivity for hydrosilylation currently not accessible using traditional homogeneous catalysis. Si–H bonds may also provide access to silylium ions or highly reactive Si–E bonds (E = S, transition metals) under enzymatic catalysis. Such approaches have been demonstrated in homogeneous catalysis using metal complexes approximating [NiFe] hydrogenases. These intermediates could form a number of Si–heteroatom bonds. Interception with arenes in a Friedel–Crafts reaction would produce arylsilanes, which have applications in pharmaceuticals, agrochemicals, and materials. Interception with oxygen nucleophiles would generate silyl ethers or siloxane bonds. Nitrogen nucleophiles would afford silazanes, another common class of silicon compounds. Directed evolution of enzymes may allow access to chemoselectivities not possible under standard reaction conditions.

### 2.4.6 Biologically Templated Inorganic Materials

Silicatein enzymes are responsible for the formation of vast quantities of inorganic silica structures in nature. Engineering silicateins or enzymes with similar mechanisms may enable the construction of an array of small molecule organosilicon species bearing complex functionalities and may also be employed to synthesize inorganic materials (*32*, *37*, *102*).

Recent work has shown that the post-translational modifications that decorate diatom silaffins can be modulated to generate diverse silica morphologies (*103*). A suite of enzymes was used to decorate the R5 silaffin with modifications including the native phosphorylation as well as methylation, acetylation, and myristoylation. These modifying enzymes and the R5 silaffin, when co-expressed in E. coli, were able to precipitate silica and form nanostructured silica with diverse, controlled physicochemical characteristics and morphologies.

Silsesquioxanes are a class of organosilicon compounds that adopt three-dimensional cage-like conformations via a repeating motif wherein each silicon atom is bonded to three oxygen atoms and a functional group ($RSiO_{3/2}$) (*104*). Of particular relevance for materials applications are polyoctahedral silsesquioxanes (POSSs) which form cubic cages that can be used as precursors to polymers. The inorganic Si–O–Si backbone of silsesquioxanes is stable, enabling the construction of polymeric compounds, while the functional groups allow installation of potentially diverse reactivities to meet applications in nanocomposites, optoelectronics, catalysis, high-temperature composites, and biomaterials (**Figure 2-6E**) (*104*). Controlling the functional substituents on silsesquioxanes remains an outstanding

challenge and is an area where the chemo- and regioselectivity of enzymes may aid in precisely functionalizing silicon centers *en route* to designer silsesquioxanes.

### 2.5 Summary and Outlook

Advances in molecular biology and protein engineering techniques combined with the ever-increasing diversity of known protein sequences have expanded the ability to access biocatalysts with new-to-nature reactivities. Simultaneously, synthetic chemists have accessed organosilicon compounds exhibiting rich structural and functional diversity. The developed molecules and polymers are useful as synthetic reagents, pharmaceuticals, and materials.

The common refrain has been that organosilicon species are inaccessible to enzymes. However, recent studies have highlighted natural enzymes that act on silicon species and have demonstrated the adaptability of engineered enzymes to perform reactions on silicon species. With the proof-of-principle that enzymes can perform catalytic transformations of silicon species, the doors to merging biocatalysis and organosilicon chemistry have been opened. We encourage researchers in biocatalysis and organosilicon chemistry to use biocatalysis as another tool to access organosilicon transformations with the sustainability and selectivity inherent to biocatalytic platforms.

### Chapter II Bibliography

1. E. Struyf, A. Smis, S. Van Damme, P. Meire, D. J. Conley, The global biogeochemical silicon cycle. *Silicon*. **1**, 207–213 (2009).
2. P. Tréguer, D. M. Nelson, A. J. V. Bennekom, D. J. DeMaster, A. Leynaert, B. Quéguiner, The silica balance in the world ocean: A reestimate. *Science*. **268**, 375–379 (1995).

3. J. Chelikowsky, "Introduction: Silicon in All Its Forms" in *Silicon: Evolution and Future of a Technology*, P. Siffert, E. F. Krimmel, Eds. (Springer, Berlin, Heidelberg, 2004), pp. 1–22.

4. C. Rücker, K. Kümmerer, Environmental chemistry of organosiloxanes. *Chem. Rev.* **115**, 466–524 (2015).

5. G. Bertrand, The modest undressing of a silicon center. *Science*. **305**, 783–785 (2004).

6. C. Marschner, T. D. Tilley, Current advances in the chemistry of silicon: Not exactly a carbon copy. *Dalton Trans.* **46**, 8699–8700 (2017).

7. N. Auner, J. Weis, *Organosilicon Chemistry III: From Molecules to Materials* (John Wiley & Sons, 2008).

8. F. Hanusch, L. Groll, S. Inoue, Recent advances of group 14 dimetallenes and dimetallynes in bond activation and catalysis. *Chem. Sci.* **12**, 2001–2015 (2021).

9. R. Ramesh, D. S. Reddy, Quest for novel chemical entities through incorporation of silicon in drug scaffolds. *J. Med. Chem.* **61**, 3779–3798 (2018).

10. R. D. Miller, J. Michl, Polysilane high polymers. *Chem. Rev.* **89**, 1359–1410 (1989).

11. J. J. Petkowski, W. Bains, S. Seager, On the potential of silicon as a building block for life. *Life*. **10**, 84 (2020).

12. E. V. Armbrust, The life of diatoms in the world's oceans. *Nature*. **459**, 185–192 (2009).

13. P. Tréguer, C. Bowler, B. Moriceau, S. Dutkiewicz, M. Gehlen, O. Aumont, L. Bittner, R. Dugdale, Z. Finkel, D. Iudicone, O. Jahn, L. Guidi, M. Lasbleiz, K. Leblanc, M. Levy, P. Pondaven, Influence of diatom diversity on the ocean biological carbon pump. *Nat. Geosci.* **11**, 27–37 (2018).

14. M. Luyckx, J.-F. Hausman, S. Lutts, G. Guerriero, Silicon and plants: Current knowledge and technological perspectives. *Front. Plant Sci.* **8** (2017).

15. Y. Wang, X. Xiao, Y. Xu, B. Chen, Environmental Effects of silicon within biochar (Sichar) and carbon–silicon coupling mechanisms: A critical review. *Environ. Sci. Technol.* **53**, 13570–13582 (2019).

16. A. K. Franz, S. O. Wilson, Organosilicon molecules with medicinal applications. *J. Med. Chem.* **56**, 388–405 (2013).

17. T. H. Chan, D. Wang, Chiral organosilicon compounds in asymmetric synthesis. *Chem. Rev.* **92**, 995–1006 (1992).

18. D. T. Hurd, G. F. Roedel, Vinyl and allyl silicone polymers and copolymers. *Ind. Eng. Chem.* **40**, 2078–2081 (1948).

19. A. Colas, “Silicones: Preparation, Properties and Performance” (Dow Corning, Life Sciences, 2005).

20. E. M. Leitao, T. Jurca, I. Manners, Catalysis in service of main group chemistry offers a versatile approach to p -block molecules and materials. *Nat. Chem.* **5**, 817–829 (2013).

21. D. Seyferth, Dimethyldichlorosilane and the direct synthesis of methylchlorosilanes. The key to the silicones industry. *Organometallics*. **20**, 4978–4992 (2001).

22. J. M. Roberts, V. V. Pushkarev, J. J. Sturm, D. E. Katsoulis, Toward a new direct process: Synthesis of methylmethoxysilanes from dimethyl carbonate and pentacopper silicide. *Ind. Eng. Chem. Res.* **59**, 7457–7465 (2020).

23. L. Rösch, P. John, R. Reitmeier, "Silicon Compounds, Organic" in *Ullmann’s Encyclopedia of Industrial Chemistry* (Wiley-VCH Verlag GmbH & Co. KGaA, 2000).

24. R. A. Sheldon, D. Brady, The limits to biocatalysis: Pushing the envelope. *Chem. Commun.* **54**, 6088–6104 (2018).

25. U. T. Bornscheuer, The fourth wave of biocatalysis is approaching. *Philos. Trans. R. Soc. A*. **376**, 20170063 (2018).

26. S. B. J. Kan, R. D. Lewis, K. Chen, F. H. Arnold, Directed evolution of cytochrome c for carbon–silicon bond formation: Bringing silicon to life. *Science*. **354**, 1048–1051 (2016).

27. S. B. J. Kan, X. Huang, Y. Gumulya, K. Chen, F. H. Arnold, Genetically programmed chiral organoborane synthesis. *Nature*. **552**, 132–136 (2017).

28. F. H. Arnold, Directed evolution: Bringing new chemistry to life. *Angew. Chem. Int. Ed.* **57**, 4143–4148 (2018).

29. N. Poulsen, M. Sumper, N. Kroger, Biosilica formation in diatoms: Characterization of native silaffin-2 and its role in silica morphogenesis. *Proc. Natl. Acad. Sci. U.S.A.* **100**, 12075–12080 (2003).

30. H. Lutz, V. Jaeger, L. Schmüser, M. Bonn, J. Pfaendtner, T. Weidner, The structure of the diatom silaffin peptide R5 within freestanding two-dimensional biosilica sheets. *Angew. Chem. Int. Ed.* **56**, 8277–8280 (2017).

31. N. Kröger, N. Poulsen, Diatoms—From cell wall biogenesis to nanotechnology. *Annu. Rev. Genet.* **42**, 83–107 (2008).

32. R. L. Brutchey, D. E. Morse, Silicatein and the translation of its molecular mechanism of biosilicification into low temperature nanomaterial synthesis. *Chem. Rev.* **108**, 4915–4934 (2008).

33. K. Shimizu, J. Cha, G. D. Stucky, D. E. Morse, Silicatein α: Cathepsin L-like protein in sponge biosilica. *Proc. Natl. Acad. Sci. U.S.A.* **95**, 6234–6238 (1998).

34. Y. Zhou, K. Shimizu, J. N. Cha, G. D. Stucky, D. E. Morse, Efficient catalysis of polysiloxane synthesis by silicatein α requires specific hydroxy and imidazole functionalities. *Angew. Chem. Int. Ed.* **38**, 779–782 (1999).

35. J. N. Cha, K. Shimizu, Y. Zhou, S. C. Christiansen, B. F. Chmelka, G. D. Stucky, D. E. Morse, Silicatein filaments and subunits from a marine sponge direct the polymerization of silica and silicones in vitro. *Proc. Natl. Acad. Sci. U.S.A.* **96**, 361–365 (1999).

36. M. Jensen, R. Keding, T. Höche, Y. Yue, Biologically formed mesoporous amorphous silica. *J. Am. Chem. Soc.* **131**, 2717–2721 (2009).

37. S. Y. Tabatabaei Dakhili, S. A. Caslin, A. S. Faponle, P. Quayle, S. P. de Visser, L. S. Wong, Recombinant silicateins as model biocatalysts in organosiloxane chemistry. *Proc. Natl. Acad. Sci. U.S.A.* **114**, E5285–E5291 (2017).

38. J. S. Thayer, Biological methylation of less-studied elements. *Appl. Organomet. Chem.* **16**, 677–691 (2002).

39. A. D. Ryabov, The biochemical reactions of organometallics with enzymes and proteins. *Angew. Chem. Int. Ed.* **30**, 931–941 (1991).

40. R. Tacke, Milestones in the biochemistry of silicon: From basic research to biotechnological applications. *Angew. Chem. Int. Ed.* **38**, 3015–3018 (1999).

41. M. B. Frampton, P. M. Zelisko, Organosilicon biotechnology. *Silicon*. **1**, 147–163 (2009).

42. M. B. Frampton, P. M. Zelisko, Biocatalysis in silicon chemistry. *Chem. Asian J.* **12**, 1153–1167 (2017).

43. K. F. Brandstadt, Inspired by nature: An exploration of biocatalyzed siloxane bond formation and cleavage. *Curr. Opin. Biotechnol.* **16**, 393–397 (2005).

44. V. Abbate, A. R. Bassindale, K. F. Brandstadt, R. Lawson, P. G. Taylor, Enzyme mediated silicon–oxygen bond formation; the use of Rhizopus oryzae lipase, lysozyme and phytase under mild conditions. *Dalton Trans.* **39**, 9361 (2010).

45. A. R. Bassindale, K. F. Brandstadt, T. H. Lane, P. G. Taylor, Enzyme-catalysed siloxane bond formation. *J. Inorg. Biochem.* **96**, 401–406 (2003).

46. M. B. Frampton, P. M. Zelisko, A comparison of protease active sites and their ability to process silicon-based substrates. *Silicon*. **4**, 51–56 (2012).

47. M. B. Frampton, I. Subczynska, P. M. Zelisko, Biocatalytic synthesis of silicone polyesters. *Biomacromolecules*. **11**, 1818–1825 (2010).

48. M. B. Frampton, R. Simionescu, T. Dudding, P. M. Zelisko, The enzymatic cleavage of Si–O bonds: A kinetic analysis of the biocatalyzed hydrolysis of phenyltrimethoxysilane. *J. Mol. Catal. B Enzym.* **66**, 105–112 (2010).

49. M. B. Frampton, J. P. Séguin, D. Marquardt, T. A. Harroun, P. M. Zelisko, Synthesis of polyesters containing disiloxane subunits: Structural characterization, kinetics, and an examination of the thermal tolerance of Novozym-435. *J. Mol. Catal. B Enzym.* **85–86**, 149–155 (2013).

50. M. B. Frampton, P. M. Zelisko, Synthesis of lipase-catalysed silicone-polyesters and silicone-polyamides at elevated temperatures. *Chem. Commun.* **49**, 9269–9271 (2013).

51. M. Frampton, A. Vawda, J. Fletcher, P. M. Zelisko, Enzyme-mediated sol–gel processing of alkoxysilanes. *Chem. Commun.*, 5544–5546 (2008).

52. S. Varaprath, J. M. McMahon, K. P. Plotzke, Metabolites of hexamethyldisiloxane and decamethylcyclopentasiloxane in Fischer 344 rat urine—A comparison of a linear and a cyclic siloxane. *Drug Metab. Dispos.* **31**, 206–214 (2003).

53. S. Varaprath, K. L. Salyers, K. P. Plotzke, S. Nanavati, Identification of metabolites of octamethylcyclotetrasiloxane ($D_4$) in rat urine. *Drug Metab. Dispos.* **27**, 1267–1273 (1999).

54. E. Boada, E. Santos-Clotas, S. Bertran, A. Cabrera-Codony, M. J. Martín, L. Bañeras, F. Gich, Potential use of Methylibium sp. as a biodegradation tool in organosilicon and volatile compounds removal for biogas upgrading. *Chemosphere*. **240**, 124908 (2020).

55. C. L. Sabourin, J. C. Carpenter, T. K. Leib, J. L. Spivack, Biodegradation of dimethylsilanediol in soils. *Appl. Environ. Microbiol.* **62**, 4352–4360 (1996).

56. S. Varaprath, K. L. Salyers, K. P. Plotzke, S. Nanavati, Extraction of octamethylcyclotetrasiloxane and its metabolites from biological matrices. *Anal. Biochem.* **256**, 14–22 (1998).

57. K. P. Plotzke, S. D. Crofoot, E. S. Ferdinandi, J. G. Beattie, R. H. Reitz, D. A. McNett, R. G. Meeks, Disposition of radioactivity in Fischer 344 rats after single and multiple inhalation exposure to [14C]octamethylcyclotetrasiloxane ([14C]D4). *Drug Metab. Dispos.* **28**, 192–204 (2000).

58. M. B. Reddy, M. E. Andersen, P. E. Morrow, I. D. Dobrev, S. Varaprath, K. P. Plotzke, M. J. Utell, Physiological modeling of inhalation kinetics of octamethylcyclotetrasiloxane in humans during rest and exercise. *Toxicol. Sci.* **72**, 3–18 (2003).

59. A. G. Brook, Molecular rearrangements of organosilicon compounds. *Acc. Chem. Res.* **7**, 77–84 (1974).

60. Z. Wu, S. B. J. Kan, R. D. Lewis, B. J. Wittmann, F. H. Arnold, Machine learning-assisted directed protein evolution with combinatorial libraries. *Proc. Natl. Acad. Sci. U.S.A.* **116**, 8852–8858 (2019).

61. O. F. Brandenberg, R. Fasan, F. H. Arnold, Exploiting and engineering hemoproteins for abiological carbene and nitrene transfer reactions. *Curr. Opin. Biotechnol.* **47**, 102–111 (2017).

62. K. Chen, F. H. Arnold, Engineering new catalytic activities in enzymes. *Nat. Catal.* **3**, 203–213 (2020).

63. S. E. Denmark, C. S. Regens, Palladium-catalyzed cross-coupling reactions of organosilanols and their salts: Practical alternatives to boron- and tin-based methods. *Acc. Chem. Res.* **41**, 1486–1499 (2008).

64. A. Mori, Y. Danda, T. Fujii, K. Hirabayashi, K. Osakada, Hydroxorhodium complex-catalyzed carbon−carbon bond-forming reactions of silanediols with α,β-unsaturated carbonyl compounds. Mizoroki-Heck-type reaction vs conjugate addition. *J. Am. Chem. Soc.* **123**, 10774–10775 (2001).

65. U. Ritter, N. Winkhofer, H.-G. Schmidt, H. W. Roesky, New cobalt catalysts for hydroformylations in two-phase systems. *Angew. Chem. Int. Ed.* **35**, 524–526 (1996).

66. K. Hirabayashi, A. Mori, J. Kawashima, M. Suguro, Y. Nishihara, T. Hiyama, Palladium-catalyzed cross-coupling of silanols, silanediols, and silanetriols promoted by silver(I) oxide. *J. Org. Chem.* **65**, 5342–5349 (2000).

67. S. E. Denmark, M. H. Ober, Cross-coupling reactions of arylsilanols with substituted aryl halides. *Org. Lett.* **5**, 1357–1360 (2003).

68. Y. Kim, S. Farrah, R. H. Baney, Structure–antimicrobial activity relationship for silanols, a new class of disinfectants, compared with alcohols and phenols. *Int. J. Antimicrob. Agents*. **29**, 217–222 (2007).

69. K. Valliant-Saunders, E. Gunn, G. R. Shelton, D. A. Hrovat, W. T. Borden, J. M. Mayer, Oxidation of tertiary silanes by osmium tetroxide. *Inorg. Chem.* **46**, 5212–5219 (2007).

70. D. Limnios, C. G. Kokotos, Organocatalytic oxidation of organosilanes to silanols. *ACS Catal.* **3**, 2239–2243 (2013).

71. M. Lee, S. Ko, S. Chang, Highly selective and practical hydrolytic oxidation of organosilanes to silanols catalyzed by a ruthenium complex. *J. Am. Chem. Soc.* **122**, 12011–12012 (2000).

72. G. H. Barnes, N. E. Daughenbaugh, The preparation of organosilanols via the metal-catalyzed reaction of organosilicon hydrides with water. *J. Org. Chem.* **31**, 885–887 (1966).

73. Y. Lee, D. Seomoon, S. Kim, H. Han, S. Chang, P. H. Lee, Highly efficient iridium-catalyzed oxidation of organosilanes to silanols. *J. Org. Chem.* **69**, 1741–1743 (2004).

74. S. Bähr, S. Brinkmann-Chen, M. Garcia-Borràs, J. M. Roberts, D. E. Katsoulis, K. N. Houk, F. H. Arnold, Selective enzymatic oxidation of silanes to silanols. *Angew. Chem. Int. Ed.* **59**, 15507–15511 (2020).

75. J. F. Hyde, P. L. Brown, A. L. Smith, Inductive effects in the chlorosilane hydrolysis equilibrium. *J. Am. Chem. Soc.* **82**, 5854–5858 (1960).

76. P. D. Lickiss, "The Synthesis and Structure of Organosilanols" in *Advances in Inorganic Chemistry*, A. G. Sykes, Ed. (Academic Press, 1995), vol. 42, pp. 147–262.

77. V. Chandrasekhar, R. Boomishankar, S. Nagendran, Recent developments in the synthesis and structure of organosilanols. *Chem. Rev.* **104**, 5847–5910 (2004).

78. W. Bains, R. Tacke, Silicon chemistry as a novel source of chemical diversity in drug design. *Curr. Opin. Drug Discov. Devel.* **6**, 526–543 (2003).

79. R. Tacke, F. Popp, B. Müller, B. Theis, C. Burschka, A. Hamacher, M. U. Kassack, D. Schepmann, B. Wünsch, U. Jurva, E. Wellner, Sila-Haloperidol, a silicon analogue of the dopamine (D2) receptor antagonist Haloperidol: Synthesis, pharmacological properties, and metabolic fate. *ChemMedChem*. **3**, 152–164 (2008).

80. Y. Nakajima, S. Shimada, Hydrosilylation reaction of olefins: Recent advances and perspectives. *RSC Adv.* **5**, 20603–20616 (2015).

81. E. Rémond, C. Martin, J. Martinez, F. Cavelier, Silicon-containing amino acids: Synthetic aspects, conformational studies, and applications to bioactive peptides. *Chem. Rev.* **116**, 11654–11684 (2016).

82. S. Pujals, J. Fernández-Carneado, M. J. Kogan, J. Martinez, F. Cavelier, E. Giralt, Replacement of a proline with silaproline causes a 20-fold increase in the cellular uptake of a Pro-rich peptide. *J. Am. Chem. Soc.* **128**, 8479–8483 (2006).

83. E. Watkins-Dulaney, S. Straathof, F. Arnold, Tryptophan synthase: Biocatalyst extraordinaire. *ChemBioChem*. **22**, 5–16 (2021).

84. P. J. Almhjell, C. E. Boville, F. H. Arnold, Engineering enzymes for noncanonical amino acid synthesis. *Chem. Soc. Rev.* **47**, 8980–8997 (2018).

85. K. Igawa, D. Yoshihiro, Y. Abe, K. Tomooka, Enantioselective synthesis of silacyclopentanes. *Angew. Chem. Int. Ed.* **55**, 5814–5818 (2016).

86. K. Igawa, K. Tomooka, "Chiral Silicon Molecules" in *Organosilicon Chemistry*, T. Hiyama, M. Oestreich, Eds. (Wiley, ed. 1, 2019), pp. 495–532.

87. G. Raabe, J. Michl, Multiple bonding to silicon. *Chem. Rev.* **85**, 419–509 (1985).

88. R. West, "History of a Paradigm Shift: Multiple Bonds to Silicon" in *Modern Aspects of Main Group Chemistry* (American Chemical Society, 2005), vol. 917 of *ACS Symposium Series*, pp. 166–178.

89. R. Tacke, S. Dörrich, "Drug Design Based on the Carbon/Silicon Switch Strategy" in *Atypical Elements in Drug Design*, J. Schwarz, Ed. (Springer International Publishing, Cham, 2016), pp. 29–59.

90. R. J. Fessenden, M. D. Coon, Silicon-substituted medicinal agents. Silacarbamates related to meprobamate. *J. Med. Chem.* **8**, 604–608 (1965).

91. M. Geyer, E. Wellner, U. Jurva, S. Saloman, D. Armstrong, R. Tacke, Can silicon make an excellent drug even better? An in vitro and in vivo head-to-head comparison between loperamide and its silicon analogue sila-loperamide. *ChemMedChem*. **10**, 911–924 (2015).

92. V. B. Kumar, E. M. Leitao, Properties and applications of polysilanes. *Appl. Organomet. Chem.* **34**, e5402 (2020).

93. M. Fujiki, J. R. Koe, K. Terao, T. Sato, A. Teramoto, J. Watanabe, Optically active polysilanes. Ten years of progress and new polymer twist for nanoscience and nanotechnology. *Polym. J.* **35**, 297–344 (2003).

94. B. M. Vis, J. Wen, S. K. Mellerup, R. D. Merchant, R. C. Mawhinney, S. D. Kinrade, Silicon forms a rich diversity of aliphatic polyol complexes in aqueous solution. *J. Am. Chem. Soc.* **142**, 9188–9202 (2020).

95. J. K. Puri, R. Singh, V. K. Chahal, Silatranes: A review on their synthesis, structure, reactivity and applications. *Chem. Soc. Rev.* **40**, 1791–1840 (2011).

96. J. Henker, J. Wirmer-Bartoschek, L. E. Bendel, Y. Xiang, C. Fu, K. Harms, H. Schwalbe, E. Meggers, Progress in the synthesis and bioactivity of hexacoordinate silicon(IV) complexes. *Eur. J. Inorg. Chem.* **2016**, 5161–5170 (2016).

97. C. Chuit, R. J. P. Corriu, C. Reye, J. C. Young, Reactivity of penta- and hexacoordinate silicon compounds and their role as reaction intermediates. *Chem. Rev.* **93**, 1371–1448 (1993).

98. A. A. Toutov, W.-B. Liu, K. N. Betz, A. Fedorov, B. M. Stoltz, R. H. Grubbs, Silylation of C–H bonds in aromatic heterocycles by an Earth-abundant metal catalyst. *Nature*. **518**, 80–84 (2015).

99. W. Ridley, L. Dizikes, J. Wood, Biomethylation of toxic elements in the environment. *Science*. **197**, 329–332 (1977).

100. O. S. Fatoki, Biomethylation in the natural environment: A review. *S. Afr. J. Sci.* **93**, 366–370 (1997).

101. E. G. Rochow, The direct synthesis of organosilicon compounds. *J. Am. Chem. Soc.* **67**, 963–965 (1945).

102. M. B. Dickerson, K. H. Sandhage, R. R. Naik, Protein- and peptide-directed syntheses of inorganic materials. *Chem. Rev.* **108**, 4935–4978 (2008).

103. A. K. Wallace, N. Chanut, C. A. Voigt, Silica nanostructures produced using diatom peptides with designed post-translational modifications. *Adv. Funct. Mater.*, 2000849 (2020).

104. D. B. Cordes, P. D. Lickiss, F. Rataboul, Recent developments in the chemistry of cubic polyhedral oligosilsesquioxanes. *Chem. Rev.* **110**, 2081–2173 (2010).

Chapter III

# DIRECTED EVOLUTION OF ENZYMATIC SILICON–CARBON BOND CLEAVAGE IN SILOXANES

Material from this chapter appears in: **N. S. Sarai**, T. J. Fulton, R. L. O'Meara, K. E. Johnston, S. Brinkmann-Chen, R. R. Maar, R. E. Tecklenburg, J. M. Roberts, J. C. T. Reddel, D. E. Katsoulis, F. H. Arnold, Directed evolution of enzymatic silicon–carbon bond cleavage in siloxanes. *Submitted.*

# ABSTRACT

The volatile siloxane building blocks of silicones are produced at megaton scale and are non-biodegradable, leading to concerns over their potential for environmental persistence, long-range transport, and bioaccumulation. We discovered an engineered variant of bacterial cytochrome $P450_{BM3}$ that can cleave siloxane Si–C bonds, an activity not previously demonstrated with an enzyme. To accomplish this transformation, the enzyme catalyzes two chemically distinct steps: C–H hydroxylation produces a carbinol species whose Si–C bond is subsequently broken via a [1,2]-Brook-like rearrangement followed by hydrolysis. We enhanced this promiscuous function on cyclic and linear siloxanes using directed evolution.

## 3.1 Introduction

Linear and cyclic volatile methylsiloxanes (VMS), the building blocks of silicone polymers, are anthropogenic compounds whose unique material properties such as high backbone flexibility and low surface tension make them useful in many consumer applications, from detergents and antifoaming agents to lotions, shampoos, and hair conditioners (*1–4*). Cyclic VMS are also important feedstocks for the synthesis of silicone polymers (*5*). To satisfy consumer and feedstock demand for siloxanes, annual production is on the order of megatons per year (*4*).

The open use and high vapor pressures of VMS lead to wide distribution of these compounds and cause them to migrate between environmental compartments via long-range atmospheric transport (*6–12*). Regulations on VMS vary in different regions of the world. For example, octamethylcyclotetrasiloxane (**3**) is designated as a Substance of Very High Concern (SVHC) by the European Chemicals Agency on the basis of persistence, bioaccumulation and suspected reproductive toxicity (*13*, *14*). Given the prevalence and utility of siloxanes, their degradation is of significant interest.

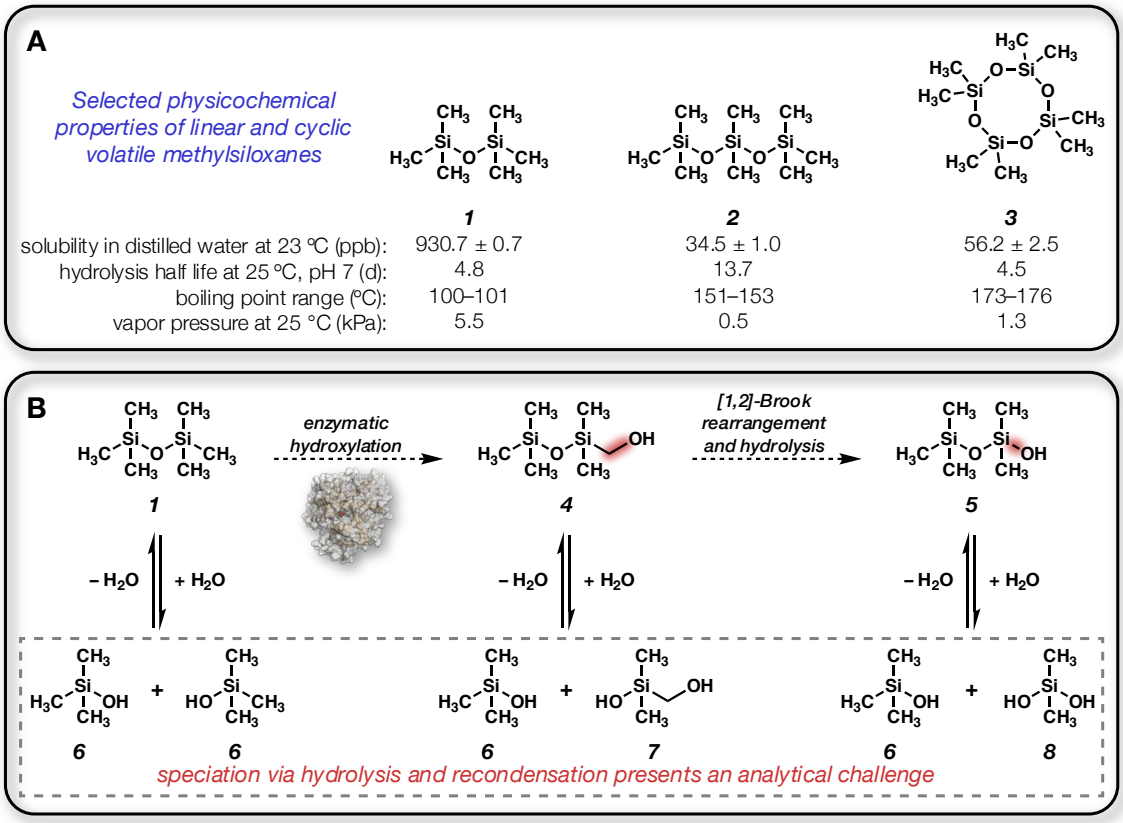


**Figure 3-1. Siloxanes have diverse molecular structures and are prone to complex interconversion reactions. A)** Physicochemical properties of selected volatile siloxanes and their structures. **B)** Hypothesis for enzymatic Si–C bond cleavage in hexamethyldisiloxane (**1**) initiated by a siloxane C–H bond hydroxylation followed by [1,2]-Brook rearrangement and hydrolysis of carbinol **4** to silanol **5**. Possible hydrolytic pathways are shown to demonstrate the complex nature of the product manifold of even the simplest siloxane, hexamethyldisiloxane (**1**). The hydrolysis products can recombine to form a diversity of condensation products.

Degradation of VMS is non-trivial due to their high thermal stability and lack of functional group handles. Hydrolysis of the Si–O bonds merely leads to speciation, producing silanols and siloxanediols, and complete degradation requires cleavage of the relatively inert Si–C bonds, which is generally initiated by one or more C–H oxidation events on siloxane methyl groups (*4*). The difficulty of this oxidation is highlighted by the limited examples of means to accomplish it, primarily $TiO_2$ photocatalysis, pyrolysis, and atmospheric $HO^{\bullet}$

oxidation (*4*, *15*, *16*). Enzymatic oxidation would offer an environmentally benign alternative that could unlock a mechanism for siloxane degradation that is adaptable to a variety of environmental conditions (*17–19*).

We hypothesized that enzymatic hydroxylation of a siloxane methyl group C–H bond would install a functional group handle that could facilitate Si–C bond cleavage. Studies on the fate of siloxanes in higher organisms have found that siloxanes are metabolized to a bevy of products when administered via IV or gavage, including products indicative of Si–C cleavage, which is proposed to occur following a C–H hydroxylation event (*20–22*). However, no enzyme capable of hydroxylating the siloxane C–H bond nor facilitating breakage of an Si–C bond has ever been identified (*4*, *23*, *24*).

### 3.2 Discovery of Siloxane C–H Hydroxylation Activity

Cytochromes P450 are known to insert oxygen into strong C–H bonds through an iron-oxo intermediate (*25–28*). Given the ability of these enzymes to oxidize unactivated alkyl C–H bonds, we envisaged that they might also be able to overcome the similar bond-dissociation energies of siloxane C–H bonds. We began by evaluating a panel of cytochrome $P450_{BM3}$ enzymes for their ability to oxidize the siloxane C–H bond in hexamethyldisiloxane (**1**). Cytochrome $P450_{BM3}$ is a self-sufficient enzyme comprised of a heme domain fused to an NADPH-dependent reductase domain. This soluble bacterial enzyme has been engineered to catalyze myriad non-native hydroxylations (*28*, *29*).

We hypothesized that successful hydroxylation of one of the C–H bonds would lead to carbinol **4**, which can then undergo a [1,2]-Brook rearrangement and subsequent hydrolysis

to the desired Si–C bond cleavage product (*30*, *31*), silanol **5** (**Figure 3-1**). We anticipated that such a rearrangement would be feasible in aqueous conditions (*4*); however, known siloxane hydrolysis and recondensation pathways could result in an analytical quagmire for characterization of the products. The diverse physical properties of the product analyte manifold make achieving a quantitative mass balance intractable using a single high-throughput analytical method to screen the large number of variants required for directed evolution. Additionally, we anticipated that the volatility of hexamethyldisiloxane (**1**) coupled with its low aqueous solubility would pose a challenge for finding initial enzyme activity, expected to be at trace levels at best for this non-native substrate (see **Figure 3-1A**). We proceeded with GC/MS analysis of enzymatic reaction mixtures in *Escherichia coli* lysate, which allowed quantification of carbinol **4** and silanol **5**, as these compounds could be formed only by enzymatic C–H hydroxylation. We tested eleven variants from our large collection of engineered cytochromes $P450_{BM3}$ and identified several variants capable of catalyzing the desired transformation at very low levels, as evidenced by formation of both carbinol **4** and silanol **5**; reactions with wild-type $P450_{BM3}$ do not result in formation of either species. We selected an unpublished variant from previous work on Si–H oxidation (*32*) as the parent enzyme and performed several generations of directed evolution to improve its activity on **1**, resulting in variant *L*SilOx4 (Linear Siloxane Oxidase generation 4) which furnishes 51 units of total product per unit of enzyme (**Figure 3-2A**), defined as total product concentration / enzyme concentration.

### 3.3 Investigation of Product Hydrolysis and Enzymatic Si–C Cleavage

Throughout this enzyme engineering effort, carbinol **4** and silanol **5** were difficult to quantify reliably, which limited the rate at which we could discover activating mutations. We observed that the concentration of authentic carbinol **4** decreases upon incubation in aqueous conditions, regardless of the presence of enzyme. Absent the enzyme, the decay is a result of hydrolysis, not conversion to silanol **5**. In the presence of enzyme, however, silanol **5** also forms, which we hypothesized is due to an enzyme-catalyzed [1,2]-Brook rearrangement and subsequent hydrolysis (**Figure 3-2B and 3-2C**) (*20*). We did not observe formation of silanol **5** upon incubation of siloxane **1** with free heme, ferric chloride, non-heme proteins, *E. coli* lysate, or heat-treated *L*SilOx4 (**Figure 3-2B**) (*see Supplementary Materials for controls*). However, cytochrome $P450_{BM3}$ variants from the lineage evolved for hexamethyldisiloxane (**1**) oxidation catalyze the formation of silanol **5** using siloxane **1** as substrate. Reactions performed in parallel using authentic carbinol **4** as substrate mirrored these results with the notable exception that wild-type $P450_{BM3}$ catalyzes the formation of silanol **5** directly from carbinol **4**, albeit with lower conversion than the engineered enzymes**,** even though it is unable to form silanol **5** from hexamethyldisiloxane (**1**) (**Figure 3-2C**).

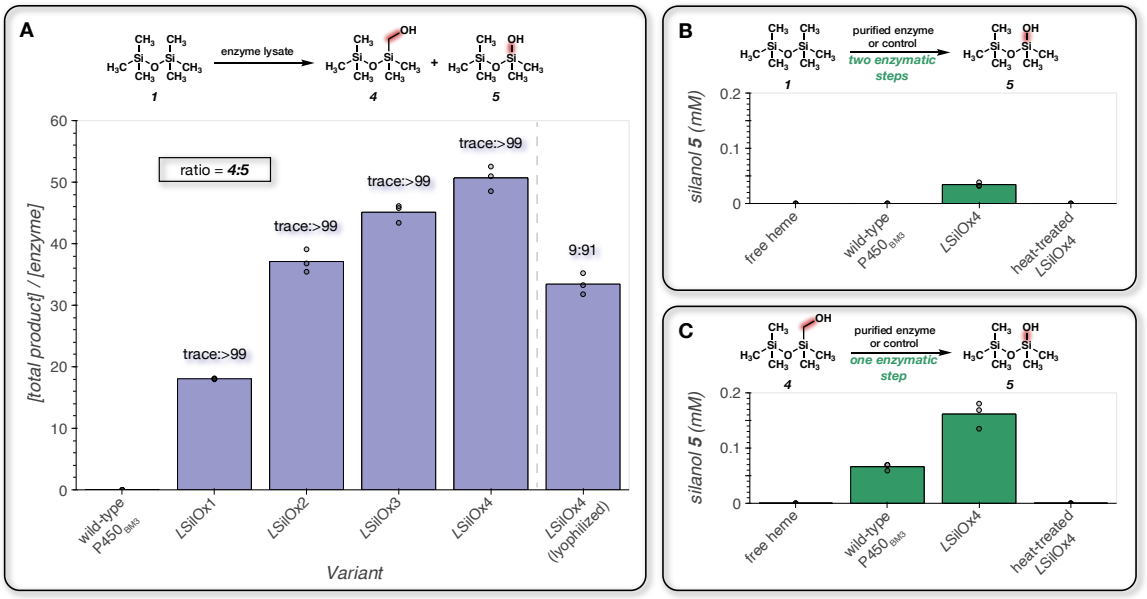


**Figure 3-2. Engineered variants catalyze both hydroxylation and [1,2]-Brook-like rearrangement steps of Si–C cleavage. A)** Enzymatic reaction of hexamethyldisiloxane (**1**) assayed for formation of carbinol **4** and silanol **5**; the ratio of carbinol **4** to silanol **5** is indicated above each bar. Directed evolution on hexamethyldisiloxane (**1**) yielded variant *L*SilOx4 which gives 51 units of total product per unit of enzyme. **B)** Silanol **5** is formed from siloxane **1** only in the presence of engineered enzyme. Wild-type $P450_{BM3}$ does not catalyze this transformation. **C)** Silanol **5** is formed from carbinol **4** by $P450_{BM3}$ variants. Wild-type cytochrome $P450_{BM3}$ can also catalyze this reaction step. Enzymatic reactions were performed with purified enzyme, heat-treated purified enzyme, lysate, or lyophilized lysate, with 5 mM substrate, 3.6% ethanol, 0.5 mM $NADP^+$, 2 U/mL G6PD, and 40 mM G6P, all in 100 mM Tris buffer at pH 7.0. Free heme controls were performed using hemin chloride (2.5 μM) in 100 mM Tris buffer at pH 7.0 instead of enzyme and the NADPH recycling system (see Supplementary Materials). Heat-treated *L*SilOx4 was obtained by denaturing purified *L*SilOx4 at 100 ºC for 5 min prior to the reaction (see Supplementary Materials). All reactions were performed aerobically at 23 °C for 4 h under agitation at 800 rpm. Abbreviations: G6PD – glucose-6-phosphate dehydrogenase, G6P – D-glucose-6-phosphate, Tris – tris(hydroxymethyl)aminomethane buffer.

### 3.4 Directed Evolution on Cyclic and Linear Siloxane Substrates

To continue directed evolution, we hypothesized that hydroxylation of siloxanes with lower volatility, such as linear siloxane **2** and cyclic siloxane **3** (**Figure 3-1A**), would reduce variation in the activity assay and provide advantages for sample handling in higher-throughput workflows. Indeed, these factors led to greater reproducibility and enabled

higher-throughput enzymatic reactions with siloxanes **2** and **3**. We began the evolutionary campaign targeting linear siloxane **2** by performing error-prone mutagenesis on *L*SilOx4 and identified improved variant *L*SilOx5. This variant also exhibits activity on cyclic siloxane **3**, thus serving as a suitable starting point for evolution on this substrate. We proceeded to target these two important classes of siloxanes—linear and cyclic—in parallel, resulting in distinct enzyme evolution lineages for each one. The final enzyme in the lineage evolved for linear siloxane **2**, *L*SilOx7, furnishes 35 units of total product per unit of enzyme (**Figure 3-3A**). We do not observe products that would result from hypothetical activity on the internal silicon center of linear siloxane **2** (**Figure 3-3B**). The final enzyme for cyclic siloxane **3,** *C*SilOx3 (Cyclic Siloxane Oxidase generation 3), furnishes 31 units of total product per unit of enzyme (**Figure 3-3C**). The amino acid substitutions present in the initial variant (*L*SilOx1) relative to wild type are imposed as small gray spheres on a structure of wild-type $P450_{BM3}$ (PDB: 2IJ2) (*33*) (**Figure 3-3D**). The substitutions accumulated during evolution of the *L*SilOx and *C*SilOx lineages relative to their initial variants are shown as lavender and peach spheres, respectively. The final variants for linear siloxanes **1** and **2** as well as cyclic siloxane **3** also retain >50% of their activity when formulated as freeze-dried lysate powders (**Figures 3-2A and 3-3A/C**).

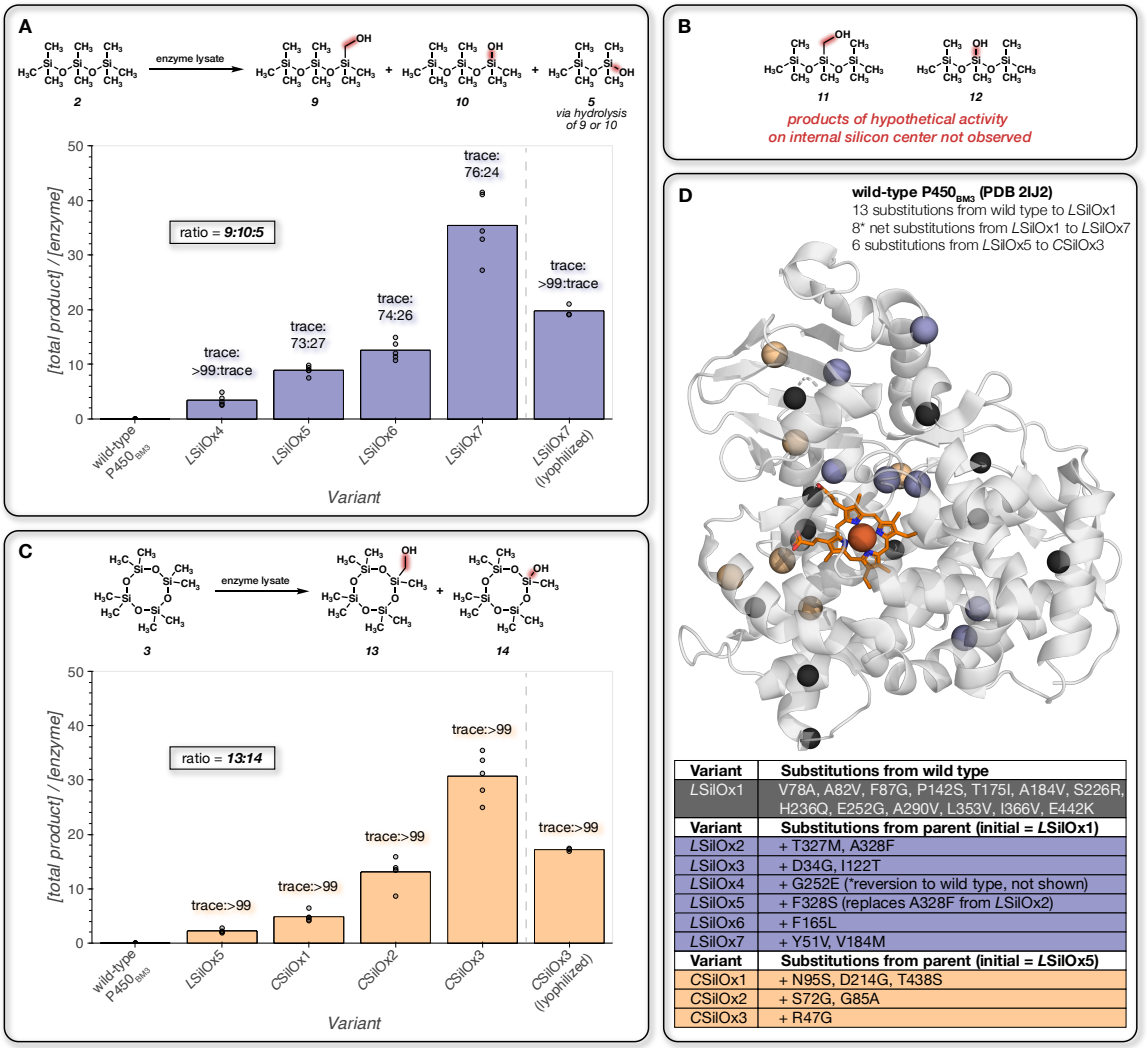


| Variant | Substitutions from wild type |
|---|---|
| *L*SilOx1 | V78A, A82V, F87G, P142S, T175I, A184V, S226R, H236Q, E252G, A290V, L353V, I366V, E442K |
| **Variant** | **Substitutions from parent (initial = *L*SilOx1)** |
| *L*SilOx2 | + T327M, A328F |
| *L*SilOx3 | + D34G, I122T |
| *L*SilOx4 | + G252E (*reversion to wild type, not shown) |
| *L*SilOx5 | + F328S (replaces A328F from *L*SilOx2) |
| *L*SilOx6 | + F165L |
| *L*SilOx7 | + Y51V, V184M |
| **Variant** | **Substitutions from parent (initial = *L*SilOx5)** |
| *C*SilOx1 | + N95S, D214G, T438S |
| *C*SilOx2 | + S72G, G85A |
| *C*SilOx3 | + R47G |

**Figure 3-3. Directed evolution with octamethyltrisiloxane (2) and octamethylcyclotetrasiloxane (3) as substrates.** **A)** Reaction of octamethyltrisiloxane (**2**) with P450$_{BM3}$ variants assayed for formation of carbinol **9**, silanol **10**, and silanol **5**; the ratio of carbinol **9** to silanol **10** to silanol **5** is indicated above each bar. Directed evolution on octamethyltrisiloxane (**2**) yielded variant *L*SilOx7 which gives 35 units of total product per unit of enzyme. Reactions were performed with enzyme lysate or lyophilized lysate, 5 mM substrate, 3.6% acetonitrile, 0.5 mM NADP$^+$, 2 U/mL G6PD, and 40 mM G6P, all in 100 mM Tris buffer at pH 7.0. Reactions were performed aerobically at 23 °C for 4 h under agitation at 800 rpm. **B)** Products formed from enzymatic activity on the internal silicon center are not detected. **C)** Reaction of octamethylcyclotetrasiloxane (**3**) with P450$_{BM3}$ variants assayed for formation of carbinol **13** and silanol **14**; the ratio of carbinol **13** to silanol **14** is indicated above each bar. Directed evolution on octamethylcyclotetrasiloxane (**3**) yielded variant *C*SilOx3 which gives 31 units of product per unit of enzyme. Reactions were conducted under the same conditions as in panel A, but with 3.6% ethanol instead of acetonitrile. **D)** Structure of wild-type P450$_{BM3}$ (PDB: 2IJ2) (*33*) with amino acid

substitutions accumulated during directed evolution highlighted. Substitutions present in the initial variant, *L*SilOx1, relative to wild-type $P450_{BM3}$ are shown as small gray spheres. Substitutions accrued in the *L*SilOx lineage relative to initial variant *L*SilOx1 are shown as lavender spheres. Substitutions accrued in the *C*SilOx lineage relative to initial variant *L*SilOx5 are shown as peach spheres. Abbreviations: G6PD – glucose-6-phosphate dehydrogenase, G6P – D-glucose-6-phosphate, Tris – tris(hydroxymethyl)aminomethane buffer.

### 3.5 Unlocking New-to-Nature Degradation Activities in the Laboratory

The body of directed evolution literature demonstrates that even trace activities can be amplified to yield powerful new biocatalysts with activities not yet found in nature (*17*, *34*), including enzymes that forge (*35*), and now break, Si–C bonds. Enzymatic activities for degradation of anthropogenic compounds can also evolve in microorganisms which derive a selective advantage from doing so. For example, *Ideonella sakaiensis,* isolated from sediment collected near a recycling plant rich in polyethylene terephthalate (PET), has a set of PET-degrading enzymes that enable the bacteria to grow on PET as a sole carbon source (*36*, *37*). That an enzyme for siloxane Si–C cleavage has not been discovered may be because it does not exist, due to the dilute occurrence of siloxanes in the environment (*4*) or because there is no selective advantage to an organism to drive its evolution; another possibility is that this activity exists but has not yet been found. One can argue, however, that a microorganism would gain little benefit from devoting resources to metabolize VMS. To gain a single carbon atom by cleaving an Si–C bond, the microorganism would need to perform both chemical steps: hydroxylation of a C–H bond adjacent to a silicon center, followed by a [1,2]-Brook-like rearrangement and subsequent hydrolysis. Furthermore, because silicon is rarely used in microbial metabolism, the silicon-containing byproducts are unlikely to provide benefit (*23*).

Directed evolution bypasses these limitations on natural evolution of new activities by decoupling enzyme evolution from the requirement to provide selective advantage and instead explores what is chemically possible, such as biocatalytic scission of siloxane Si–C bonds. This bond cleavage is the result of tandem reactions performed by engineered cytochrome $P450_{BM3}$ enzymes: C–H hydroxylation and [1,2]-Brook-like rearrangement followed by hydrolysis to a silanol. Interestingly, wild-type $P450_{BM3}$ performs the second step of the reaction—a 'promiscuous function' unrelated to its natural reactivity of fatty acid hydroxylation—but cannot access the carbinol species. Strikingly, engineered variants of this enzyme catalyze both steps. The cleavage of a single siloxane Si–C bond catalyzed by these enzymes is a proof of principle which may extend to scission of multiple siloxane Si–C bonds and represents a first step towards full degradation of these stable, man-made compounds.

**Chapter III Bibliography**


1. J. Chelikowsky, "Introduction: Silicon in All Its Forms" in *Silicon: Evolution and Future of a Technology*, P. Siffert, E. F. Krimmel, Eds. (Springer, Berlin, Heidelberg, 2004), pp. 1–22.

2. W. Noll, Ed., "Applications of Technical Silicone Products in Various Branches of Industry" in *Chemistry and Technology of Silicones* (Academic Press, 1968), pp. 531–638.

3. A. J. O'Lenick, *Silicones for Personal Care* (Allured Publishing, 2008).

4. C. Rücker, K. Kümmerer, Environmental chemistry of organosiloxanes. *Chem. Rev.* **115**, 466–524 (2015).

5. W. Noll, Ed., "Preparation of Polyorganosiloxanes" in *Chemistry and Technology of Silicones* (Academic Press, 1968), pp. 190–245.

6. K. Mojsiewicz-Pieńkowska, D. Krenczkowska, Evolution of consciousness of exposure to siloxanes—review of publications. *Chemosphere*. **191**, 204–217 (2018).

7. S. Genualdi, T. Harner, Y. Cheng, M. MacLeod, K. M. Hansen, R. van Egmond, M. Shoeib, S. C. Lee, Global distribution of linear and cyclic volatile methyl siloxanes in air. *Environ. Sci. Technol.* **45**, 3349–3354 (2011).

8. D.-G. Wang, W. Norwood, M. Alaee, J. D. Byer, S. Brimble, Review of recent advances in research on the toxicity, detection, occurrence and fate of cyclic volatile methyl siloxanes in the environment. *Chemosphere*. **93**, 711–725 (2013).

9. X. Xiang, N. Liu, L. Xu, Y. Cai, Review of recent findings on occurrence and fates of siloxanes in environmental compartments. *Ecotoxicol. Environ. Saf.* **224**, 112631 (2021).

10. N. A. Warner, A. Evenset, G. Christensen, G. W. Gabrielsen, K. Borgå, H. Leknes, Volatile siloxanes in the European Arctic: Assessment of sources and spatial distribution. *Environ. Sci. Technol.* **44**, 7705–7710 (2010).

11. O. L. Flaningam, Vapor pressures of poly(dimethylsiloxane) oligomers. *J. Chem. Eng. Data*. **31**, 266–272 (1986).

12. Y. D. Lei, F. Wania, D. Mathers, Temperature-dependent vapor pressure of selected cyclic and linear polydimethylsiloxane oligomers. *J. Chem. Eng. Data*. **55**, 5868–5873 (2010).

13. ECHA (European Chemicals Agency), "Inclusion of substances of very high concern in the Candidate List for eventual inclusion in Annex XIV" (ED/61/2018, 2018), (available at https://echa.europa.eu/documents/10162/2be7bcbf-f797-c28c-2c67-939664155c7c).

14. ECHA (European Chemicals Agency), "Support Document for Identification of Octamethylcyclotetrasiloxane ($D_4$) as a Substance of Very High Concern because of its PBT and vPvB properties." (57D & E, 2018), (available at https://echa.europa.eu/documents/10162/115f70a9-a387-1525-d49f-b715e84996e4).

15. E. C. Tuazon, S. M. Aschmann, R. Atkinson, Atmospheric degradation of volatile methyl-silicon compounds. *Environ. Sci. Technol.* **34**, 1970–1976 (2000).

16. M. W. Alton, E. C. Browne, Atmospheric degradation of cyclic volatile methyl siloxanes: Radical chemistry and oxidation products. *ACS Environ. Au*. **2**, 263–274 (2022).

17. F. H. Arnold, Directed evolution: Bringing new chemistry to life. *Angew. Chem. Int. Ed.* **57**, 4143–4148 (2018).

18. R. A. Sheldon, J. M. Woodley, Role of biocatalysis in sustainable chemistry. *Chem. Rev.* **118**, 801–838 (2018).

19. T. Sutherland, I. Horne, K. Weir, C. Coppin, M. Williams, M. Selleck, R. Russell, J. Oakeshott, Enzymatic bioremediation: From enzyme discovery to applications. *Clin. Exp. Pharmacol.* **31**, 817–821 (2004).

20. S. Varaprath, J. M. McMahon, K. P. Plotzke, Metabolites of hexamethyldisiloxane and decamethylcyclopentasiloxane in Fischer 344 rat urine—A comparison of a linear and a cyclic siloxane. *Drug Metab. Dispos.* **31**, 206–214 (2003).

21. S. Varaprath, K. L. Salyers, K. P. Plotzke, S. Nanavati, Identification of metabolites of octamethylcyclotetrasiloxane ($D_4$) in rat urine. *Drug Metab. Dispos.* **27**, 1267–1273 (1999).

22. M. B. Reddy, M. E. Andersen, P. E. Morrow, I. D. Dobrev, S. Varaprath, K. P. Plotzke, M. J. Utell, Physiological modeling of inhalation kinetics of octamethylcyclotetrasiloxane in humans during rest and exercise. *Toxicol. Sci.* **72**, 3–18 (2003).

23. N. S. Sarai, B. J. Levin, J. M. Roberts, D. E. Katsoulis, F. H. Arnold, Biocatalytic transformations of silicon—the other Group 14 element. *ACS Cent. Sci.* **7**, 944–953 (2021).

24. C. Rücker, E. Grabitz, K. Kümmerer, Are Si–C bonds cleaved by microorganisms? A critical review on biodegradation of methylsiloxanes. *Chemosphere*. **321**, 137858 (2023).

25. N. P. Dunham, F. H. Arnold, Nature's machinery, repurposed: Expanding the repertoire of iron-dependent oxygenases. *ACS Catal.* **10**, 12239–12255 (2020).

26. K. Mittra, M. T. Green, Reduction potentials of P450 Compounds I and II: Insight into the thermodynamics of C–H bond activation. *J. Am. Chem. Soc.* **141**, 5504–5510 (2019).

27. J. Münch, P. Püllmann, W. Zhang, M. J. Weissenborn, Enzymatic hydroxylations of $sp^3$-carbons. *ACS Catal.* **11**, 9168–9203 (2021).

28. C. J. C. Whitehouse, S. G. Bell, L.-L. Wong, $P450_{BM3}$ (CYP102A1): Connecting the dots. *Chem. Soc. Rev.* **41**, 1218–1260 (2012).

29. S. T. Jung, R. Lauchli, F. H. Arnold, Cytochrome P450: Taming a wild type enzyme. *Curr. Opin. Biotechnol.* **22**, 809–817 (2011).

30. A. G. Brook, Molecular rearrangements of organosilicon compounds. *Acc. Chem. Res.* **7**, 77–84 (1974).

31. L. Gao, W. Yang, Y. Wu, Z. Song, "The Brook Rearrangement" in *Organic Reactions* (John Wiley & Sons, Ltd, 2020), pp. 1–612.

32. S. Bähr, S. Brinkmann-Chen, M. Garcia-Borràs, J. M. Roberts, D. E. Katsoulis, K. N. Houk, F. H. Arnold, Selective enzymatic oxidation of silanes to silanols. *Angew. Chem. Int. Ed.* **59**, 15507–15511 (2020).

33. H. M. Girvan, H. E. Seward, H. S. Toogood, M. R. Cheesman, D. Leys, A. W. Munro, Structural and spectroscopic characterization of P450 BM3 mutants with unprecedented P450 heme iron ligand sets: New heme ligation states influence conformational equilibria in P450 BM3. *J. Biol. Chem.* **282**, 564–572 (2007).

34. K. Chen, F. H. Arnold, Engineering new catalytic activities in enzymes. *Nat. Catal.* **3**, 203–213 (2020).

35. S. B. J. Kan, R. D. Lewis, K. Chen, F. H. Arnold, Directed evolution of cytochrome c for carbon–silicon bond formation: Bringing silicon to life. *Science*. **354**, 1048–1051 (2016).

36. I. Taniguchi, S. Yoshida, K. Hiraga, K. Miyamoto, Y. Kimura, K. Oda, Biodegradation of PET: Current status and application aspects. *ACS Catal.* **9**, 4089–4105 (2019).

37. S. Yoshida, K. Hiraga, T. Takehana, I. Taniguchi, H. Yamaji, Y. Maeda, K. Toyohara, K. Miyamoto, Y. Kimura, K. Oda, A bacterium that degrades and assimilates poly(ethylene terephthalate). *Science*. **351**, 1196–1199 (2016).

# Appendix A

# SUPPLEMENTARY INFORMATION FOR CHAPTER III

## A.1 Materials and Methods

### A.1.1 General

Expression vector pET22(b)+ was used, and cloning was performed using Gibson assembly (*1*). *Escherichia coli* cells were grown using Luria-Bertani medium or Terrific Broth with 100 μg/mL carbenicillin ($LB_{carb}$ or $TB_{carb}$). T7 Express competent *Escherichia coli* cells were purchased from New England Biolabs Inc (NEB, Ipswich, MA). T5 exonuclease, Phusion polymerase, and Taq ligase were purchased from NEB. Tris(hydroxymethyl)aminomethane buffer (abbreviated as Tris, pH 7.0) was used as a buffering system for cell lysates and purified proteins, unless otherwise specified.

Biocatalytic reaction analysis was performed with an Agilent 7820A or an Agilent 8890 gas chromatograph equipped with a 5977B mass spectrometer detector and a DB-5MS capillary column (30 m length, 0.250 mm diameter, 0.25 μm film thickness using split-mode capillary injection and electron-impact ionization). Calibration curves were generated using serial dilutions of the appropriate material with 5 mM 1,3,5-trimethoxybenzene as an internal standard. Yields were determined by adjusting the calculated concentration of product relative to internal standard, accounting for the dilution factor of enzymatic reaction extraction.

Glucose-6-phosphate dehydrogenase (196 U/mg) was dissolved in pH 7.4 sodium citrate buffer to give a final concentration of 196 U/mL. The stock of glucose-6-phosphate dehydrogenase was aliquoted in 200-μL portions into individual PCR tubes and flash-frozen in liquid nitrogen ($LN_2$) or powdered dry ice prior to storage. For biocatalytic reactions, a

stock of the NADPH cofactor regeneration system was prepared by combining 14 mM $NADP^+$, 1.12 M glucose-6-phosphate, and 56 U/mL glucose-6-phosphate dehydrogenase (stock concentrations) in 100 mM pH 7 Tris buffer.

### A.1.2 Cloning, Mutagenesis, and Plasmid Isolation

*Site-saturation mutagenesis*

Site-saturation mutagenesis (SSM) experiments were performed using primers bearing degenerate codons (NDT, VHG, TGG) as per the "22-codon trick" using a modified QuikChange protocol (*2*). A break in the ampicillin cassette was introduced, resulting in two fragments. The degenerate primer targeting the site of interest (forward) and the Amp_int_reverse (reverse) primer were used to yield one fragment. The primer targeting the site of interest (reverse) and the Amp_int_forward (forward) primer were used to yield the other fragment. The PCR conditions were as follows (final concentrations): Phusion GC Buffer 1x, 200 mM dNTPs, 0.5 μM of forward primer, 0.5 μM reverse primer, and 0.02 U/μL of Phusion polymerase. Thermocycling conditions are outlined below (Table A-1). Upon completion of PCRs, the remaining template DNA was digested with *Dpn*I (1 μL). Gel purification was performed using gel electrophoresis (1% agarose gel containing a SYBR Gold nucleic acid gel stain), and DNA was visualized on a blue transilluminator. DNA was isolated using a Zymoclean DNA gel recovery kit. The purified PCR product was then assembled using the Gibson assembly protocol (*1*).

**Table A-1.** Thermocycler conditions for SSM protocol.

| Step | Temperature (ºC) | Time (min:sec) | Number of Cycles |
|---|---|---|---|
| Initial Denaturation | 98 | 00:30 | 1 |
| Denaturation | 98 | 00:10 | 5 |
| Annealing | 98 to 55 at 1 ºC/s | 00:15 | |
| Extension | 72 | 2:06 | |
| Denaturation | 98 | 0:10 | 25 |
| Annealing | 55 | 0:15 | |
| Extension | 72 | 2:06 | |
| Extension | 72 | 5:00 | 1 |
| Hold | 10 | – | |

*Random Mutagenesis*

Random mutations were introduced using error-prone PCR with the addition of 200–500 µM MnCl2 to a *Taq* PCR using the primers described below (Table A-2).

**Table A-2.** Primers used for PCR mutagenesis and amplification.

| Primer | Amplicon | Sequence (5' to 3') |
|---|---|---|
| RLO005 | Insert forward (use with v4) | GGATAACAATTCCCCTCTAGAAATAATTTTGTTTAACTTTAAGAAGGAGATATACATATG |
| RLO007 | BB1 reverse (use with v4) | CATATGTATATCTCCTTCTTAAAGTTAAACAAAATTATTTCTAGAGGGGAATTGTTATCC |
| NSS005 | Insert forward (use with v2) | AACTTTAAGAAGGAGATATACATATGACAATTAAAGAAATGCCTCAGCCA |
| NSS007 | BB1 reverse (use with v2) | TGGCTGAGGCATTTCTTTAATTGTCATATGTATATCTCCTTCTTAAAGTT |
| HR1-v2 | insert reverse (use with NSS) | CTTTTTTAGCAGACTGTTCAGTGCTAGGTGAAGGAATACC |
| HR1-v4 | insert reverse (use with RLO) | CGTATTATGAGCGTTTTCTGCCTTTTTGCG |
| HF1-v2 | BB2 forward (use with NSS) | GGTATTCCTTCACCTAGCACTGAACAGTCTGCTAAAAAAG |
| HF1-v4 | BB2 forward (use with RLO) | CGCAAAAAGGCAGAAAACGCTCATAATACG |
| Amp_int_forward | BB1 forward | GCTAACCGCTTTTTTGCACAACATG |
| Amp_int_reverse | BB2 reverse | TTGTGCAAAAAAGCGGTTAGCTCC |

A break in the ampicillin cassette was introduced in error-prone PCRs, resulting in two backbone fragments (BB1/BB2), while a third fragment (insert) was amplified that encodes the heme domain of the enzyme. Mutations within this third fragment were introduced by varying the concentration of $MnCl_2$ during PCR amplification. The insert PCR conditions were as follows (final concentrations): standard *Taq* buffer 1x, 200 mM dNTPs, 0.5 μM forward primer, 0.5 μM reverse primer, and 0.08 U/μL of *Taq* polymerase, and 200–400 μM $MnCl_2$. The two backbone PCR conditions were as follows: Phusion GC buffer 1x, 5% DMSO, 200 mM dNTPs, 0.5 μM forward primer, 0.5 μM reverse primer, and 0.02 U/μL of Phusion polymerase. Primers NSS005 (forward) with HR1-v2 (reverse) or RLO005 (forward) with HR1-v4 (reverse) were used to amplify the region encoding the enzyme (insert). Two primer pairs (Amp_int_forward (forward) with NSS007 (reverse) or RLO007 (reverse)) and (HF1-v2 (forward) or HF1-v4 (forward) and Amp_int_reverse (reverse)) were used to amplify the backbone fragments (BB1/BB2) using Phusion polymerase and the parent DNA template. Thermocycler conditions for the insert and BB1/BB2 are outlined below (Tables A-3 and A-4). Upon completion of PCRs, remaining template DNA was digested using *Dpn*I (1 μL). The amplified fragments were purified gel electrophoresis (1% agarose gel containing a SYBR Gold nucleic acid gel stain), and DNA was visualized on a blue transilluminator. The three amplified fragments were then assembled into a circular plasmid using a Gibson assembly protocol (*1*).

**Table A-3.** Thermocycler conditions for insert PCR.

| Step | Temperature (ºC) | Time (min:sec) | Number of Cycles |
|---|---|---|---|
| Initial Denaturation | 98 | 5:00 | 1 |
| Denaturation | 98 | 00:30 | 30 |
| Annealing | 64 | 00:30 | |
| Extension | 72 | 1:30 | |
| Extension | 72 | 5:00 | 1 |
| Hold | 10 | – | |

**Table A-4.** Thermocycler conditions for BB1/BB2.

| Step | Temperature (ºC) | Time (min:sec) | Number of Cycles |
|---|---|---|---|
| Initial Denaturation | 98 | 00:30 | 1 |
| Denaturation | 98 | 00:10 | 5 |
| Annealing | 98 to 64 at 1 ºC/sec | 00:15 | |
| Extension | 72 | 2:06 | |
| Denaturation | 98 | 0:10 | 25 |
| Annealing | 64 | 0:15 | |
| Extension | 72 | 2:06 | |
| Extension | 72 | 5:00 | 1 |
| Hold | 10 | – | |

*Recombination via Staggered Extension Process*

Staggered extension process (StEP) PCR was performed using a mixture of plasmids of the variants to be recombined in equimolar fashion, using this mixture as the template DNA. The StEP PCR was then conducted by varying the annealing temperature and by using a shorter extension time following a standard protocol (*3*, *4*). The PCR conditions were as follows (final concentrations): standard *Taq* buffer 1x, 200 mM dNTPs, 0.5 µM of primer NSS005 and 0.5 µM of primer HR1-v2 or µM of primer RLO005 and 0.5 µM of primer HR1-v4, and 0.08 U/µL of *Taq* polymerase. Amplification of the recombined fragment was conducted using a Phusion PCR protocol. Thermocycling conditions are outlined below (Tables A-5 and A-6). Upon completion of PCRs, the remaining template DNA was digested with *Dpn*I (1 µL). The PCR product was purified by purified gel electrophoresis (1% agarose gel containing a SYBR Gold nucleic acid gel stain), and DNA was visualized on a blue

transilluminator. The recombined insert library was purified and inserted into the pET22(b)+ vector using a Gibson assembly (*1*) with BB1/BB2 fragments as outlined in the section *Error-Prone PCR Mutagenesis*.

**Table A-5.** Thermocycler conditions for recombination of PCR products.

| Step | Temperature (ºC) | Time (min:sec) | Number of Cycles |
|---|---|---|---|
| Initial Denaturation | 95 | 5:00 | 1 |
| Denaturation | 95 | 0:10 | 120 |
| Annealing | 55 | 0:05 | |
| Extension | Gradient (50->72°C) | 0:05 | |
| Hold | 10 | – | |

**Table A-6.** Thermocycler conditions for amplification of StEP insert.

| Step | Temperature (ºC) | Time (min:sec) | Number of Cycles |
|---|---|---|---|
| Initial Denaturation | 98 | 5:00 | 1 |
| Denaturation | 98 | 00:30 | 30 |
| Annealing | 64 | 00:30 | |
| Extension | 72 | 1:30 | |
| Extension | 72 | 5:00 | 1 |
| Hold | 10 | – | |

*Transformation of T7 Express chemically competent* E. coli *cells and Isolation of Plasmids/Gibson Products*

T7 Express Competent *E. coli* cells were utilized for all experiments. Plasmids were mixed with competent cells on ice in PCR tubes. The mixture was kept on ice for 30 min, after which time transformation was accomplished by heat shocking the mixture in a 42 ºC water bath for exactly 10 seconds. After a 5-min recovery on ice, the cells were diluted with SOC medium and plated on $LB_{carb}$ agar plates.

Plasmids were isolated from stationary-phase cultures by miniprep (Qiagen), and sequencing was performed by Laragen, Inc. (Culver City, CA) using T7 promoter and HR1-V2 terminator primers.

### A.1.3 Small-Scale Enzymatic Reactions to Identify Improved Variants

Enzyme mutant libraries were evaluated on a 350-µL scale using crude cell lysate in individual snap-cap 2.0-mL microtubes or 96-well plates constructed from individual 1.0-mL autosampler neckless shell vials. The 96-well plates of individual shell vials were constructed by inserting 1.0-mL autosampler neckless shell vials into a 96-well microtiter plate using a USA Scientific 1000-µL pipette tip rack as an alignment guide. The snap-cap vials were sealed by individual capping after the addition of all biocatalytic reaction components. The 96-well shell vial plates were sealed by capping with an additional 96-well microtiter plate and centrifugation (3,000 *g*, 1 min, 25 ºC).

After a site-saturation mutagenesis (SSM), error-prone PCR (epPCR), or staggered extension process (StEP) library was generated, 84 single colonies were randomly picked and cultured in 400 µL of LB medium with 0.1 mg/mL carbenicillin ($LB_{carb}$) in a sterilized 96-well culture plate (2-mL well volume). The plate typically contained eight wells inoculated with single colonies expressing the parent enzyme, two sterile wells, and two wells inoculated with single colonies expressing tryptophan synthase variant *Tm*9D8* (*5*). The cultures were covered with EasyApp microporous film and grown at 37 ºC, 220 rpm, and 80% relative humidity for 12–16 h. A separate, sterilized 96-well culture plate was filled with 930 µL of Terrific Broth medium containing 0.1 mg/mL carbenicillin ($TB_{carb}$). The plate with $TB_{carb}$ was inoculated with the $LB_{carb}$ preculture (20 µL/well) and incubated at 37 ºC, 220 rpm, and 80% relative humidity for 3 h. The plate was then cooled on ice for 30 min, induced with 0.5 mM IPTG, 1 mM ALA, and 3.5 mM $FeCl_3$ and 1:1000 trace metals master mix (as described in (*6*)) (final concentrations), and then expressed at 22 ºC and 220 rpm for 16–22 h. After

expression, the cells were pelleted (4,500 *g*, 15 min, 4 ºC) via centrifugation and the supernatant was discarded. The pelleted cells were sealed with a TempPlate sealing foil and stored in a –20 ºC freezer for at least 16 h prior to lysis.

The 96-well plates containing frozen cell cultures were thawed for 10 min at 25 ºC and the pelleted cells were then resuspended in lysis buffer (400 µL/well) containing 1 mg/mL lysozyme, 0.07 mg/mL DNAse, and 2 mM $MgCl_2$. The cells were then lysed at 37 ºC and 160 rpm for 1 h. Cell debris was then pelleted by centrifugation (4,500 *g*, 15 min, 4 ºC). The biocatalytic reaction vessels were then charged with the NADPH cofactor regeneration system (12.5 µL/vessel) to give final reaction concentrations of 0.5 mM $NADP^+$, 40 mM glucose-6-phosphate, and 2 U/mL of glucose-6-phosphate dehydrogenase. A 140 mM substrate stock was prepared by dissolving the appropriate substrate in the specified cosolvent. The cell lysate was then added (325 µL/reaction) to the reaction vessel, followed by the substrate (12.5 µL/reaction) to give a final concentration of 5 mM substrate. The reaction vessels were sealed immediately after the addition of substrate and shaken at 800 rpm for 4 h at 25 ºC. After the 4 h reaction, the reaction vessels were unsealed and 5 mM 1,3,5-trimethoxybenzene in ethyl acetate were added (450 µL/well) quickly. The organic and aqueous phases were mixed by using a vortex mixer (microtubes) or by pipetting the mixture up and down with a multi-channel pipette (glass shells). Phase separation in microtubes was facilitated by centrifugation at 20,817 *g* and 4 ºC for 15 min. The 96-well shell vial plates were sealed with TempPlate sealing foil and centrifuged at 4,000 *g* and 4 ºC for 15 min. Aliquots of the organic phase (300 µL/reaction) were then transferred to individual 400 µL flat bottom glass inserts in 2-mL screw-cap vials which were sealed with red sil septum screw

caps. Analysis was performed using GC/MS with product concentrations and yield determined by response relative to the 1,3,5-trimethoxybenzene internal standard using a calibration curve.

### A.1.4 Determination of Hemeprotein Concentration

Hemeprotein concentration was determined for purified protein and cell lysate by performing a CO-binding assay (*7*, *8*). Hemeprotein solution was added to Greiner Bio-One clear plastic flat-bottomed 96-well plates (180 µL/well) in 3–6 technical replicates per protein. To the wells was then added a solution of 300 mM sodium dithionite in 1 M potassium phosphate buffer ($KP_i$), pH 8.0 (20 µL/well). Absorbance was measured at 450 nm and 490 nm using a Tecan Spark multimode microplate reader. The 96-well plate was then placed in a CO-chamber. The atmosphere in the chamber was evacuated with a vacuum pump, and the chamber was refilled to atmospheric pressure with CO. The 96-well plate was incubated in the CO atmosphere for 30 min, then measured again using the microplate reader at 450 nm and 490 nm. Beer's law was used to determine the hemeprotein concentration of the solution using the ΔA450–490 between the CO-bound and reduced samples, the ε450–490 value of 0.091, dilution factor of 1.1, and the pathlength of 0.74 cm.

### A.1.5 Protein Purification

For purification, cell pellets were frozen at −20 °C for at least 24 hours. Cells were thawed and resuspended in binding buffer (20 mM Tris·HCl, 100 mM sodium chloride, 20 mM imidazole, pH 7.0, ~5 mL/g wet cells) and lysed by sonication (QSonica Q500 sonicator, 25% amplitude, 33% duty cycle, 2 minutes). The lysate was clarified by centrifugation (20,000 *g*, 10 min, 4 °C) followed by filtration (0.20 µm syringe filter). The protein was

purified using an Äkta Purifier with a HisTrap HP column (GE Healthcare), eluting with a gradient of 20–500 mM imidazole. Fractions containing purified enzyme were pooled and concentrated with repeated centrifugation and dilution in 100 mM Tris, pH 7.0 in an Amicon ultra-centrifugal filter (10 kDa molecular weight cutoff). The concentrated protein was divided into aliquots (100 µL), flash frozen on powdered dry ice in PCR tubes, and stored at −80 °C. Protein concentration was determined after a freeze/thaw cycle via the CO-binding assay with appropriate dilutions of the protein solutions (0 to 20-fold).

### A.1.6 Small-Scale Enzymatic Reactions for Lineage Validation

Validation of enzymatic activity was performed as follows. *E. coli* transformed with pET22b(+) constructs encoding P450 variants were grown at 37 ºC and 220 rpm in 5-mL $LB_{carb}$ medium for 16–20 h. Subsequently, 0.5 mL of this preculture was used to inoculate 50 mL of $TB_{carb}$ medium in a sterile 125-mL Erlenmeyer flask covered with sterilized aluminum foil. The culture was incubated at 37 ºC and shaken at 220 rpm for approximately 2–4 h until the optical cell density at 600 nm ($OD_{600}$) was 0.7–0.9. Then, the expression culture was cooled in an ice bath for 30 min, induced with 0.5 mM IPTG, 1 mM ALA, and 3.5 µM $FeCl_3$ and 1:1000 trace metals master mix (as described in (*6*)) (final concentrations), and then expressed at 22 ºC and 220 rpm for 16–22 h. After expression, the cultures were transferred to tared 50-mL Falcon tubes and pelleted (4,500 *g*, 15 min, 4 ºC) via centrifugation and the supernatant was discarded. The pelleted cells were stored in a –20 ºC freezer for at least 16 h in the sealed Falcon tube prior to lysis.

The Falcon tubes containing frozen cell cultures were thawed for 10 min at 25 ºC, and the pelleted cells were resuspended in lysis buffer (4 mL/1 g of pellet) containing 1 mg/mL

lysozyme, 0.07 mg/mL DNAse, 2 mM $MgCl_2$, and, for reactions with *Tm*9D8*, 200 μM PLP. The cells were then lysed at 37 ºC and 180 rpm for 1 h. The lysed cultures were then transferred to 2.0-mL microtubes and centrifuged at 20,817 *g* and 4 ºC for 15 min. The supernatant lysates were combined in 15-mL Falcon tubes. An NADPH cofactor regeneration system (12.5 μL/vessel) was then added to 2.0-mL microtubes to give final reaction concentrations of 0.5 mM $NADP^+$, 40 mM glucose-6-phosphate, and 2 U/mL of glucose-6-phosphate dehydrogenase. A 140 mM substrate stock was prepared by dissolving the appropriate substrate in the specified cosolvent (MeCN for **3**, EtOH for **4**). The cell lysate was then added (325 μL/reaction) to the reaction vessel, followed by the substrate (12.5 μL/well) to give a final concentration of 5 mM substrate. The microtubes were sealed immediately after the addition of substrate and shaken at 800 rpm for 4 h at 23ºC. After the 4 h reaction, the reaction vessels were unsealed and 5 mM 1,3,5-trimethoxybenzene in ethyl acetate were added (450 μL/reaction) quickly. The organic and aqueous phases were mixed by using a vortex mixer. Phase separation was facilitated by centrifugation at 20,817 *g* and 4 ºC for 15 min. Aliquots of the organic phase (200–300 μL/reaction) were then transferred to individual 400-μL flat bottom glass inserts in 2-mL screw-cap vials which were sealed with red sil septum screw cap. Analysis was performed using GC/MS with product concentrations and yield determined by response relative to the 1,3,5-trimethoxybenzene internal standard using a calibration curve. Superior variants were selected for subsequent mutagenesis by comparing product yields and product yields relative to estimated protein concentration. Hemeprotein concentration was determined by performing a CO-binding assay on the cell lysate.

### A.1.7 Enzymatic Reactions with Lyophilized Enzymes

*E. coli* transformed with pET22b(+) constructs encoding P450s *L*SilOx4, *L*SilOx7, or *C*SilOx3 were grown at 37 ºC and 220 rpm in 5 mL $LB_{carb}$ medium for 16–20 h. Subsequently, 2.5 mL of this preculture were used to inoculate 250 mL of $TB_{carb}$ medium in a sterile 1-L Erlenmeyer flask covered with sterilized aluminum foil. The culture was incubated at 37 ºC and shaken at 220 rpm for approximately 2–4 h until the optical cell density at 600 nm ($OD_{600}$) was 0.7–0.9. Then, the expression culture was cooled in an ice bath for 30 min, induced with 0.5 mM IPTG, 1 mM ALA, and 3.5 µM $FeCl_3$ and 1:1000 trace metals master mix (as described in (*6*)) (final concentrations), and then expressed at 22 ºC and 220 rpm for 16–22 h. After expression, the cultures were transferred to tared 50-mL Falcon tubes and pelleted (4,500 *g*, 15 min, 4 ºC) via centrifugation and the supernatant was discarded. The pelleted cells were stored in a –20 ºC freezer for at least 16 h prior to lysis in the sealed Falcon tube.

The Falcon tubes containing frozen cell cultures were thawed for 10 min at 25 ºC and the pelleted cells were then resuspended in lysis buffer (4 mL/1 g of pellet) containing 1 mg/mL lysozyme, 0.07 mg/mL DNAse, and 2 mM $MgCl_2$. The cells were then lysed at 37 ºC and 180 rpm for 1 h. The lysed cultures were then transferred to 2.0-mL microtubes and centrifuged at 20,817 *g* and 4 ºC for 15 min. The supernatant lysates were collected via syringe and passed through a sterile syringe filter (0.20 µm) into 15-mL Falcon tubes. The total volume of each lysate was recorded. The combined lysate was then immersed in a liquid nitrogen bath and allowed to deep freeze for 15 min. The frozen lysate was then lyophilized for 24–48 h. Prior to enzymatic reactions, the lyophilized lysate was then reconstituted in

deionized water to equal the volume noted above. Lyophilized lysate of *C*SilOx3 was reconstituted in half of the volume noted above.

An NADPH cofactor regeneration system (12.5 µL/vessel) then added to 2.0-mL microtubes to give final reaction concentrations of 0.5 mM $NADP^+$, 40 mM glucose-6-phosphate, and 2 U/mL of glucose-6-phosphate dehydrogenase. A 140 mM substrate stock was prepared by dissolving the appropriate substrate in the specified cosolvent (MeCN for **3**, EtOH for **4**). The reconstituted lysate was then added (325 µL/reaction) to the reaction vessel, followed by the substrate (12.5 µL/reaction) to give a final concentration of 5 mM substrate. The microtubes were sealed immediately after the addition of substrate and shaken at 800 rpm for 4 h at 23 ºC. After the 4 h reaction, the reaction vessels were unsealed and 5 mM 1,3,5-trimethoxybenzene in ethyl acetate were added (450 µL/reaction) quickly. The organic and aqueous phases were mixed by using a vortex mixer. Phase separation was facilitated by centrifugation at 20,817 *g* and 4 ºC for 15 min. Aliquots of the organic phase (200–300 µL/reaction) were then transferred to individual 400 µL flat bottom glass inserts in 2-mL screw-cap vials which were sealed with red sil septum screw cap. Analysis was performed using GC/MS with product concentrations and yield determined by response relative to the 5 mM 1,3,5-trimethoxybenzene internal standard using a calibration curve. Hemeprotein concentration was determined by performing a CO-binding assay on the reconstituted lysate.

### A.1.8 Enzymatic Reactions Relevant to Figure 3-2B and Figure 3-2C

All reactions were performed in 2.0-mL snap-cap microtubes on a 350-µL scale with specific conditions are outlined below. After the addition of the appropriate reagents or enzyme, 12.5 µL of substrate stock (140 mM in EtOH) were added to give a final substrate concentration

of 5 mM. After the addition of substrate, the microtubes were rapidly sealed and shaken at 800 rpm at 23 ºC in for 4 h. After 4 h, the reaction vessels were unsealed and 450 µL of a 5 mM 1,3,5-trimethoxybenzene stock in EtOAc were added. The microtubes were sealed, vortexed for 10 sec, and the aqueous and organic phases were separated by centrifugation at 20,817 *g* and 4 ºC for 20 min. If phase separation did not occur after initial centrifugation, the sample was vortexed again for 10 sec and centrifuged for an additional 20 min at 20,817 *g* and 4 ºC. Aliquots of the organic phase (200–300 µL/reaction) were then transferred to individual 400-µL flat bottom glass inserts in 2-mL screw-cap vials which were sealed with red sil septum screw caps. Analysis was then performed using GC/MS with product concentrations determined by response relative to the 1,3,5-trimethoxybenzene internal standard using a calibration curve.

100 mM Tris buffer: The reaction was performed as described above by adding the substrate stock to 325 µL of 100 mM Tris buffer.

*Tm*9D8* (lysate): A culture of *E. coli* harboring *Tm*9D8* was grown and lysed as described above (see section Small-Scale Enzymatic Reactions for Lineage Validation). To the reaction microtube were added 325 µL of the lysate containing *Tm*9D8*and PLP (200 µM in 100 mM Tris pH 7 buffer), 12.5 µL of NADPH regeneration system described above, and substrate.

hemin chloride: With minimum light exposure, a suspension of hemin chloride was freshly prepared by suspending 65.2 mg of hemin chloride in approximately 9.5 mL of 100 mM Tris pH 7 buffer. To the suspension was then added 1 M NaOH dropwise until the hemin chloride was fully dissolved (approx. 150 µL). The solution was then diluted to 10 mL with 100 mM Tris pH 7 buffer. A 100 mM stock was then

prepared by dilution. To the reaction microtube were then added 8.8 µL of the 100 mM hemin chloride and 329 µL of 100 mM Tris buffer pH 7 followed by substrate.

$FeCl_3$: To the reaction microtube were added 7.1 µL of a $FeCl_3$ stock (123.3 mM in 100 mM Tris buffer pH 7), 12.5 µL of NADPH regeneration system described above, and 318 µL of 100 mM Tris pH 7 buffer followed by substrate.

BSA: To the reaction microtube were added 0.9 µL of BSA stock (1 mM in 100 mM Tris buffer pH 7) and 337 µL of 100 mM Tris pH 7 buffer followed by substrate.

BSA/hemin chloride: To the reaction microtube were added 0.9 µL of BSA stock (1 mM in 100 mM Tris buffer pH 7), 8.8 µL of hemin chloride (100 mM in 100 mM Tris buffer pH 7, see above for preparation), and 328 µL of 100 mM Tris pH 7 Tris buffer followed by substrate.

*Tm*9D8* (purified): A frozen aliquot of purified *Tm*9D8* was thawed on ice. To the reaction microtube were added 1.9 µL of purified *Tm*9D8* (471 µM), and 336 µL of 100 mM Tris pH 7 buffer followed by substrate. *Note: purified samples of Tm*9D8**contain the prebound PLP cofactor.*

*E. coli* lysate: A culture of *E. coli* transformed with a pUC19 vector was grown and lysed as described above (see section Small-Scale Enzymatic Reactions for Lineage Validation). To the reaction microtube were added 325 µL of the lysate from this *E. coli culture* and 12.5 µL of 100 mM Tris pH 7 buffer followed by substrate. Separately, this control was also performed using 325 µL of the *E. coli* lysate, 12.5 µL of NADPH regeneration system described above, and substrate.

wild-type $P450_{BM3}$ (purified): Frozen aliquots of purified wild-type $P450_{BM3}$ (93.0 µM) were thawed on ice and a stock of 2.70 µM wild-type $P450_{BM3}$ in 100 mM Tris pH 7 buffer was prepared. To the reaction microtube were added

325 µL of the *L*SilOx4 stock and 12.5 µL of the NADPH regeneration system stock followed by substrate.

*L*SilOx4 (purified): Frozen aliquots of purified lineage enzyme *L*SilOx4 (36.9 µM) were thawed on ice and a stock of 2.70 µM *L*SilOx4 in 100 mM Tris pH 7 buffer was prepared. To the reaction microtube were added 325 µL of the *L*SilOx4 stock and 12.5 µL of the NADPH regeneration system stock followed by substrate.

*L*SilOx4 (heat-treated): Frozen aliquots of purified lineage enzyme *L*SilOx4 (36.9 µM) were thawed on ice and a stock of 2.70 µM *L*SilOx4 in 100 mM Tris pH 7 buffer was prepared. The enzyme stock was then heated in an Eppendorf thermomixer at 100 ºC for 5 min at 300 rpm. To the reaction microtube were added 325 µL of the denatured *L*SilOx4 stock and 12.5 µL of the NADPH regeneration system stock followed by substrate.

**A.2 GC/MS Analytical Methods**

GC/MS analysis was performed to analyze all biocatalytic reactions. Calibration curves were generated using series dilutions of each analyte with 5 mM 1,3,5-trimethoxybenzene as an internal standard. All calibration standards were prepared for individual analytes to prevent speciation. Three replicate injections were acquired for each calibration point. The calibration curves plot analyte response relative to the 5 mM 1,3,5-trimethoxybenzene internal standard response (y-axis) against the ratio of the analyte concentration to the internal standard concentration (x-axis). GC/MS quantification was performed using the Agilent Masshunter Quantitative Analysis software using retention time and 2–4 mass qualifiers with 20% relative mass uncertainty to identify and quantify analytes. Integration was performed using Agile2 integration with peak filtering of 10,000 total ion count.

Analytes identified below this peak integration threshold by retention time and mass fragmentation are reported as trace. Specific parameters for GC/MS and data analysis are outlined below for each analyte.

### A.2.1 Analysis of Hexamethyldisiloxane (1) Biocatalytic Reactions

*GC/MS Method Information*
Column: DB-5MS Ultra Inert, 30 m x 250 µm x 0.25 µm

**Table A-7.** GC/MS oven parameters.

| | Rate (ºC/min) | Value (ºC) | Hold Time (min) |
|---|---|---|---|
| **Initial** | | 50 | 2 |
| **Gradient** | 50 | 300 | 1 |

**Table A-8.** Mass spectrometer parameters (scan mode).

| Solvent Delay (min) | Start Mass (*m*/*z*) | End Mass (*m*/*z*) | Scan Speed (u/s) |
|---|---|---|---|
| 2.00 | 50 | 300 | 3.125 |

**Table A-9.** Summary of analytes.

| Analyte | Retention Time (min) | Qualifier Ions (*m*/*z*) (relative abundance) |
|---|---|---|
| Carbinol **4** | 4.01 | 147.0 (100), 135.0 (23.4), 118.9 (18.1), 163.0 (15.7) |
| Silanol **5** | 3.12 | 149.1 (100), 133.0 (84.7), 75.1 (10.0) |

**Figure A-1.** Representative gas chromatogram and EI mass spectrum of a 0.482 mM sample of carbinol **4** with 5 mM 1,3,5-trimethoxybenzene. *Note: the peak present at 2.491 min corresponds to ethyl propionate, an impurity present in EtOAc.*

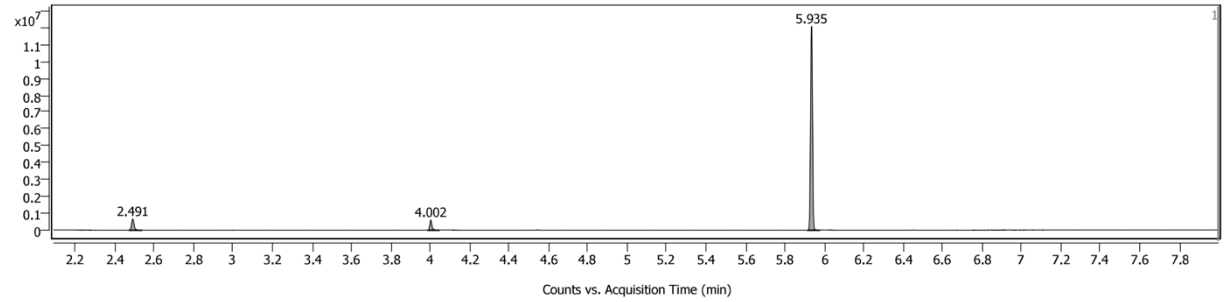


*Chromatogram Peaks*

| Peak | Start | RT | End | Height | Area | Area % | SNR |
|---|---|---|---|---|---|---|---|
| 1 | 2.470 | 2.491 | 2.540 | 659332 | 590289 | 6.77 | |
| 2 | 3.985 | 4.002 | 4.045 | 609211 | 470780 | 5.40 | |
| 3 | 5.916 | 5.935 | 5.975 | 12069331 | 8719742 | 100.00 | |

**Sample Spectra**

**+ Scan (rt: 3.958-4.072 min)**

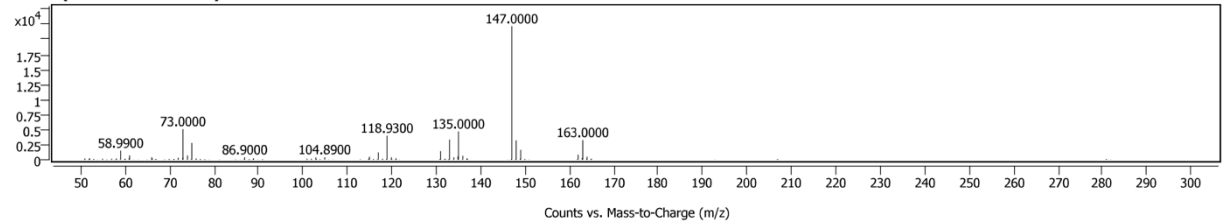

**Figure A-2.** Calibration curve for carbinol **4**.

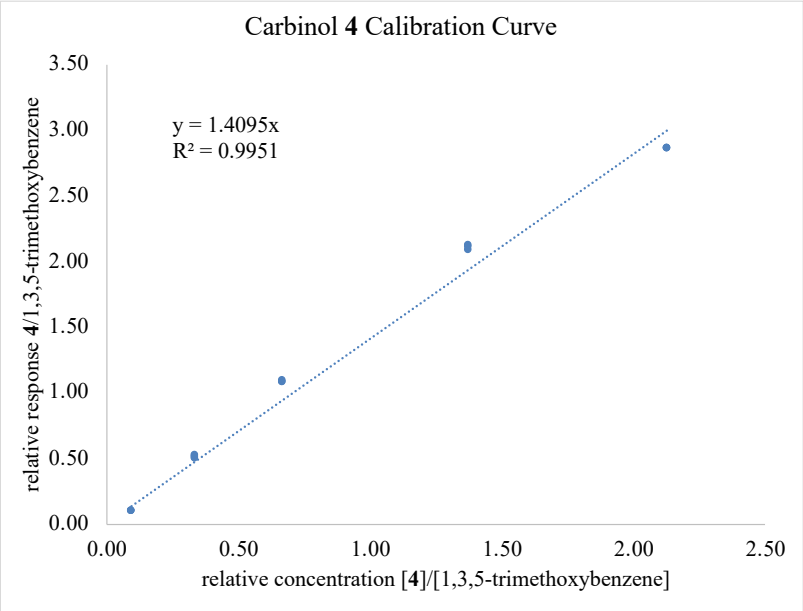


**Figure A-3.** Representative gas chromatogram and EI mass spectrum of a 0.341 mM sample of silanol **5** with 5 mM 1,3,5-trimethoxybenzene. *Note: the peak present at 2.514 min corresponds to ethyl propionate, an impurity present in EtOAc.*

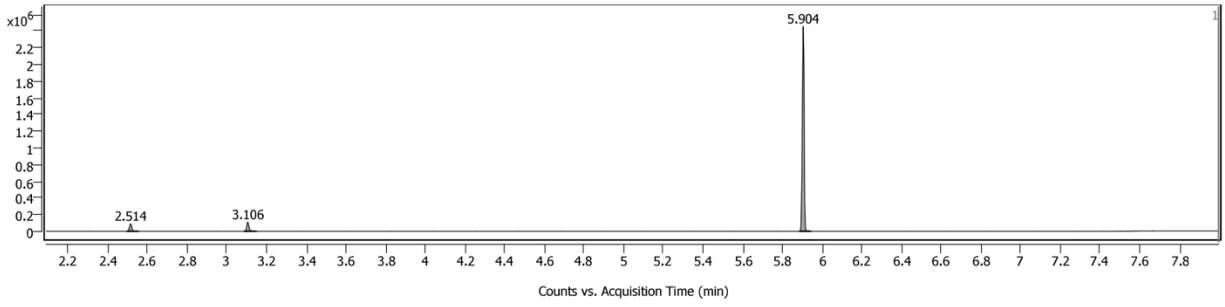


*Chromatogram Peaks*

| Peak | Start | RT | End | Height | Area | Area % | SNR |
|---|---|---|---|---|---|---|---|
| 1 | 2.494 | 2.514 | 2.557 | 90644 | 75401 | 4.76 | |
| 2 | 3.084 | 3.106 | 3.148 | 108972 | 91616 | 5.78 | |
| 3 | 5.887 | 5.904 | 5.943 | 2454124 | 1585143 | 100.00 | |

**Sample Spectra**

**+ Scan (rt: 3.051-3.165 min)**

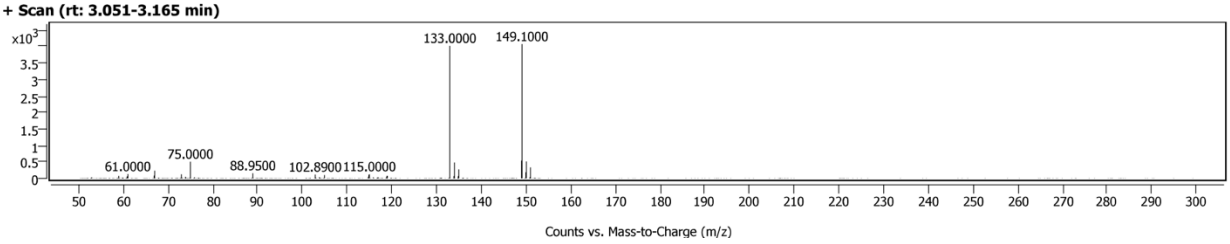

**Figure A-4.** Calibration curve for silanol **5**.

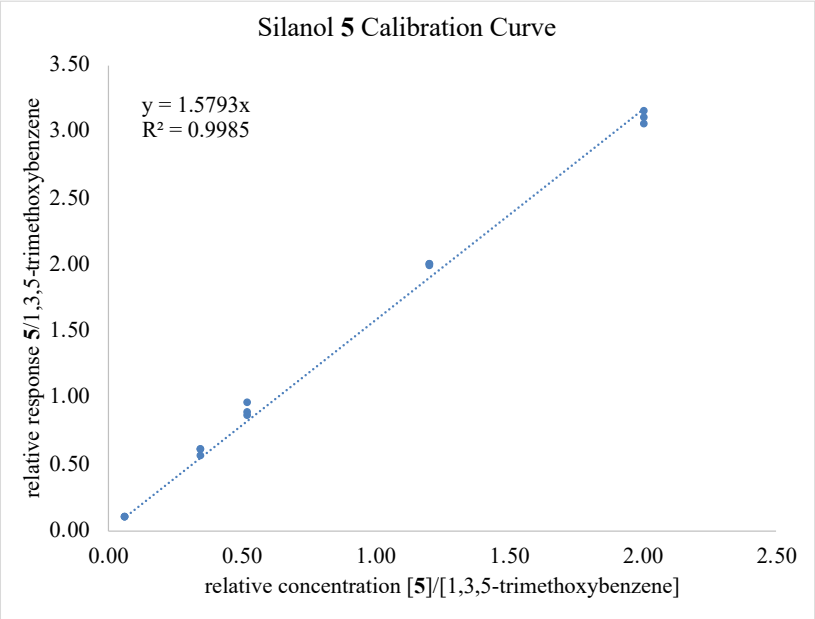


### A.2.2 Analysis of Octamethyltrisiloxane (2) Biocatalytic Reactions

*GC/MS Method Information*
Column: DB-5MS Ultra Inert, 30 m x 250 µm x 0.25 µm

**Table A-10.** GC/MS oven parameters.

| | Rate (ºC/min) | Value (ºC) | Hold Time (min) |
|---|---|---|---|
| **Initial** | | 50 | 1 |
| **Gradient 1** | 60 | 120 | 1 |
| **Gradient 2** | 60 | 300 | 1 |

**Table A-11.** Mass spectrometer parameters (scan mode).

| Solvent Delay (min) | Start Mass (*m*/*z*) | End Mass (*m*/*z*) | Scan Speed (u/s) |
|---|---|---|---|
| 2.2 | 50 | 350 | 3.125 |

**Table A-12.** Summary of analytes.

| Analyte | Retention Time (min) | Qualifier Ions (*m*/*z*) (relative abundance) |
|---|---|---|
| Carbinol **9** | 4.10 | 193.1 (100), 221.1 (64.7) |
| Silanol **10** | 3.40 | 207.1 (100), 223.1 (23.1) |
| Carbinol **11** | 4.04 | 193.0 (100), 221.0 (64.3), 237.0 (16.2) |
| Silanol **12** | 3.42 | 207.1 (100), 223.1 (23.8) |
| Silanol **5** | 2.45 | 149.1 (100), 133.0 (86.2), 75.1 (10.6) |

**Figure A-5.** Representative gas chromatogram and EI mass spectrum of a 0.328 mM sample of carbinol **9** with 5 mM 1,3,5-trimethoxybenzene.

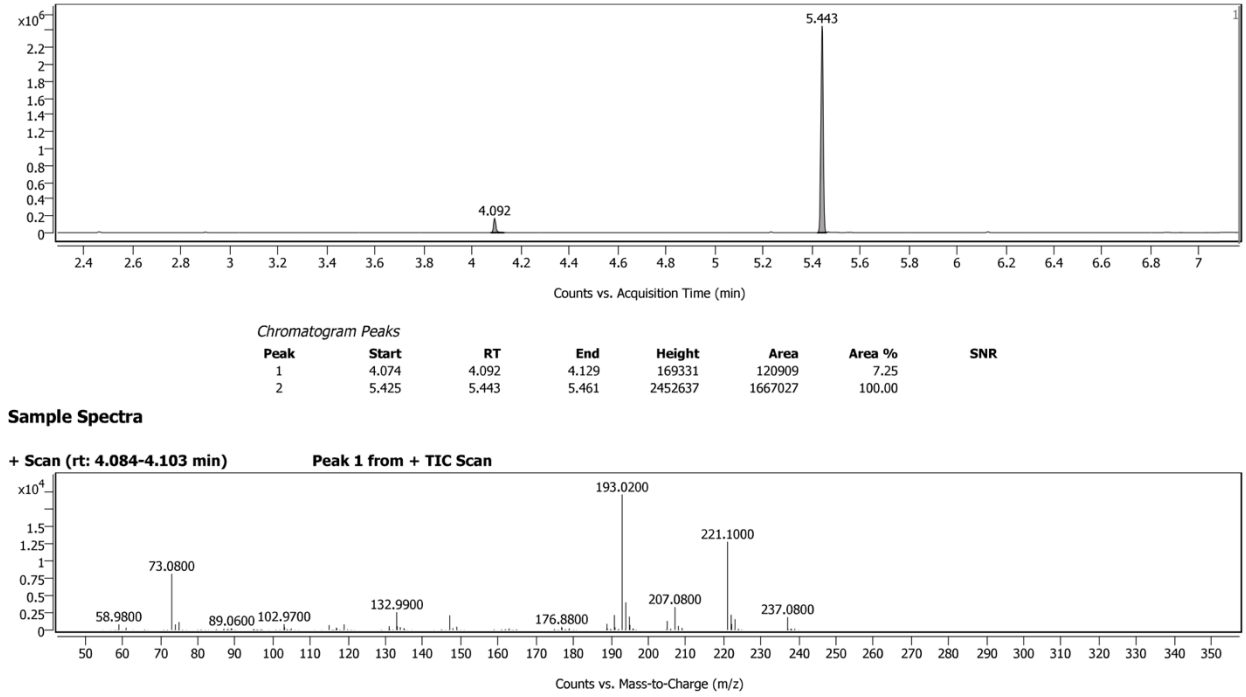


**Figure A-6.** Calibration curve for carbinol **9**.

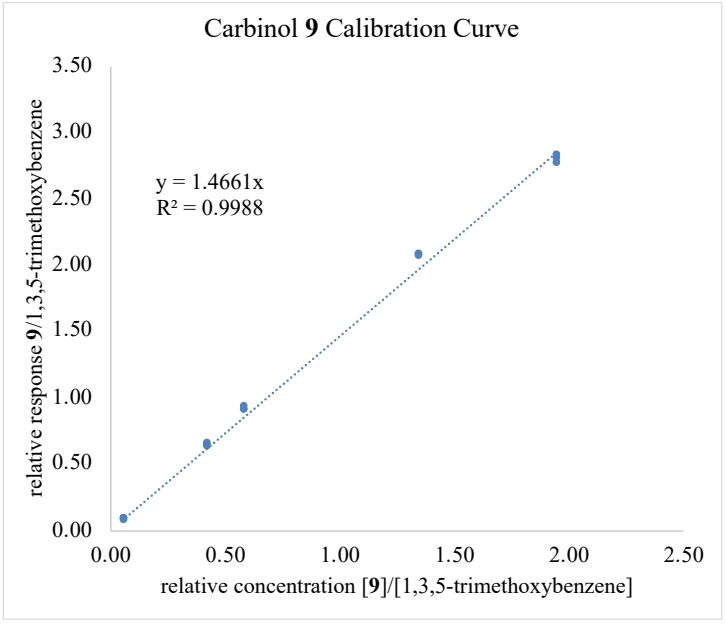

**Figure A-7.** Representative gas chromatogram and EI mass spectrum of a 0.436 mM sample of silanol **10** with 5 mM 1,3,5-trimethoxybenzene.

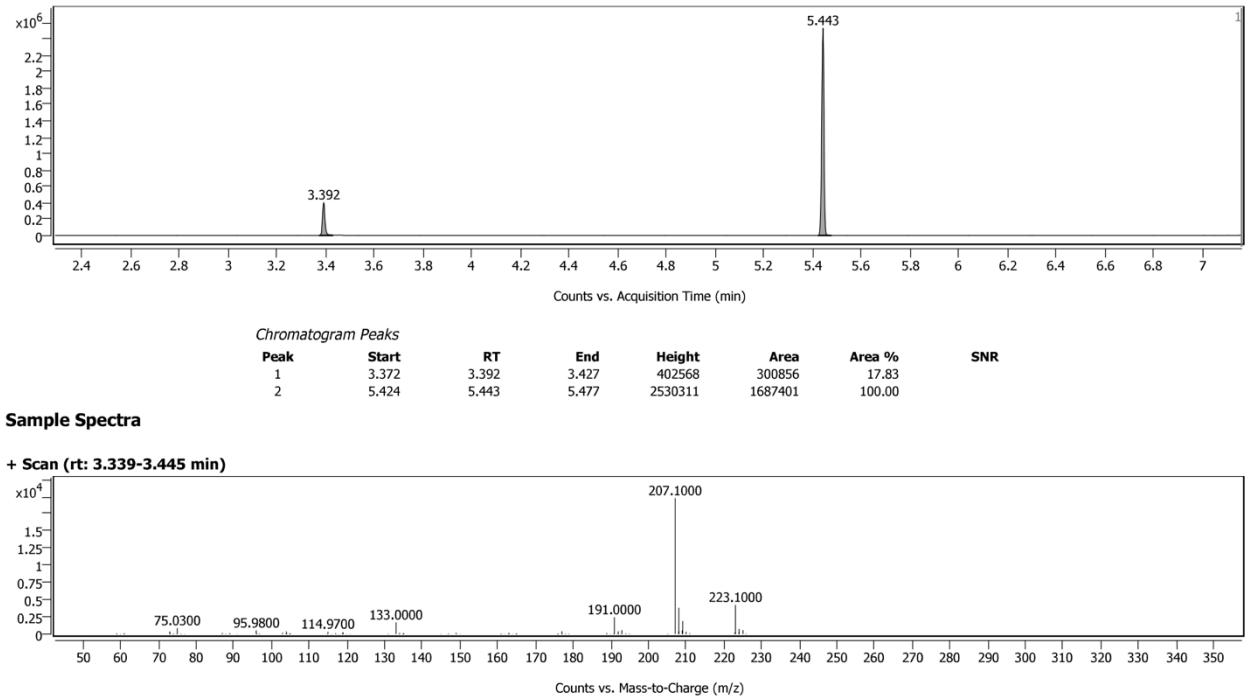


**Figure A-8.** Calibration curve for silanol **10**.

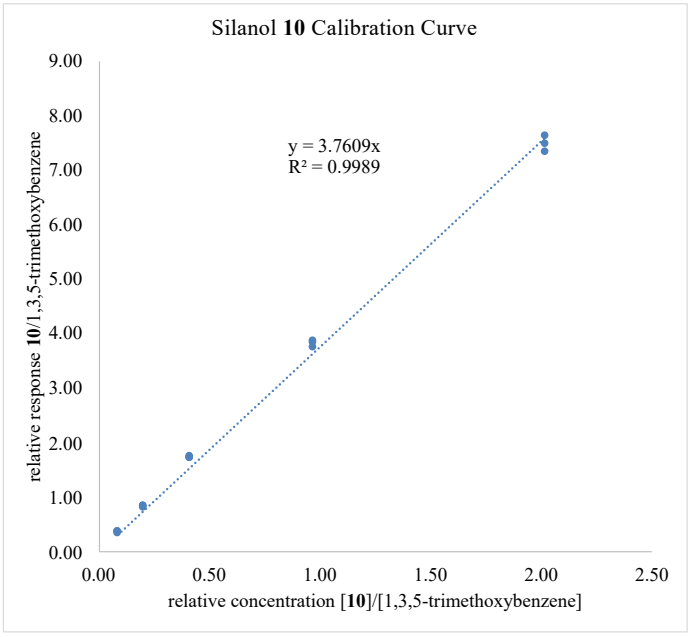

**Figure A-9.** Representative gas chromatogram and EI mass spectrum of carbinol **11**.

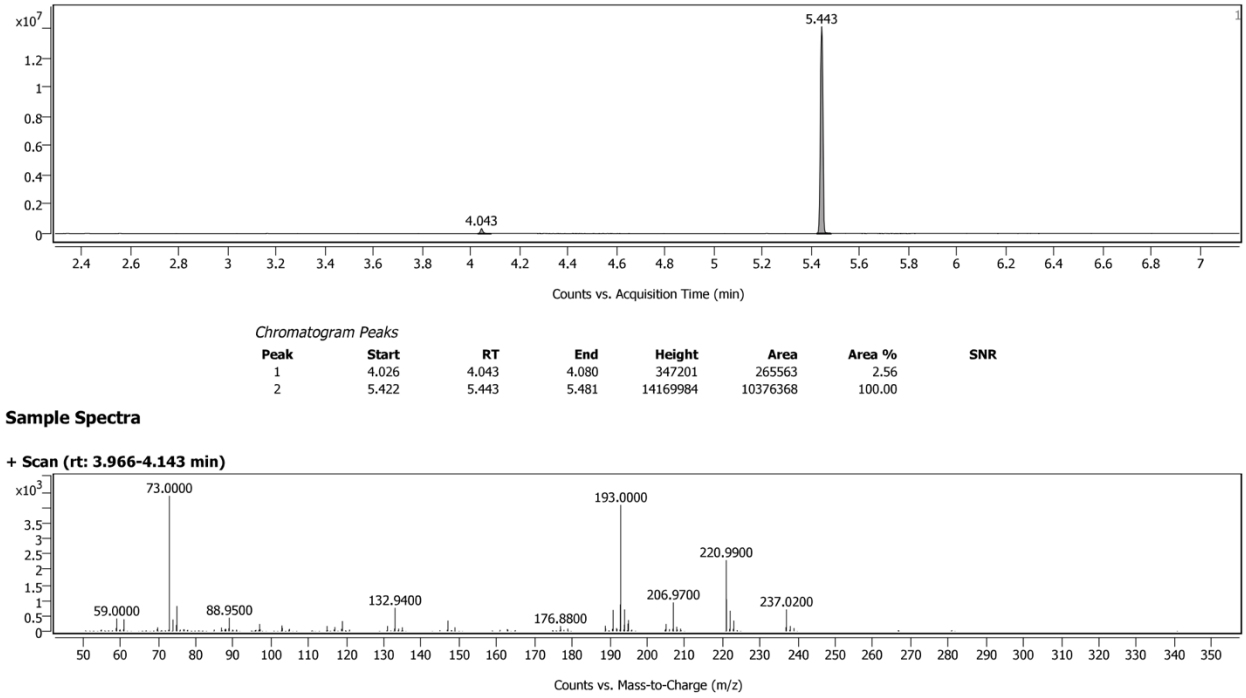


**Figure A-10.** Calibration curve for carbinol **11**.

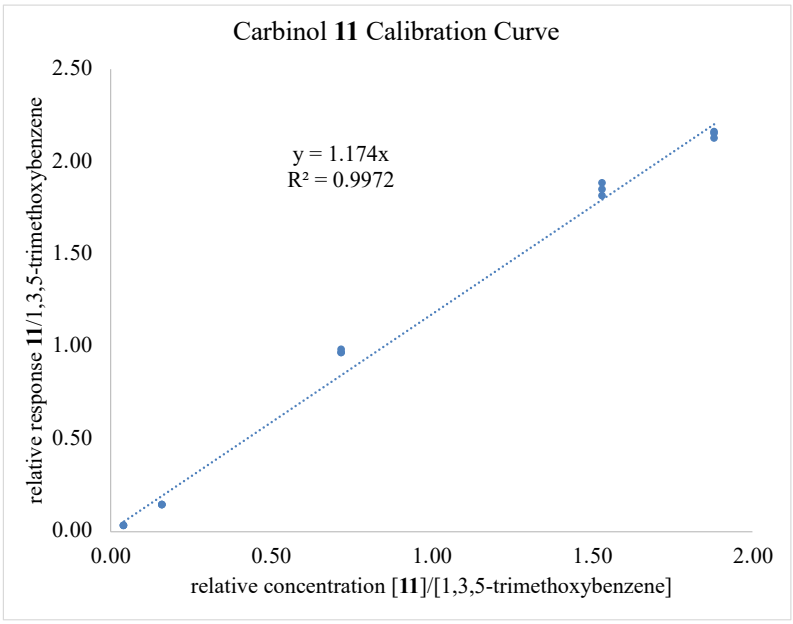

**Figure A-11.** Representative gas chromatogram and EI mass spectrum of a 0.394 mM sample of silanol **12** with 1,3,5-trimethoxybenzene.

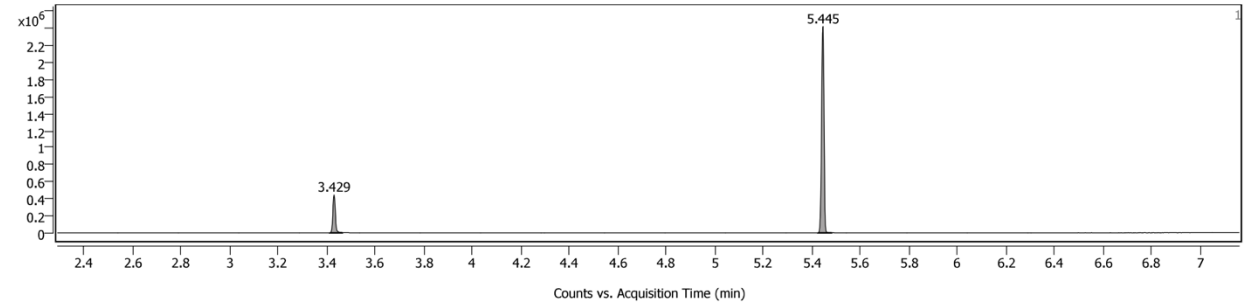


*Chromatogram Peaks*

| Peak | Start | RT | End | Height | Area | Area % | SNR |
|---|---|---|---|---|---|---|---|
| 1 | 3.411 | 3.429 | 3.462 | 447844 | 326991 | 19.57 | |
| 2 | 5.424 | 5.445 | 5.480 | 2422153 | 1670799 | 100.00 | |

**Sample Spectra**

**+ Scan (rt: 3.380-3.482 min)**

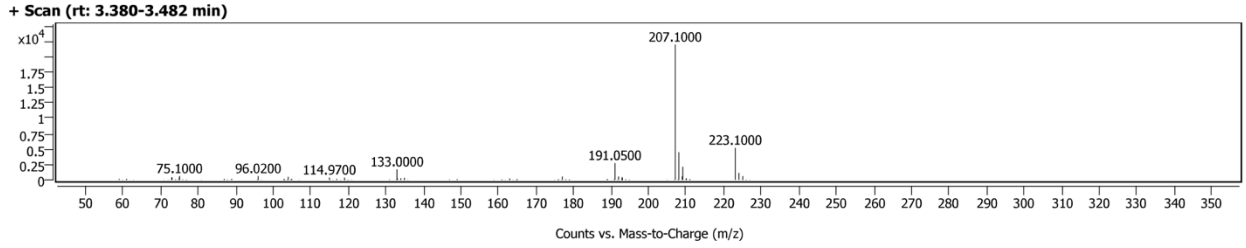


**Figure A-12.** Calibration curve for silanol **12**.

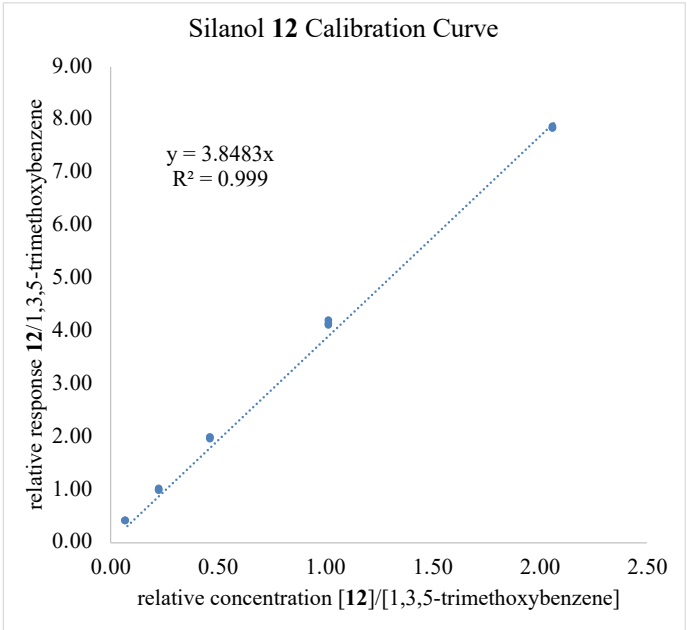

**Figure A-13.** Representative gas chromatogram and EI mass spectrum of a 0.341 mM sample of silanol **5** with 5 mM 1,3,5-trimethoxybenzene.

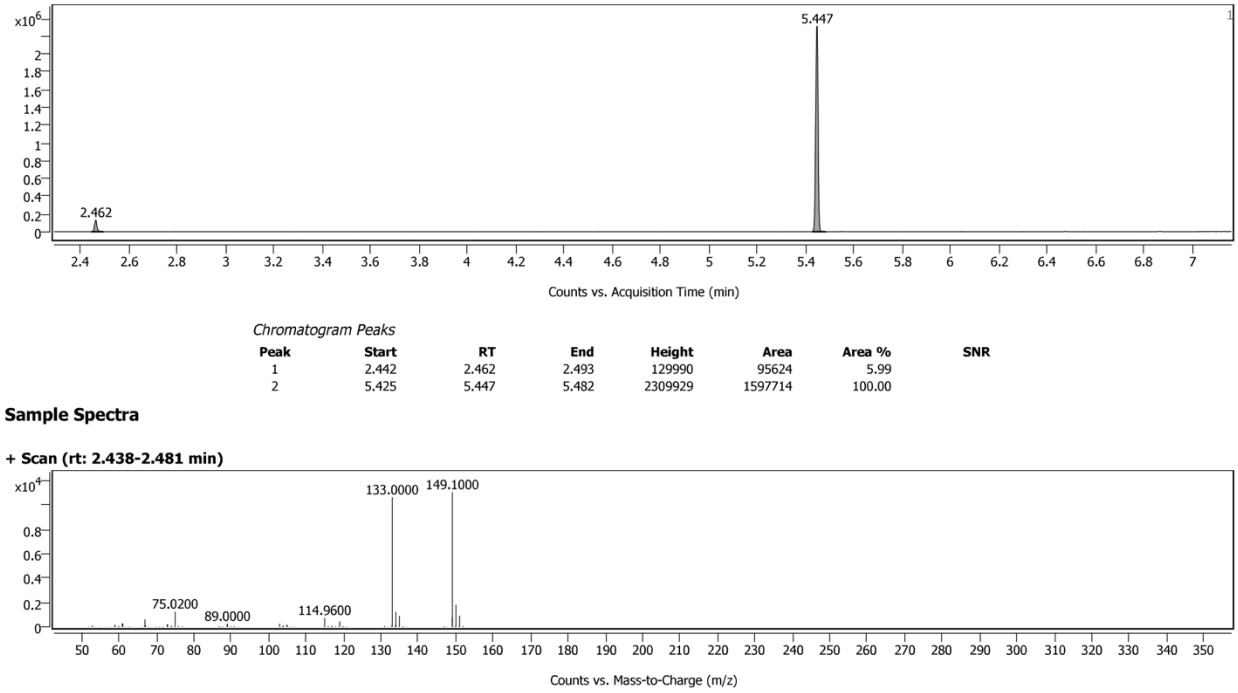


**Figure A-14.** Calibration curve for silanol **5**.

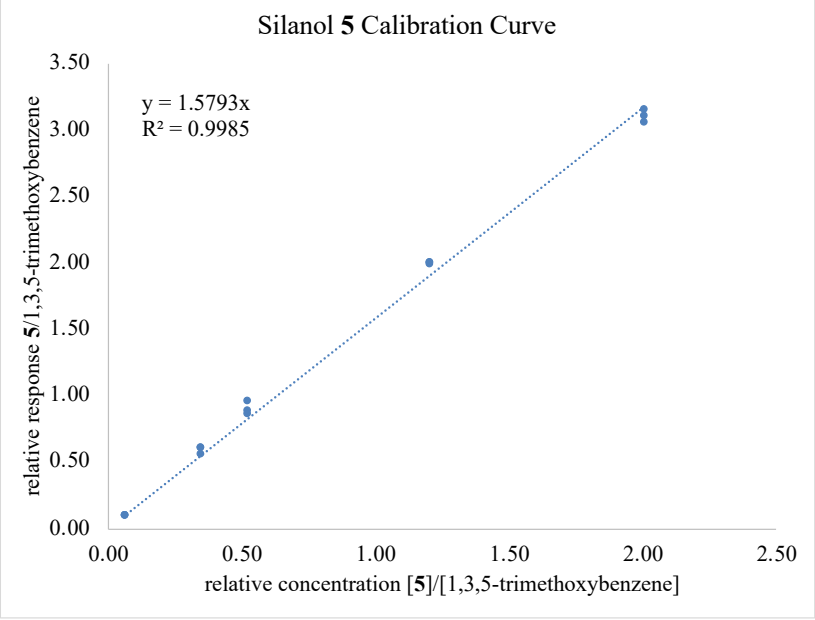

### A.2.3 Analysis of Octamethylcyclotetrasiloxane (3) Biocatalytic Reactions

*GC/MS Method Information*
Column: DB-5MS Ultra Inert, 30 m x 250 µm x 0.25 µm

**Table A-13.** GC/MS oven parameters.

| | Rate (ºC/min) | Value (ºC) | Hold Time (min) |
|---|---|---|---|
| **Initial** | | 120 | 0 |
| **Gradient** | 75 | 300 | 1.2 |

**Table A-14.** Mass spectrometer parameters (scan mode).

| Solvent Delay (min) | Start Mass (*m*/*z*) | End Mass (*m*/*z*) | Scan Speed (u/s) |
|---|---|---|---|
| 1.30 | 50 | 350 | 3.125 |

**Table A-15.** Summary of analytes.

| Analyte | Retention Time (min) | Qualifier Ions (*m*/*z*) (relative abundance) |
|---|---|---|
| Carbinol **13** | 1.87 | 281.2 (100), 253.1 (69.6), 193.1 (21.0), 264.8 (12.1) |
| Silanol **14** | 1.66 | 267.1 (100), 251.0 (15.9), 283.1 (13.7), 193.0 (12.9) |

**Figure A-15.** Representative gas chromatogram and EI mass spectrum of a 0.320 mM sample of carbinol **13** with 5 mM 1,3,5-trimethoxybenzene.

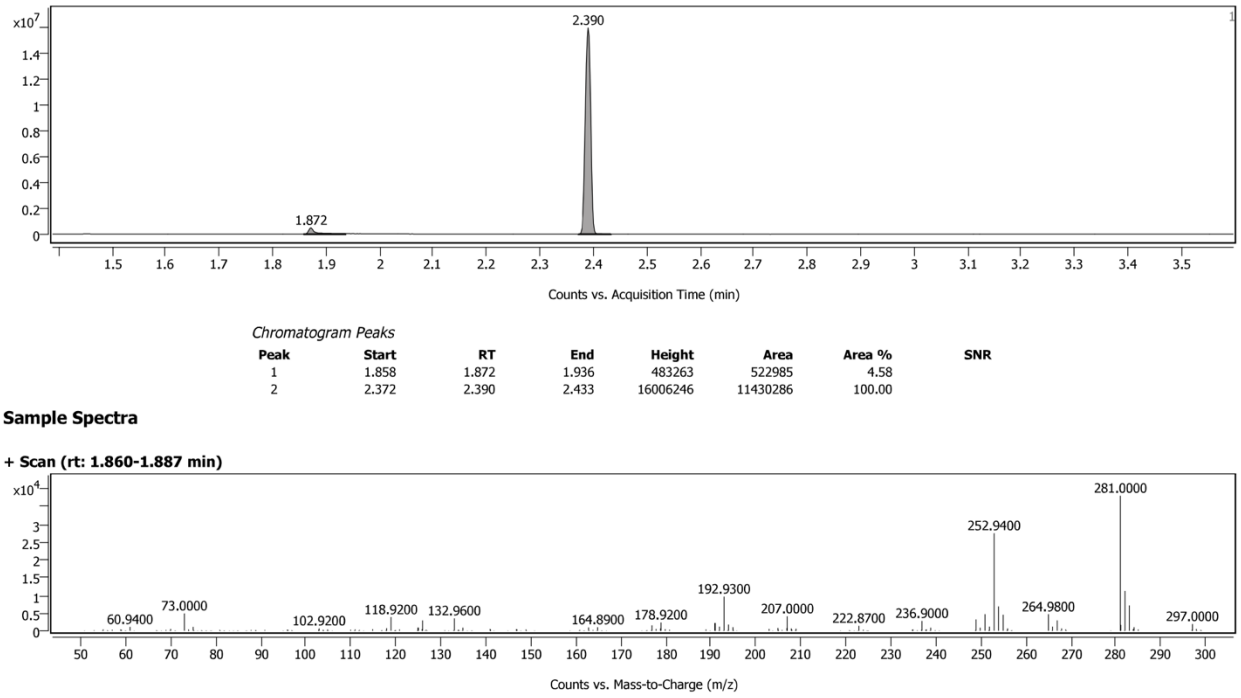

**Figure A-16.** Calibration curve for carbinol **13**.

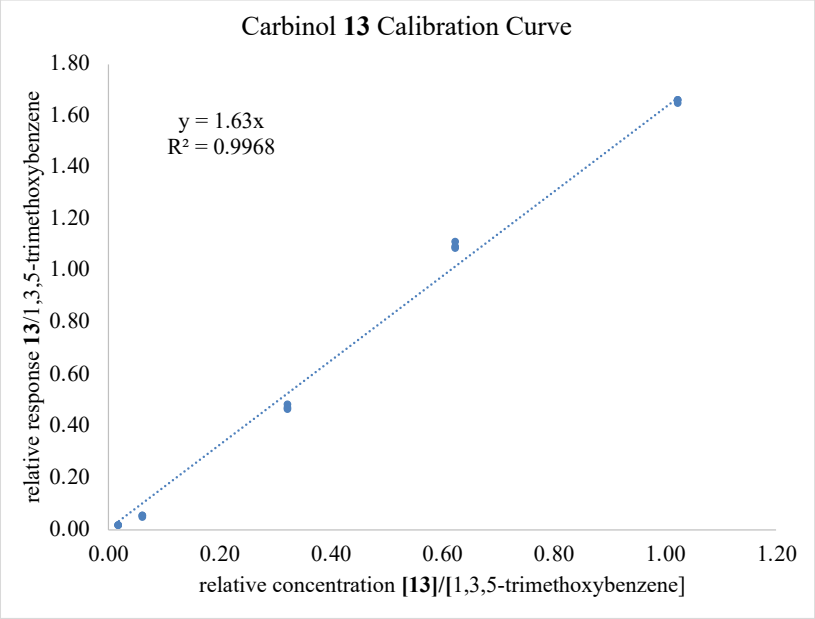


**Figure A-17.** Representative gas chromatogram and EI mass spectrum of a 0.362 mM sample of silanol **14** with 5 mM 1,3,5-trimethoxybenzene.

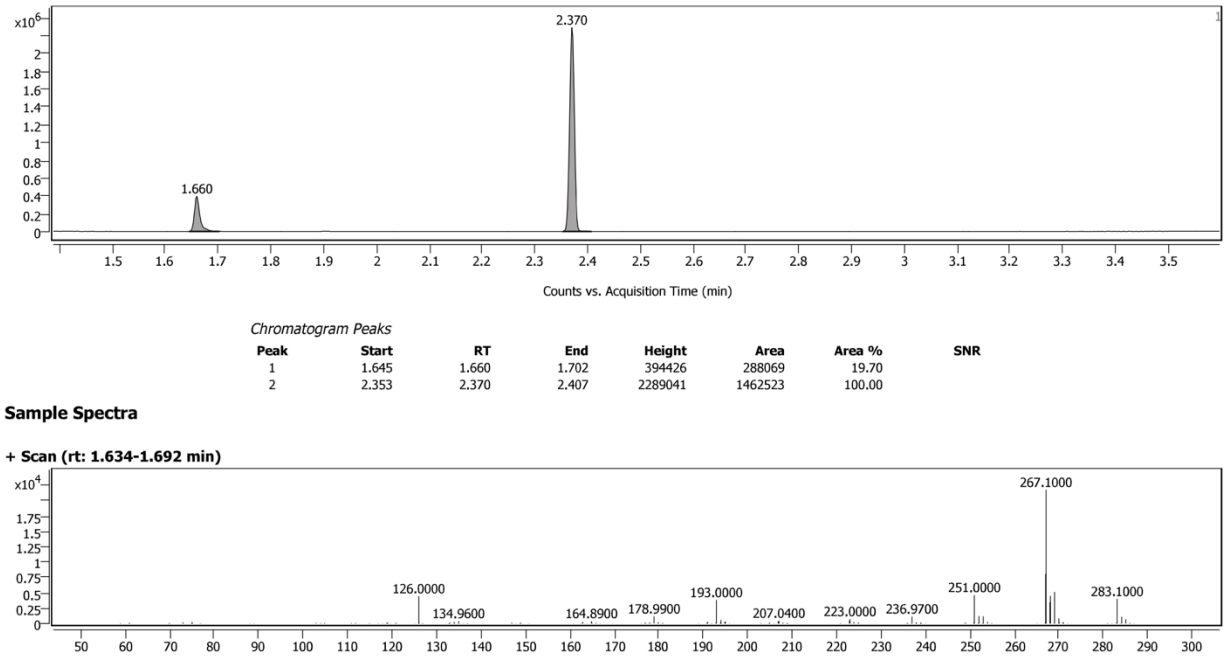

**Figure A-18.** Calibration curve for silanol **14**.

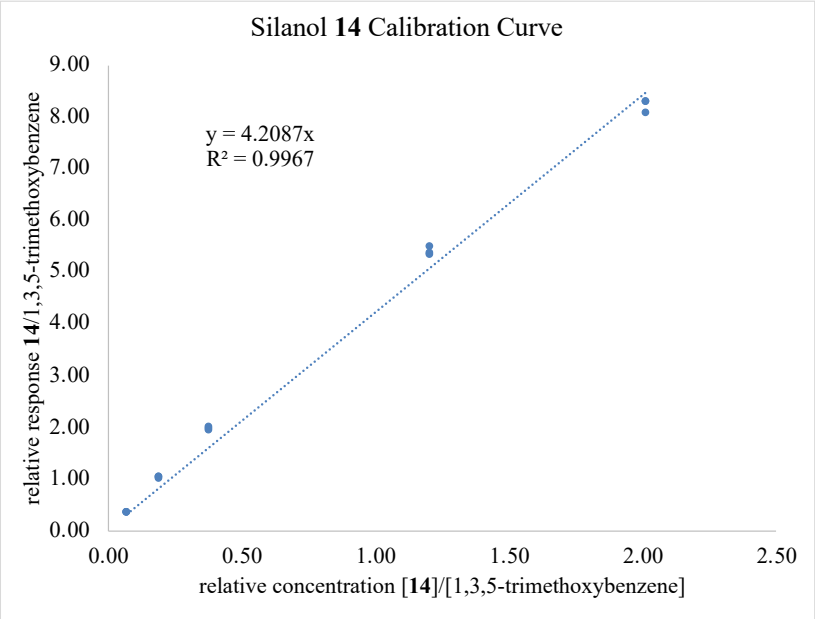


## A.3 Experimental Data Relevant to Figures

**Table A-16.** Summary of enzyme lineage for hexamethyldisiloxane (**1**).

| Variant | Mutations from Parent | Method of Mutagenesis |
|---|---|---|
| *L*SilOx1 | – | |
| *L*SilOx2 | T327M, A328F | dSSM (327X, 328X) |
| *L*SilOx3 | D34G, I122T | epPCR and StEP recombination |
| *L*SilOx4 | G252E | StEP recombination |
| *L*SilOx4 *(lyophilized)* | – | |

**Table A-17.** Experimental data relevant to Figure 3-2A.

| **Variant** | [enzyme] (μM) | [carbinol **4**] (μM) | [silanol **5**] (μM) | total product concentration / enzyme concentration |
|---|---|---|---|---|
| wild-type $P450_{BM3}$ | 4.63 | 0 | 0 | 0 |
| | 4.63 | 0 | 0 | 0 |
| | 4.63 | 0 | 0 | 0 |
| *L*SilOx1 | 4.76 | trace | 86.1 | 18.1 |
| | 4.76 | trace | 86.1 | 18.1 |
| | 4.76 | trace | 85.5 | 18.0 |
| *L*SilOx2 | 3.83 | trace | 150 | 39.1 |
| | 3.83 | trace | 136 | 35.4 |
| | 3.83 | trace | 141 | 36.8 |
| *L*SilOx3 | 1.72 | trace | 74.6 | 43.4 |
| | 1.72 | trace | 79.3 | 46.1 |
| | 1.72 | trace | 78.8 | 45.8 |
| *L*SilOx4 | 2.59 | trace | 136 | 52.5 |
| | 2.59 | trace | 132 | 51.0 |
| | 2.59 | trace | 126 | 48.5 |
| *L*SilOx4 *(lyophilized)* | 7.26 | 24.5 | 231 | 35.2 |
| | 7.26 | 23.2 | 218 | 33.3 |
| | 7.26 | 17.1 | 214 | 31.8 |

**Figure A-19**. Representative example of trace carbinol **5** detected in a biocatalytic reaction with *L*SilOx4 with ions 147.0, 135.0, 118.8, and 162.9.

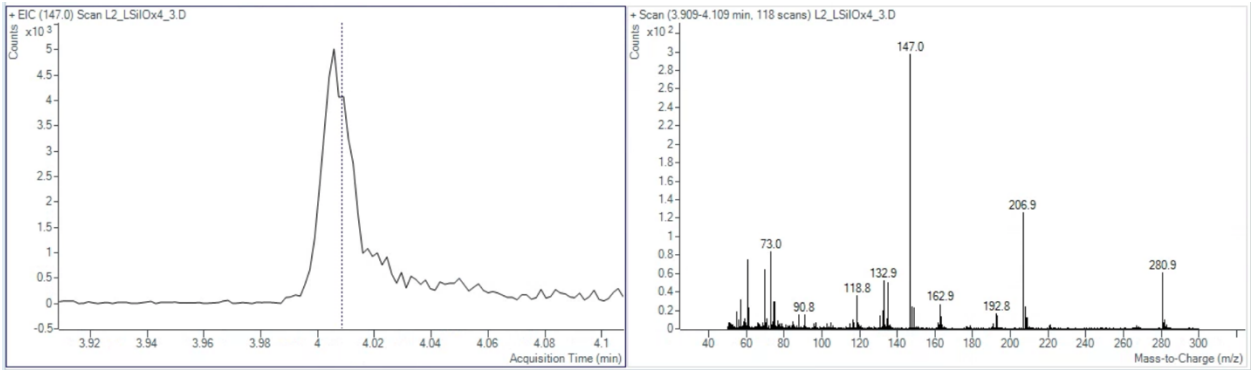

**Table A-18.** Experimental data relevant to Figure 3-2B.

| **Reaction Conditions** | [carbinol **4**] (μM) | [silanol **5**] (μM) |
|---|---|---|
| 100 mM Tris pH 7 buffer | 0 | 0 |
| | 0 | 0 |
| | 0 | 0 |
| *Tm*9D8* (lysate) | 0 | 0 |
| | 0 | 0 |
| | 0 | 0 |
| 2.5 μM hemin chloride | 0 | 0 |
| | 0 | 0 |
| | 0 | 0 |
| 2.5 μM $FeCl_3$ | 0 | 0 |
| | 0 | 0 |
| | 0 | 0 |
| 2.5 μM BSA[b] | 0 | 0 |
| | 0 | 0 |
| | 0 | 0 |
| 2.5 μM BSA and hemin chloride[b] | 0 | 0 |
| | 0 | 0 |
| | 0 | 0 |
| 2.5 μM *Tm*9D8*[a,b] | 0 | 0 |
| | 0 | 0 |
| 2.5 μM PLP[b] | 0 | 0 |
| | 0 | 0 |
| | 0 | 0 |
| *E. coli* lysate[b] | 0 | 0 |
| | 0 | 0 |
| *E. coli* lysate | 0 | 0 |
| | 0 | 0 |
| 2.5 μM wild-type $P450_{BM3}$[a] | 0 | 0 |
| | 0 | 0 |
| | 0 | 0 |
| 2.5 μM *L*SilOx4[a] | trace | 38.2 |
| | trace | 32.1 |
| | trace | 32.1 |
| 2.5 μM *L*SilOx4 (heat-treated)[a] | 0 | 0 |
| | 0 | 0 |
| | 0 | 0 |

[a]Purified protein. [b]NADPH regeneration system not added.

**Table A-19.** Experimental data relevant to Figure 3-2C.

| **Reaction Conditions** | [silanol **5**] (μM) |
|---|---|
| 100 mM Tris pH 7 buffer | 0 |
| | 0 |
| | 0 |
| *Tm*9D8* (lysate) | 0 |
| | 0 |
| | 0 |
| 2.5 μM hemin chloride | 0 |
| | 0 |
| | 0 |
| 2.5 μM $FeCl_3$ | 0 |
| | 0 |
| | 0 |
| 2.5 μM BSA[b] | 0 |
| | 0 |
| | 0 |
| 2.5 μM BSA and hemin chloride[b] | 0 |
| | 0 |
| | 0 |
| 2.5 μM *Tm*9D8*[a,b] | 0 |
| | 0 |
| 2.5 μM PLP[b] | 0 |
| | 0 |
| | 0 |
| *E. coli* lysate[b] | 0 |
| | 0 |
| *E. coli* lysate | 0 |
| | 0 |
| 2.5 μM wild-type $P450_{BM3}$[a] | 69.5 |
| | 69.5 |
| | 59.2 |
| 2.5 μM *L*SilOx4[a] | 169 |
| | 135 |
| | 180 |
| 2.5 μM *L*SilOx4 (heat-treated)[a] | 0 |
| | 0 |
| | 0 |

[a]Purified protein. [b]NADPH regeneration system not added.

**Table A-20.** Summary of enzyme lineage for octamethyltrisiloxane (**2**).

| Variant | Mutations from Parent | Method of Mutagenesis |
|---|---|---|
| *L*SilOx4 | – | – |
| *L*SilOx5 | F328S | epPCR |
| *L*SilOx6 | F165L | epPCR, then StEP recombination |
| *L*SilOx7 | Y51V, V184M | SSM of sites F42, R47, Y51, A78, G87, L181, V184, A330, then StEP recombination |

**Table A-21.** Experimental data relevant to Figure 3-3A. *Note: carbinol **11** and silanol **12** were not detected in any reactions and are therefore omitted from the table for clarity.*

| Variant | [enzyme] (μM) | [carbinol **9**] (μM) | [silanol **10**] (μM) | [silanol **5**] (μM) | $\frac{\text{total product concentration}}{\text{enzyme concentration}}$ |
|---|---|---|---|---|---|
| *L*SilOx4 | 11.0 | trace | 53.9 | trace | 4.90 |
| | 11.0 | trace | 41.7 | trace | 3.79 |
| | 11.0 | trace | 27.8 | trace | 2.52 |
| | 11.0 | trace | 34.7 | trace | 3.16 |
| | 11.0 | trace | 29.7 | trace | 2.70 |
| *L*SilOx5 | 9.20 | trace | 66.5 | 23.8 | 9.82 |
| | 9.20 | trace | 51.9 | 17.3 | 7.52 |
| | 9.20 | trace | 62.4 | 23.9 | 9.38 |
| | 9.20 | trace | 59.4 | 22.5 | 8.91 |
| | 9.20 | trace | 56.4 | 25.1 | 8.86 |
| *L*SilOx6 | 8.16 | trace | 90.3 | 31.4 | 14.9 |
| | 8.16 | trace | 83.2 | 28.6 | 13.7 |
| | 8.16 | trace | 66.2 | 21.2 | 10.7 |
| | 8.16 | trace | 74.8 | 23.4 | 12.0 |
| | 8.16 | trace | 66.3 | 26.6 | 11.4 |
| *L*SilOx7 | 4.47 | trace | 144 | 41.0 | 41.5 |
| | 4.47 | trace | 141 | 42.5 | 41.1 |
| | 4.47 | trace | 112 | 34.7 | 32.9 |
| | 4.47 | trace | 114 | 39.9 | 34.4 |
| | 4.47 | trace | 91.9 | 29.8 | 27.2 |
| *L*SilOx7 *(lyophilized)* | 3.09 | trace | 65.0 | trace | 21.0 |
| | 3.09 | trace | 59.2 | trace | 19.2 |
| | 3.09 | trace | 59.0 | trace | 19.1 |

**Figure A-20.** Representative example of trace carbinol **9** detected in a biocatalytic reaction with *L*SilOx7 with ions 192.9 and 221.0.

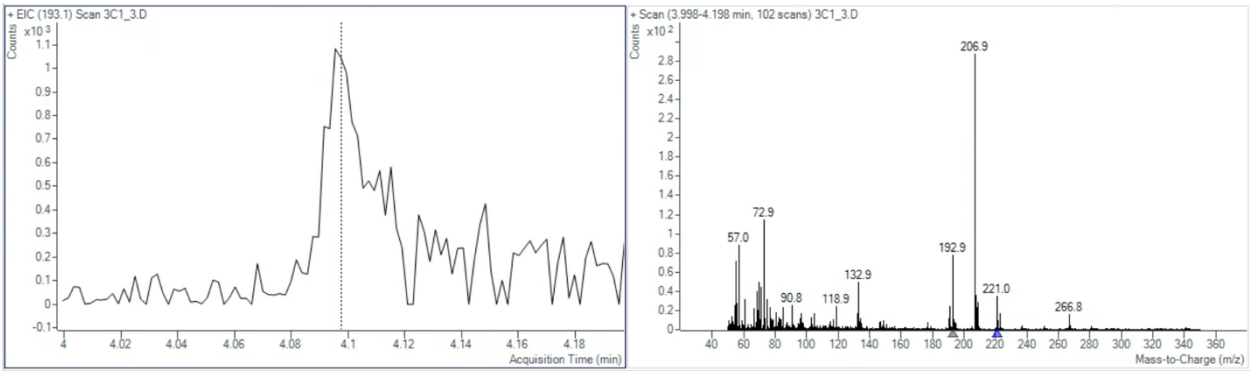


**Figure A-21.** Representative example of trace silanol **5** detected in a biocatalytic reaction with *L*SilOx4 with ions 149.0 and 132.9.

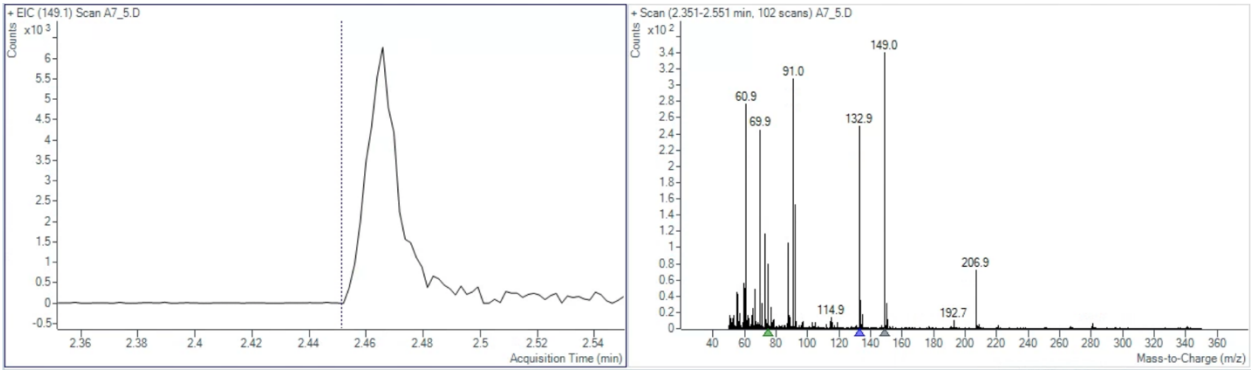


**Table A-22.** Summary of enzyme lineage for octamethylcyclotetrasiloxane (**3**).

| Leading Variant | Mutations from Parent | Method of Mutagenesis |
|---|---|---|
| *L*SilOx5 | – | – |
| *C*SilOx | N95S, D214G, T438S | epPCR, then StEP recombination |
| *C*SilOx2 | S72G, G85A | epPCR, then targeted recombination |
| *C*SilOx3 | R47G | epPCR and SSM of sites F42, R47, Y51, A78, G87, L181, V184, A330, then StEP recombination |

**Table A-23.** Experimental data relevant to Figure 3-3C.

| **Leading Variant** | [enzyme] (μM) | [carbinol **13**] (μM) | [silanol **14**] (μM) | $\frac{\text{total product concentration}}{\text{enzyme concentration}}$ |
|---|---|---|---|---|
| *L*SilOx5 | 4.20 | trace | 11.6 | 2.77 |
| | 4.20 | trace | 8.78 | 2.09 |
| | 4.20 | trace | 9.14 | 2.18 |
| | 4.20 | trace | 7.92 | 1.89 |
| | 4.20 | trace | 8.97 | 2.14 |
| *C*SilOx1 | 5.82 | trace | 37.5 | 6.44 |
| | 5.82 | trace | 27.6 | 4.74 |
| | 5.82 | trace | 27.4 | 4.70 |
| | 5.82 | trace | 24.0 | 4.13 |
| | 5.82 | trace | 24.9 | 4.28 |
| *C*SilOx2 | 2.38 | trace | 32.0 | 13.4 |
| | 2.38 | trace | 20.6 | 8.64 |
| | 2.38 | trace | 33.0 | 13.9 |
| | 2.38 | trace | 32.1 | 13.5 |
| | 2.38 | trace | 37.8 | 15.9 |
| *C*SilOx3 | 0.36 | trace | 12.1 | 33.6 |
| | 0.36 | trace | 8.99 | 25.0 |
| | 0.36 | trace | 11.2 | 31.2 |
| | 0.36 | trace | 12.8 | 35.5 |
| | 0.36 | trace | 10.1 | 28.1 |
| *C*SilOx3 *(lyophilized)* | 1.10 | trace | 18.6 | 16.9 |
| | 1.10 | trace | 19.0 | 17.3 |
| | 1.10 | trace | 19.2 | 17.4 |

**Figure A-22.** Representative example of trace carbinol **13** detected with *C*SilOx2 with ions 281.1, 252.9, and 265.1.

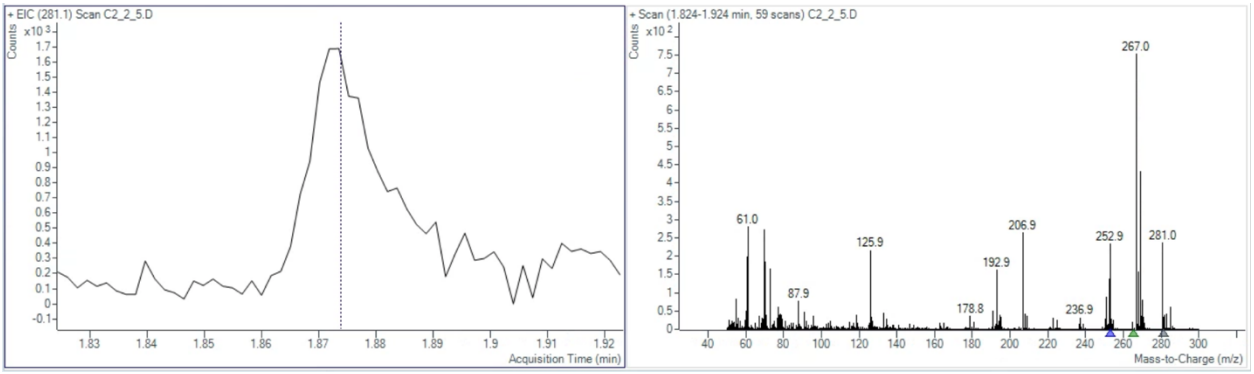


## A.4 DNA Sequences of Engineered Enzymes

### DNA Sequence of *L*SilOx1

ACAATTAAAGAAATGCCTCAGCCAAAAACGTTTGGAGAGCTTAAAAATTTACC
GTTATTAAACACAGATAAACCGGTTCAAGCTTTGATGAAAATTGCGGATGAAT
TAGGAGAAATCTTTAAATTCGAGGCGCCTGGTCGTGTAACGCGCTACTTATCA
AGTCAGCGTCTAATTAAAGAAGCATGCGATGAATCACGCTTTGATAAAAACTT
AAGTCAAGCGCTTAAATTTGCACGTGATTTTGTTGGAGACGGGTTAGGTACAA
GCTGGACGCATGAAAAAAATTGGAAAAAAGCGCATAATATCTTACTTCCAAG
CTTTAGTCAGCAGGCAATGAAAGGCTATCATGCGATGATGGTCGATATCGCCG
TGCAGCTTGTTCAAAAGTGGGAGCGTCTAAATGCAGATGAGCATATTGAAGTA
TCGGAAGACATGACACGTTTAACGCTTGATACAATTGGTCTTTGCGGCTTTAA
CTATCGCTTTAACAGCTTTTACCGAGATCAGCCTCATCCATTTATTATAAGTAT
GGTCCGTGCACTGGATGAAGTAATGAACAAGCTGCAGCGAGCAAATCCAGAC
GACCCAGCTTATGATGAAAACAAGCGCCAGTTTCAAGAAGATATCAAGGTGA
TGAACGACCTAGTAGATAAAATTATTGCAGATCGCAAAGCAAGGGGTGAACA
AAGCGATGATTTATTAACGCAGATGCTAAACGGAAAAGATCCAGAAACGGGT
GAGCCGCTTGATGACGGGAACATTCGCTATCAAATTATTACATTCTTAATTGC
GGGACACGAAACAACAAGTGGTCTTTTATCATTTGCGCTGTATTTCTTAGTGA
AAAATCCACATGTATTACAAAAAGTAGCAGAAGAAGCAGCACGAGTTCTAGT
AGATCCTGTTCCAAGCTACAAACAAGTCAAACAGCTTAAATATGTCGGCATGG
TCTTAAACGAAGCGCTGCGCTTATGGCCAACTGCTCCTGCGTTTTCCCTATATG
CAAAAGAAGATACGGTGCTTGGAGGAGAATATCCTTTAGAAAAAGGCGACGA
AGTAATGGTTCTGATTCCTCAGCTTCACCGTGATAAAACAGTTTGGGGAGACG
ATGTGGAGGAGTTCCGTCCAGAGCGTTTTGAAAATCCAAGTGCGATTCCGCAG
CATGCGTTTAAACCGTTTGGAAACGGTCAGCGTGCGTGTATCGGTCAGCAGTT
CGCTCTTCATGAAGCAACGCTGGTACTTGGTATGATGCTAAAACACTTTGACTT
TGAAGATCATACAAACTACGAGCTCGATATTAAAGAAACTTTAACGTTAAAAC
CTAAAGGCTTT

**DNA Sequence of *L*SilOx2**

ACAATTAAAGAAATGCCTCAGCCAAAAACGTTTGGAGAGCTTAAAAATTTACC
GTTATTAAACACAGATAAACCGGTTCAAGCTTTGATGAAAATTGCGGATGAAT
TAGGAGAAATCTTTAAATTCGAGGCGCCTGGTCGTGTAACGCGCTACTTATCA
AGTCAGCGTCTAATTAAAGAAGCATGCGATGAATCACGCTTTGATAAAAACTT
AAGTCAAGCGCTTAAATTTGCACGTGATTTTGTTGGAGACGGGTTAGGTACAA
GCTGGACGCATGAAAAAAATTGGAAAAAAGCGCATAATATCTTACTTCCAAG
CTTTAGTCAGCAGGCAATGAAAGGCTATCATGCGATGATGGTCGATATCGCCG
TGCAGCTTGTTCAAAAGTGGGAGCGTCTAAATGCAGATGAGCATATTGAAGTA
TCGGAAGACATGACACGTTTAACGCTTGATACAATTGGTCTTTGCGGCTTTAA
CTATCGCTTTAACAGCTTTTACCGAGATCAGCCTCATCCATTTATTATAAGTAT
GGTCCGTGCACTGGATGAAGTAATGAACAAGCTGCAGCGAGCAAATCCAGAC
GACCCAGCTTATGATGAAAACAAGCGCCAGTTTCAAGAAGATATCAAGGTGA
TGAACGACCTAGTAGATAAAATTATTGCAGATCGCAAAGCAAGGGGTGAACA
AAGCGATGATTTATTAACGCAGATGCTAAACGGAAAAGATCCAGAAACGGGT
GAGCCGCTTGATGACGGGAACATTCGCTATCAAATTATTACATTCTTAATTGC
GGGACACGAAACAACAAGTGGTCTTTTATCATTTGCGCTGTATTTCTTAGTGA
AAAATCCACATGTATTACAAAAAGTAGCAGAAGAAGCAGCACGAGTTCTAGT
AGATCCTGTTCCAAGCTACAAACAAGTCAAACAGCTTAAATATGTCGGCATGG
TCTTAAACGAAGCGCTGCGCTTATGGCCAATGTTTCCTGCGTTTTCCCTATATG
CAAAAGAAGATACGGTGCTTGGAGGAGAATATCCTTTAGAAAAAGGCGACGA
AGTAATGGTTCTGATTCCTCAGCTTCACCGTGATAAAACAGTTTGGGGAGACG
ATGTGGAGGAGTTCCGTCCAGAGCGTTTTGAAAATCCAAGTGCGATTCCGCAG
CATGCGTTTAAACCGTTTGGAAACGGTCAGCGTGCGTGTATCGGTCAGCAGTT
CGCTCTTCATGAAGCAACGCTGGTACTTGGTATGATGCTAAAACACTTTGACTT
TGAAGATCATACAAACTACGAGCTCGATATTAAAGAAACTTTAACGTTAAAAC
CTAAAGGCTTT

**DNA Sequence of *L*SilOx3**

ACAATTAAAGAAATGCCTCAGCCAAAAACGTTTGGAGAGCTTAAAAATTTACC
GTTATTAAACACAGATAAACCGGTTCAAGCTTTGATGAAAATTGCGGGTGAAT
TAGGAGAAATCTTTAAATTCGAGGCGCCTGGTCGTGTAACGCGCTACTTATCA
AGTCAGCGTCTAATTAAAGAAGCATGCGATGAATCACGCTTTGATAAAAACTT
AAGTCAAGCGCTTAAATTTGCACGTGATTTTGTTGGAGACGGGTTAGGTACAA
GCTGGACGCATGAAAAAAATTGGAAAAAAGCGCATAATATCTTACTTCCAAG
CTTTAGTCAGCAGGCAATGAAAGGCTATCATGCGATGATGGTCGATACCGCCG
TGCAGCTTGTTCAAAAGTGGGAGCGTCTAAATGCAGATGAGCATATTGAAGTA
TCGGAAGACATGACACGTTTAACGCTTGATACAATTGGTCTTTGCGGCTTTAA
CTATCGCTTTAACAGCTTTTACCGAGATCAGCCTCATCCATTTATTATAAGTAT
GGTCCGTGCACTGGATGAAGTAATGAACAAGCTGCAGCGAGCAAATCCAGAC
GACCCAGCTTATGATGAAAACAAGCGCCAGTTTCAAGAAGATATCAAGGTGA
TGAACGACCTAGTAGATAAAATTATTGCAGATCGCAAAGCAAGGGGTGAACA
AAGCGATGATTTATTAACGCAGATGCTAAACGGAAAAGATCCAGAAACGGGT
GAGCCGCTCGATGACGGGAACATTCGCTATCAAATTATTACATTCTTAATTGC
GGGACACGAAACAACAAGTGGTCTTTTATCATTTGCGCTGTATTTCTTAGTGA

AAAATCCACATGTATTACAAAAAGTAGCAGAAGAAGCAGCACGAGTTCTAGT
AGATCCTGTTCCAAGCTACAAACAAGTCAAACAGCTTAAATATGTCGGCATGG
TCTTAAACGAAGCGCTGCGCTTATGGCCAATGTTTCCTGCGTTTTCCCTATATG
CAAAAGAGGATACGGTGCTAGGAGGAGAATATCCTTTAGAAAAAGGCGACGA
AGTAATGGTTCTGATTCCTCAGCTTCACCGTGATAAAACAGTTTGGGGAGACG
ATGTGGAGGAGTTCCGTCCAGAGCGTTTTGAGAATCCAAGTGCGATTCCACAG
CATGCGTTTAAACCGTTTGGAAACGGTCAGCGTGCGTGTATCGGTCAGCAGTT
CGCTCTTCATGAAGCAACGCTGGTACTTGGTATGATGCTAAAACACTTTGACTT
TGAAGATCATACAAACTACGAGCTCGATATTAAAGAAACTTTAACGTTAAAAC
CTAAAGGCTTT

**DNA Sequence of *L*SilOx4**

ACAATTAAAGAAATGCCTCAGCCAAAAACGTTTGGAGAGCTTAAAAATTTACC
GTTATTAAACACAGATAAACCGGTTCAAGCTTTGATGAAAATTGCGGGTGAAT
TAGGAGAAATCTTTAAATTCGAGGCGCCTGGTCGTGTAACGCGCTACTTATCA
AGTCAGCGTCTAATTAAAGAAGCATGCGATGAATCACGCTTTGATAAAAACTT
AAGTCAAGCGCTTAAATTTGCACGTGATTTTGTTGGAGACGGGTTAGGTACAA
GCTGGACGCATGAAAAAAATTGGAAAAAAGCGCATAATATCTTACTTCCAAG
CTTTAGTCAGCAGGCAATGAAAGGCTATCATGCGATGATGGTCGATACCGCCG
TGCAGCTTGTTCAAAAGTGGGAGCGTCTAAATGCAGATGAGCATATTGAAGTA
TCGGAAGACATGACACGTTTAACGCTTGATACAATTGGTCTTTGCGGCTTTAA
CTATCGCTTTAACAGCTTTTACCGAGATCAGCCTCATCCATTTATTATAAGTAT
GGTCCGTGCACTGGATGAAGTAATGAACAAGCTGCAGCGAGCAAATCCAGAC
GACCCAGCTTATGATGAAAACAAGCGCCAGTTTCAAGAAGATATCAAGGTGA
TGAACGACCTAGTAGATAAAATTATTGCAGATCGCAAAGCAAGGGGTGAACA
AAGCGATGATTTATTAACGCAGATGCTAAACGGAAAAGATCCAGAAACGGGT
GAGCCGCTTGATGACGAGAACATTCGCTATCAAATTATTACATTCTTAATTGC
GGGACACGAAACAACAAGTGGTCTTTTATCATTTGCGCTGTATTTCTTAGTGA
AAAATCCACATGTATTACAAAAAGTAGCAGAAGAAGCAGCACGAGTTCTAGT
AGATCCTGTTCCAAGCTACAAACAAGTCAAACAGCTTAAATATGTCGGCATGG
TCTTAAACGAAGCGCTGCGCTTATGGCCAATGTTTCCTGCGTTTTCCCTATATG
CAAAAGAAGATACGGTGCTTGGAGGAGAATATCCTTTAGAAAAAGGCGACGA
AGTAATGGTTCTGATTCCTCAGCTTCACCGTGATAAAACAGTTTGGGGAGACG
ATGTGGAGGAGTTCCGTCCAGAGCGTTTTGAAAATCCAAGTGCGATTCCGCAG
CATGCGTTTAAACCGTTTGGAAACGGTCAGCGTGCGTGTATCGGTCAGCAGTT
CGCTCTTCATGAAGCAACGCTGGTACTTGGTATGATGCTAAAACACTTTGACTT
TGAAGATCATACAAACTACGAGCTCGATATTAAAGAAACTTTAACGTTAAAAC
CTAAAGGCTTT

**DNA Sequence of *L*SilOx5**

ACAATTAAAGAAATGCCTCAGCCAAAAACGTTTGGAGAGCTTAAAAATTTACC
GTTATTAAACACAGATAAACCGGTTCAAGCTTTGATGAAAATTGCGGGTGAAT
TAGGAGAAATCTTTAAATTCGAGGCGCCTGGTCGTGTAACGCGCTACTTATCA
AGTCAGCGTCTAATTAAAGAAGCATGCGATGAATCACGCTTTGATAAAAACTT
AAGTCAAGCGCTTAAATTTGCACGTGATTTTGTTGGAGACGGGTTAGGTACAA

GCTGGACGCATGAAAAAAATTGGAAAAAAGCGCATAATATCTTACTTCCAAG
CTTTAGTCAGCAGGCAATGAAAGGCTATCATGCGATGATGGTCGATACCGCCG
TGCAGCTTGTTCAAAAGTGGGAGCGTCTAAATGCAGATGAGCATATTGAAGTA
TCGGAAGACATGACACGTTTAACGCTTGATACAATTGGTCTTTGCGGCTTTAA
CTATCGCTTTAACAGCTTTTACCGAGATCAGCCTCATCCATTTATTATAAGTAT
GGTCCGTGCACTGGATGAAGTAATGAACAAGCTGCAGCGAGCAAATCCAGAC
GACCCAGCTTATGATGAAAACAAGCGCCAGTTTCAAGAAGATATCAAGGTGA
TGAACGACCTAGTAGATAAAATTATTGCAGATCGCAAAGCAAGGGGTGAACA
AAGCGATGATTTATTAACGCAGATGCTAAACGGAAAAGATCCAGAAACGGGT
GAGCCGCTTGATGACGAGAACATTCGCTATCAAATTATTACATTCTTAATTGC
GGGACACGAAACAACAAGTGGTCTTTTATCATTTGCGCTGTATTTCTTAGTGA
AAAATCCACATGTATTACAAAAAGTAGCAGAAGAAGCAGCACGAGTTCTAGT
AGATCCTGTTCCAAGCTACAAACAAGTCAAACAGCTTAAATATGTCGGCATGG
TCTTAAACGAAGCGCTGCGCTTATGGCCAATGTCTCCTGCGTTTTCCCTATATG
CAAAAGAAGATACGGTGCTTGGAGGAGAATATCCTTTAGAAAAAGGCGACGA
AGTAATGGTTCTGATTCCTCAGCTTCACCGTGATAAAACAGTTTGGGGAGACG
ATGTGGAGGAGTTCCGTCCAGAGCGTTTTGAAAATCCAAGTGCGATTCCGCAG
CATGCGTTTAAACCGTTTGGAAACGGTCAGCGTGCGTGTATCGGTCAGCAGTT
CGCTCTTCATGAAGCAACGCTGGTACTTGGTATGATGCTAAAACACTTTGATTT
TGAAGATCATACAAACTACGAGCTCGATATTAAAGAAACTTTAACGTTAAAAC
CTAAAGGCTTT

**DNA Sequence of *L*SilOx6**

ACAATTAAAGAAATGCCTCAGCCAAAAACGTTTGGAGAGCTTAAAAATTTACC
GTTATTAAACACAGATAAACCGGTTCAAGCTTTGATGAAAATTGCGGGTGAAT
TAGGAGAAATCTTTAAATTCGAGGCGCCTGGTCGTGTAACGCGCTACTTATCA
AGTCAGCGTCTAATTAAAGAAGCATGCGATGAATCACGCTTTGATAAAAACTT
AAGTCAAGCGCTTAAATTTGCACGTGATTTTGTTGGAGACGGGTTAGGTACAA
GCTGGACGCATGAAAAAAATTGGAAAAAAGCGCATAATATCTTACTTCCAAG
CTTTAGTCAGCAGGCAATGAAAGGCTATCATGCGATGATGGTCGATACCGCCG
TGCAGCTTGTTCAAAAGTGGGAGCGTCTAAATGCAGATGAGCATATTGAAGTA
TCGGAAGACATGACACGTTTAACGCTTGATACAATTGGTCTTTGCGGCTTTAA
CTATCGCTTTAACAGCCTTTACCGAGATCAGCCTCATCCATTTATTATAAGTAT
GGTCCGTGCACTGGATGAAGTAATGAACAAGCTGCAGCGAGCAAATCCAGAC
GACCCAGCTTATGATGAAAACAAGCGCCAGTTTCAAGAAGATATCAAGGTGA
TGAACGACCTAGTAGATAAAATTATTGCAGATCGCAAAGCAAGGGGTGAACA
AAGCGATGATTTATTAACGCAGATGCTAAACGGAAAAGATCCAGAAACGGGT
GAGCCGCTTGATGACGAGAACATTCGCTATCAAATTATTACATTCTTAATTGC
GGGACACGAAACAACAAGTGGTCTTTTATCATTTGCGCTGTATTTCTTAGTGA
AAAATCCACATGTATTACAAAAAGTAGCAGAAGAAGCAGCACGAGTTCTAGT
AGATCCTGTTCCAAGCTACAAACAAGTCAAACAGCTTAAATATGTCGGCATGG
TCTTAAACGAAGCGCTGCGCTTATGGCCAATGTCTCCTGCGTTTTCCCTATATG
CAAAAGAAGATACGGTGCTTGGAGGAGAATATCCTTTAGAAAAAGGCGACGA
AGTAATGGTTCTGATTCCTCAGCTTCACCGTGATAAAACAGTTTGGGGAGACG
ATGTGGAGGAGTTCCGTCCAGAGCGTTTTGAAAATCCAAGTGCGATTCCGCAG

CATGCGTTTAAACCGTTTGGAAACGGTCAGCGTGCGTGTATCGGTCAGCAGTT
CGCTCTTCATGAAGCAACGCTGGTACTTGGTATGATGCTAAAACACTTTGATTT
TGAAGATCATACAAACTACGAGCTCGATATTAAAGAAACTTTAACGTTAAAAC
CTAAAGGCTTT

**DNA Sequence of *L*SilOx7**

ACAATTAAAGAAATGCCTCAGCCAAAAACGTTTGGAGAGCTTAAAAATTTACC
GTTATTAAACACAGATAAACCGGTTCAAGCTTTGATGAAAATTGCGGGTGAAT
TAGGAGAAATCTTTAAATTCGAGGCGCCTGGTCGTGTAACGCGCGTTTTATCA
AGTCAGCGTCTAATTAAAGAAGCATGCGATGAATCACGCTTTGATAAAAACTT
AAGTCAAGCGCTTAAATTTGCACGTGATTTTGTTGGAGACGGGTTAGGTACAA
GCTGGACGCATGAAAAAAATTGGAAAAAAGCGCATAATATCTTACTTCCAAG
CTTTAGTCAGCAGGCAATGAAAGGCTATCATGCGATGATGGTCGATACCGCCG
TGCAGCTTGTTCAAAAGTGGGAGCGTCTAAATGCAGATGAGCATATTGAAGTA
TCGGAAGACATGACACGTTTAACGCTTGATACAATTGGTCTTTGCGGCTTTAA
CTATCGCTTTAACAGCCTTTACCGAGATCAGCCTCATCCATTTATTATAAGTAT
GGTCCGTGCACTGGATGAAATGATGAACAAGCTGCAGCGAGCAAATCCAGAC
GACCCAGCTTATGATGAAAACAAGCGCCAGTTTCAAGAAGATATCAAGGTGA
TGAACGACCTAGTAGATAAAATTATTGCAGATCGCAAAGCAAGGGGTGAACA
AAGCGATGATTTATTAACGCAGATGCTAAACGGAAAAGATCCAGAAACGGGT
GAGCCGCTTGATGACGAGAACATTCGCTATCAAATTATTACATTCTTAATTGC
GGGACACGAAACAACAAGTGGTCTTTTATCATTTGCGCTGTATTTCTTAGTGA
AAAATCCACATGTATTACAAAAAGTAGCAGAAGAAGCAGCACGAGTTCTAGT
AGATCCTGTTCCAAGCTACAAACAAGTCAAACAGCTTAAATATGTCGGCATGG
TCTTAAACGAAGCGCTGCGCTTATGGCCAATGTCTCCTGCGTTTTCCCTATATG
CAAAAGAAGATACGGTGCTTGGAGGAGAATATCCTTTAGAAAAAGGCGACGA
AGTAATGGTTCTGATTCCTCAGCTTCACCGTGATAAAACAGTTTGGGGAGACG
ATGTGGAGGAGTTCCGTCCAGAGCGTTTTGAAAATCCAAGTGCGATTCCGCAG
CATGCGTTTAAACCGTTTGGAAACGGTCAGCGTGCGTGTATCGGTCAGCAGTT
CGCTCTTCATGAAGCAACGCTGGTACTTGGTATGATGCTAAAACACTTTGATTT
TGAAGATCATACAAACTACGAGCTCGATATTAAAGAAACTTTAACGTTAAAAC
CTAAAGGCTTT

**DNA Sequence of *C*SilOx1**

ACAATTAAAGAAATGCCTCAGCCAAAAACGTTTGGAGAGCTTAAAAATTTACC
GTTATTAAACACAGATAAACCGGTTCAAGCTTTGATGAAAATTGCGGGTGAAT
TAGGAGAAATCTTTAAATTCGAGGCGCCTGGTCGTGTAACGCGCTACTTATCA
AGTCAGCGTCTAATTAAAGAAGCATGCGATGAATCACGCTTTGATAAAAACTT
AAGTCAAGCGCTTAAATTTGCACGTGATTTTGTTGGAGACGGGTTAGGTACAA
GCTGGACGCATGAAAAAAGTTGGAAAAAAGCGCATAATATCTTACTTCCAAG
CTTTAGTCAGCAGGCAATGAAAGGCTATCATGCGATGATGGTCGATACCGCCG
TGCAGCTTGTTCAAAAGTGGGAGCGTCTAAATGCAGATGAGCATATTGAAGTA
TCGGAAGACATGACACGTTTAACGCTTGATACAATTGGTCTTTGCGGCTTTAA
CTATCGCTTTAACAGCTTTTACCGAGATCAGCCTCATCCATTTATTATAAGTAT
GGTCCGTGCACTGGATGAAGTAATGAACAAGCTGCAGCGAGCAAATCCAGAC

GACCCAGCTTATGATGAAAACAAGCGCCAGTTTCAAGAAGATATCAAGGTGA
TGAACGGCCTAGTAGATAAAATTATTGCAGATCGCAAAGCAAGGGGTGAACA
AAGCGATGATTTATTAACGCAGATGCTAAACGGAAAAGATCCAGAAACGGGT
GAGCCGCTTGATGACGAGAACATTCGCTATCAAATTATTACATTCTTAATTGC
GGGACACGAAACAACAAGTGGTCTTTTATCATTTGCGCTGTATTTCTTAGTGA
AAAATCCACACGTATTACAAAAAGTAGCAGAAGAAGCAGCACGAGTTCTAGT
AGATCCTGTTCCAAGCTACAAACAAGTCAAACAGCTTAAATATGTCGGCATGG
TCTTAAACGAAGCGCTGCGCTTATGGCCAATGTCTCCTGCGTTTTCCCTATATG
CAAAAGAAGATACGGTGCTTGGAGGAGAATATCCTTTAGAAAAAGGCGACGA
AGTAATGGTTCTGATTCCTCAGCTTCACCGTGATAAAACAGTTTGGGGAGACG
ATGTGGAGGAGTTCCGTCCAGAGCGTTTTGAAAATCCAAGTGCGATTCCGCAG
CATGCGTTTAAACCGTTTGGAAACGGTCAGCGTGCGTGTATCGGTCAGCAGTT
CGCTCTTCATGAAGCAACGCTGGTACTTGGTATGATGCTAAAACACTTTGATTT
TGAAGATCATACAAACTACGAGCTCGATATTAAAGAAACTTTATCGTTAAAAC
CTAAAGGCTTT

**DNA Sequence of *C*SilOx2**

ACAATTAAAGAAATGCCTCAGCCAAAAACGTTTGGAGAGCTTAAAAATTTACC
GTTATTAAACACAGATAAACCGGTTCAAGCTTTGATGAAAATTGCGGGTGAAT
TAGGAGAAATCTTTAAATTCGAGGCGCCTGGTCGTGTAACGCGCTACTTATCA
AGTCAGCGTCTAATTAAAGAAGCATGCGATGAATCACGCTTTGATAAAAACTT
AGGTCAAGCGCTTAAATTTGCACGTGATTTTGTTGGAGACGCGTTAGGTACAA
GCTGGACGCATGAAAAAAGTTGGAAAAAAGCGCATAATATCTTACTTCCAAG
CTTTAGTCAGCAGGCAATGAAAGGCTATCATGCGATGATGGTCGATACCGCCG
TGCAGCTTGTTCAAAAGTGGGAGCGTCTAAATGCAGATGAGCATATTGAAGTA
TCGGAAGACATGACACGTTTAACGCTTGATACAATTGGTCTTTGCGGCTTTAA
CTATCGCTTTAACAGCTTTTACCGAGATCAGCCTCATCCATTTATTATAAGTAT
GGTCCGTGCACTGGATGAAGTAATGAACAAGCTGCAGCGAGCAAATCCAGAC
GACCCAGCTTATGATGAAAACAAGCGCCAGTTTCAAGAAGATATCAAGGTGA
TGAACGGCCTAGTAGATAAAATTATTGCAGATCGCAAAGCAAGGGGTGAACA
AAGCGATGATTTATTAACGCAGATGCTAAACGGAAAAGATCCAGAAACGGGT
GAGCCGCTTGATGACGAGAACATTCGCTATCAAATTATTACATTCTTAATTGC
GGGACACGAAACAACAAGTGGTCTTTTATCATTTGCGCTGTATTTCTTAGTGA
AAAATCCACACGTATTACAAAAAGTAGCAGAAGAAGCAGCACGAGTTCTAGT
AGATCCTGTTCCAAGCTACAAACAAGTCAAACAGCTTAAATATGTCGGCATGG
TCTTAAACGAAGCGCTGCGCTTATGGCCAATGTCTCCTGCGTTTTCCCTATATG
CAAAAGAAGATACGGTGCTTGGAGGAGAATATCCTTTAGAAAAAGGCGACGA
AGTAATGGTTCTGATTCCTCAGCTTCACCGTGATAAAACAGTTTGGGGAGACG
ATGTGGAGGAGTTCCGTCCAGAGCGTTTTGAAAATCCAAGTGCGATTCCGCAG
CATGCGTTTAAACCGTTTGGAAACGGTCAGCGTGCGTGTATCGGTCAGCAGTT
CGCTCTTCATGAAGCAACGCTGGTACTTGGTATGATGCTAAAACACTTTGATTT
TGAAGATCATACAAACTACGAGCTCGATATTAAAGAAACTTTATCGTTAAAAC
CTAAAGGCTTT

**DNA Sequence of *C*SilOx3**

ATGACAATTAAAGAAATGCCTCAGCCAAAAACGTTTGGAGAGCTTAAAAATTT
ACCGTTATTAAACACAGATAAACCGGTTCAAGCTTTGATGAAAATTGCGGGTG
AATTAGGAGAAATCTTTAAATTCGAGGCGCCTGGTGGTGTAACGCGCTACTTA
TCAAGTCAGCGTCTAATTAAAGAAGCATGCGATGAATCACGCTTTGATAAAAA
CTTAGGTCAAGCGCTTAAATTTGCACGTGATTTTGTTGGAGACGCGTTAGGTA
CAAGCTGGACGCATGAAAAAAGTTGGAAAAAAGCGCATAATATCTTACTTCC
AAGCTTTAGTCAGCAGGCAATGAAAGGCTATCATGCGATGATGGTCGATACCG
CCGTGCAGCTTGTTCAAAAGTGGGAGCGTCTAAATGCAGATGAGCATATTGAA
GTATCGGAAGACATGACACGTTTAACGCTTGATACAATTGGTCTTTGCGGCTTT
AACTATCGCTTTAACAGCTTTTACCGAGATCAGCCTCATCCATTTATTATAAGT
ATGGTCCGTGCACTGGATGAAGTAATGAACAAGCTGCAGCGAGCAAATCCAG
ACGACCCAGCTTATGATGAAAACAAGCGCCAGTTTCAAGAAGATATCAAGGT
GATGAACGGCCTAGTAGATAAAATTATTGCAGATCGCAAAGCAAGGGGTGAA
CAAAGCGATGATTTATTAACGCAGATGCTAAACGGAAAAGATCCAGAAACGG
GTGAGCCGCTTGATGACGAGAACATTCGCTATCAAATTATTACATTCTTAATTG
CGGGACACGAAACAACAAGTGGTCTTTTATCATTTGCGCTGTATTTCTTAGTGA
AAAATCCACACGTATTACAAAAAGTAGCAGAAGAAGCAGCACGAGTTCTAGT
AGATCCTGTTCCAAGCTACAAACAAGTCAAACAGCTTAAATATGTCGGCATGG
TCTTAAACGAAGCGCTGCGCTTATGGCCAATGTCTCCTGCGTTTTCCCTATATG
CAAAAGAAGATACGGTGCTTGGAGGAGAATATCCTTTAGAAAAAGGCGACGA
AGTAATGGTTCTGATTCCTCAGCTTCACCGTGATAAAACAGTTTGGGGAGACG
ATGTGGAGGAGTTCCGTCCAGAGCGTTTTGAAAATCCAAGTGCGATTCCGCAG
CATGCGTTTAAACCGTTTGGAAACGGTCAGCGTGCGTGTATCGGTCAGCAGTT
CGCTCTTCATGAAGCAACGCTGGTACTTGGTATGATGCTAAAACACTTTGATTT
TGAAGATCATACAAACTACGAGCTCGATATTAAAGAAACTTTATCGTTAAAAC
CTAAAGGCTTT

## A.5 Materials and Methods for Analytical Standard Preparations

Unless otherwise stated, reactions were performed in flame-dried glassware under an argon or nitrogen atmosphere using anhydrous solvents. Anhydrous solvents were purchased in septum-sealed bottles from Sigma-Aldrich or Tokyo Chemical Industry and used as received. Reaction progress was monitored by gas chromatography/mass spectrometry (GC/MS) or thin-layer chromatography (TLC). GC/MS analysis was performed on an Agilent 8890 gas chromatograph equipped with a 5977B mass spectrometer detector and a DB-5MS capillary column (30 m length, 0.250 mm diameter, 0.25 μm film thickness using split-mode capillary

injection and electron-impact ionization).. TLC was performed using E. Merck silica gel 60 F254 precoated glass plates (0.25 mm) and visualized by UV fluorescence quenching, *p*-anisaldehyde, or $KMnO_4$ staining. Silicycle SiliaFlash® P60 Academic Silica gel (particle size 40–63 μm) was used for flash column chromatography. $^1H$ NMR spectra were recorded on Varian Inova 500 MHz and Bruker 400 MHz spectrometers and are reported relative to residual $C_6H_6$ (δ 7.16 ppm). $^{13}C$ NMR spectra were recorded on a Bruker 400 MHz spectrometer (100 MHz) and are reported relative to $C_6H_6$ (δ 128.1 ppm). Data for $^1H$ NMR are reported as follows: chemical shift (δ ppm) (multiplicity, coupling constant (Hz), integration). Multiplicities are reported as follows: s = singlet, d = doublet, t = triplet, q = quartet, p = pentet, sept = septuplet, m = multiplet, br s = broad singlet, br d = broad doublet. Data for $^{13}C$ NMR are reported in terms of chemical shifts (δ ppm). High resolution mass spectra (HRMS) were obtained at the Caltech CCE Multiuser Mass Spectrometry lab using a JMS-T2000GC AccuTOF™ GC-Alpha in field ionization (FI+) mode. Reagents were purchased from commercial sources and used as received. 2,2,5,5-tetramethyl-1,4-dioxa-2,5-disilacyclohexane was prepared as previously described (*9*).

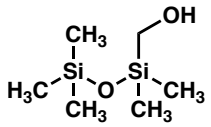


***4***

Carbinol **4**

Prepared as previously described (*10*) and isolated as a clear, colorless oil; $^{1}$H NMR (400 MHz, $C_6D_6$) δ 3.15 (s, 1H), 0.15 (s, 3H), 0.13 (s, 5H); $^{13}$C NMR (100 MHz, $C_6D_6$) δ 56.0, 2.0, –1.1; HRMS (MM:FI+) *m*/*z* calc'd for $C_6H_{18}O_2Si_2$ $[M]^+$ 178.08453, found 178.08526.

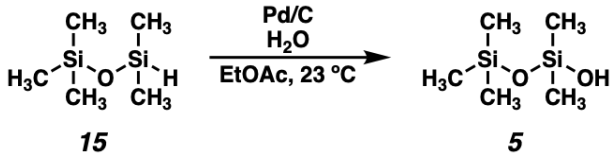


***15*** ***5***

Silanol **5**

To a 100-mL round-bottom flask equipped with a Teflon-coated magnetic stirring bar were added EtOAc (15 mL), deionized water (810 µL, 45.0 mmol, 3.0 equiv), and Pd/C (8.0 mg, 10 wt%, 7.5 mmol, 0.0005 equiv). The resulting black suspension was stirred rapidly at 23 ºC, and pentamethyldisiloxane (2.93 mL, 15.0 mmol, 1.0 equiv) was added dropwise over 5 min. *Caution: addition of siloxane **15** results in rapid evolution of hydrogen gas*. After the complete addition of siloxane **15**, the flask was equipped with a rubber septum which was pierced by an 18-G needle. After 1 h, gas evolution ceased, and consumption of siloxane **15** was observed by GC/MS analysis. The reaction mixture was filtered directly through a 6 x 4 cm pad of neutral alumina and washed with an additional 50 mL of EtOAc. The crude product was concentrated via rotary evaporation (60 mmHg) while cooled in an ice bath. The crude, colorless oil was purified by column chromatography (0 to 25% $Et_2O$/Hexanes) to yield silanol **4** as a colorless oil (1.9816 g, 12.06 mmol, 80% yield); $^1$H NMR (500 MHz, $C_6D_6$) δ 2.91 (s, 1H), 0.17 (s, 9H), 0.14 (s, 6H); $^{13}$C NMR (100 MHz, $C_6D_6$) δ 2.0, 0.7; HRMS (MM:FI+) *m/z* calc'd for $C_5H_{17}O_2Si_2$ $[M+H]^+$ 165.07671, found 165.07618.

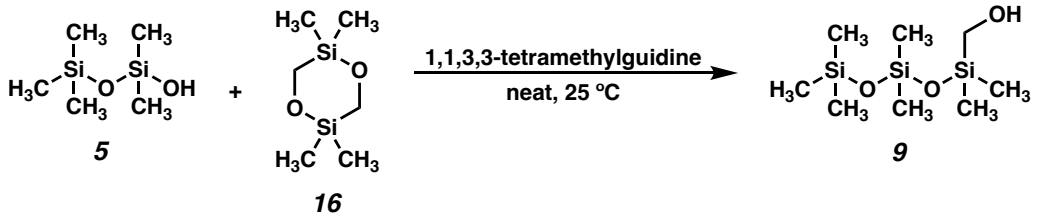


*5* *16* *9*

Carbinol **9**

To a ½-dram, septum-capped vial equipped with a Teflon-coated magnetic stirring bar were added silanol **5** (197.2 mg, 1.2 mmol, 1.2 equiv), 2,2,5,5-tetramethyl-1,4-dioxa-2,5-disilacyclohexane (**17**) (176.4 mg, 1.00 mmol, 1.0 equiv), and 1,1,3,3-tetramethylguanidine (12.5 μL, 0.10 mmol, 0.1 equiv). The vial was quickly evacuated and placed under an Ar atmosphere. After stirring for 1 h, full conversion of 2,2,5,5-tetramethyl-1,4-dioxa-2,5-disilacyclohexane was observed by GC/MS analysis. The reaction mixture was purified directly by flash column chromatography (0 to 25% $Et_2O$/hexanes) to yield carbinol **9** as a clear, colorless oil (223.8 mg, 0.886 mmol, 89% yield); $^1$H NMR (500 MHz, $C_6D_6$) δ 3.21 (s, 2H), 0.20 (s, 6H), 0.17 (s, 9H), 0.16 (s, 6H); $^{13}$C NMR (100 MHz, $C_6D_6$) δ 55.9, 1.9, 1.4, –1.3**;** HRMS (MM:FI+) *m*/*z* calc'd for $C_8H_{25}O_3Si_3$ $[M+H]^+$ 253.11115, found 253.11216.

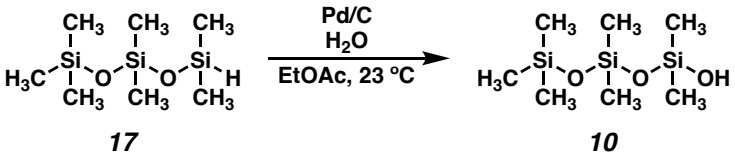


***17*** ***10***

Silanol **10**

To a 100-mL round-bottom flask equipped with a Teflon-coated magnetic stirring bar were added EtOAc (15 mL), deionized water (810 μL, 45.0 mmol, 3.0 equiv), and Pd/C (16.0 mg, 10 wt%, 0.015 mmol, 0.001 equiv). The resulting black suspension was stirred rapidly at 23 ºC, and 1,1,1,3,3,5,5-heptamethyltrisiloxane (4.03 mL, 15.0 mmol, 1.0 equiv) was added dropwise over 5 min. *Caution: addition of siloxane **17** results in rapid evolution of hydrogen gas*. After the complete addition of siloxane **17**, the flask was equipped with a rubber septum which was pierced by an 18-G needle. After 1 h, gas evolution ceased, and consumption of siloxane **17** was observed by GC/MS analysis. The reaction mixture was filtered directly through a 6 x 4 cm pad of neutral alumina and washed with an additional 50 mL of EtOAc to yield siloxane **10** as a clear, colorless oil (3.08 g, 12.9 mmol, 86% yield) which was used without further purification; (3.0820 g, 12.92 mmol, 86% yield); $^{1}$H NMR (400 MHz, $C_6D_6$) δ 0.17 (s, 6H), 0.17 (s, 9H), 0.13 (s, 6H); $^{13}$C NMR (100 MHz, $C_6D_6$) δ 2.0, 1.4, 0.7; HRMS (MM:FI+) *m*/*z* calc'd for $C_7H_{23}O_3Si_3$ $[M+H]^+$ 239.09550, found 239.09478.

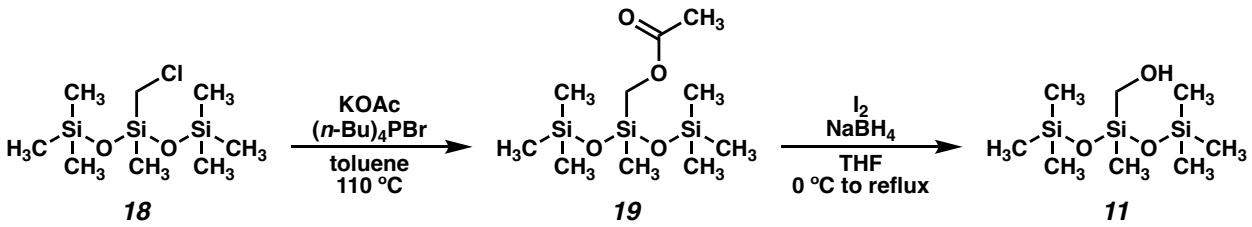


*18* *19* *11*

Carbinol **11**

An oven-dried 25-mL round bottom flask equipped with a Teflon-coated magnetic stirring bar was charged with KOAc (3.68 g, 37.5 mmol, 1.25 equiv). The flask was then evacuated and immersed in a 130 ºC oil bath for 4 h to dry the KOAc. The flask was then cooled to 23 ºC affixed with an oven-dried Liebig condenser under Ar. The flask was then charged with ($n$-Bu)$_4$PBr (203.6 mg, 0.60 mmol, 0.02 equiv), toluene (6.0 mL), and 3-(chloromethyl)-1,1,1,3,5,5,5-heptamethyltrisiloxane (**18**) (8.78 mL, 30.0 mmol, 1.0 equiv). The resulting white suspension was stirred rapidly and immersed in a 110 ºC oil bath for 24 h, after which time GC/MS analysis showed full conversion of 3-(chloromethyl)-1,1,1,3,5,5,5-heptamethyltrisiloxane (**18**). The reaction mixture was then cooled to 23 ºC and transferred to a separatory funnel with deionized water (40 mL) and EtOAc (30 mL). The layers were separated, and the aqueous phase was extracted twice with EtOAc (2 x 15 mL). The combined organics were dried over $Na_2SO_4$, filtered, and concentrated to a clear, colorless oil. The crude product was purified by flash column chromatography (0 to 30% $Et_2O$/hexanes) to yield acetate **19** as a clear, colorless oil with minor impurities (2.0217 g, 6.86 mmol, 23% yield); $^1$H NMR (400 MHz, $C_6D_6$) δ 3.80 (s, 2H), 1.73 (s, 3H), 0.19 (s, 3H), 0.14 (s, 18H); $^{13}$C NMR (100 MHz, $C_6D_6$) δ 168.9, 55.0, 18.8, 0.2, –2.7; HRMS (MM:FI+) $m/z$ calc'd for $C_{10}H_{26}O_4Si_3$ $[M]^+$ 294.11389, found 294.11534.

To a flame-dried 25-mL, two-necked round-bottom flask equipped with a Teflon-coated magnetic stirring bar, a central Liebig condenser, and a rubber septum was added acetate **19** (589.1 mg, 2.00 mmol, 1.0 equiv) and THF (6.7 mL). The resulting clear, colorless solution was cooled in an ice bath for 5 min, after which time $NaBH_4$ (181.6 mg, 4.80 mmol, 2.4 equiv) was added through the side neck in a single portion to afford a white suspension. To a separate, flame-dried 5-mL flask were added $I_2$ (507.6 mg, 2.00 mmol, 1.0 equiv) and THF (3.3 mL). The $I_2$ solution was gently swirled to mix, and the solution was added to the rapidly stirring white suspension via the side neck septum over 1 h using a syringe pump. As the $I_2$

solution is added, the reaction mixture becomes dark brown and gradually fades to white. After complete addition of the $I_2$ solution, the reaction mixture is colorless and a white precipitate forms. The reaction flask was removed from the cooling bath, and the side neck septum was replaced with an oven-dried glass stopper. The reaction mixture was then heated to reflux by immersion in a 72 ºC oil bath. After 2 h, acetate **19** was consumed by GC/MS analysis. The reaction was cooled in an ice bath for 10 min, after which time MeOH (2 mL) was added dropwise over 20 min. *Addition of MeOH is highly exothermic and results in the rapid evolution of hydrogen gas and should be performed cautiously.* After gas evolution had ceased, the reaction mixture was transferred to a separatory funnel with EtOAc (15 mL) and deionized water (15 mL). The layers were separated, and the aqueous phase was extracted twice with EtOAc (2 x 5 mL). The combined organics were washed with brine (10 mL), dried over $Na_2SO_4$, filtered, and concentrated to a clear, colorless oil. The crude product was purified by flash column chromatography (0 to 12% EtOAc/hexanes) to yield carbinol **11** as a clear, colorless oil (302.4 mg, 1.20 mmol, 60% yield); $^1$H NMR (400 MHz, $C_6D_6$) δ 3.13 (s, 2H), 0.21 (s, 3H), 0.17 (s, 18H); $^{13}$C NMR (100 MHz, $C_6D_6$) δ 55.1, 1.9, –1.6; HRMS (MM:FI+) *m*/*z* calc'd for $C_8H_{24}O_3Si_3$ $[M]^+$ 252.10332, found 252.10486.

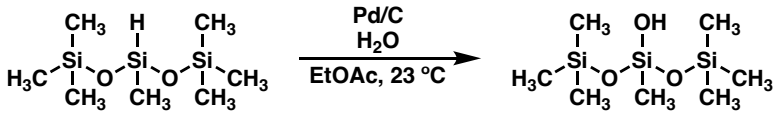


***20*** ***12***

Silanol **12**

To a 100-mL round-bottom flask equipped with a Teflon-coated magnetic stirring bar were added EtOAc (15 mL), deionized water (810 μL, 45.0 mmol, 3.0 equiv), and Pd/C (16.0 mg, 10 wt%, 0.015 mmol, 0.001 equiv). The resulting black suspension was stirred rapidly at 23 ºC, and 1,1,1,3,3,5,5-heptamethyltrisiloxane (4.03 mL, 15.0 mmol, 1.0 equiv) was added dropwise over 5 min. *Caution: addition of siloxane **20** results in rapid evolution of hydrogen gas*. After the complete addition of siloxane **20**, the flask was equipped with a rubber septum which was pierced by an 18-G needle. After 1 h, gas evolution ceased, and consumption of siloxane **20** was observed by GC/MS analysis. The reaction mixture was filtered directly through a 6 x 4 cm pad of neutral alumina and washed with an additional 50 mL of EtOAc to yield siloxane **12** as a clear, colorless oil (3.08 g, 12.9 mmol, 86% yield) which was used without further purification; (3.21 g, 13.5 mmol, 90% yield); $^{1}$H NMR (400 MHz, $C_6D_6$) δ 0.18 (s, 18H), 0.13 (s, 3H); $^{13}$C NMR (100 MHz, $C_6D_6$) δ 1.8, –2.5; HRMS (MM:FI+) *m*/*z* calc'd for $C_7H_{23}O_3Si_3$ $[M+H]^+$ 239.09550, found 239.09455.

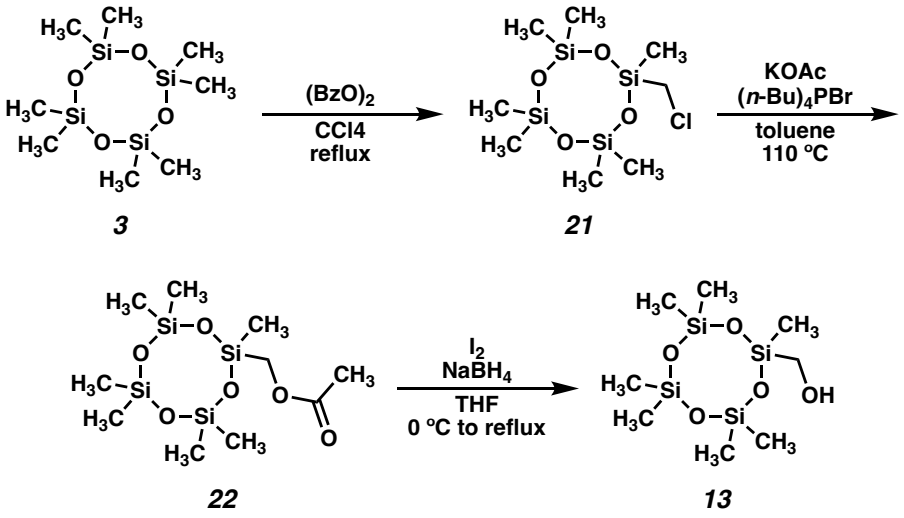


Carbinol **13**

To a flame-dried, 250-mL round bottom flask equipped with a Teflon-coated magnetic stirring bar and a Liebig condenser were added octamethylcyclotetrasiloxane (**3**) (24.8 mL, 80.0 mmol, 2.0 equiv), $CCl_4$ (28 mL), and $SO_2Cl_2$ (3.2 mL, 40 mmol, 1.0 equiv). The resulting clear, colorless solution was stirred rapidly and $(BzO)_2$ (484.5 mg, 2.00 mmol, 0.05 equiv) was added in a single portion. The clear, colorless reaction was then heated to reflux by immersion in an 80 ºC oil bath. After 6 h, the clear, colorless reaction mixture was cooled to 23 ºC. The reaction mixture was concentrated via rotary evaporation, and the resulting clear, colorless oil was transferred to a separatory funnel with 100 mL EtOAc and washed twice with saturated aqueous $NaHCO_3$ (2 x 20 mL) and once with brine (20 mL). The organic layer was then dried over $Na_2SO_4$, filtered, and concentrated to a clear, colorless oil. The resulting crude mixture containing octamethylcyclotetrasiloxane, chloride **21**, and impurities was used directly without purification.

An oven-dried 100-mL round bottom flask equipped with a Teflon-coated magnetic stirring bar was charged with KOAc (9.81 g, 100 mmol, 1.25 equiv). The flask was then evacuated and immersed in a 130 ºC oil bath for 4 h to dry the KOAc. The flask was then cooled to 23 ºC affixed with an oven-dried Liebig condenser under Ar. The flask was then charged with ($n$-Bu)$_4$PBr (542.9 mg, 1.60 mmol, 0.02 equiv), toluene (16.0 mL), and the crude mixture containing chloride **21** as prepared above. The resulting white suspension was stirred rapidly and immersed in a 110 ºC oil bath for 24 h, after which time GC/MS analysis showed full

conversion of chloride **21**. The reaction mixture was then cooled to 23 ºC and transferred to a separatory funnel with deionized water (50 mL) and EtOAc (50 mL). The layers were separated and the aqueous phase was extracted twice with EtOAc (2 x 30 mL). The combined organics were dried over $Na_2SO_4$, filtered, and concentrated to a clear, colorless oil. Octamethylcyclotetrasiloxane was removed from the crude product under high vacuum (600 mTorr), and the remaining crude product was purified by flash column chromatography (0 to 30% $Et_2O$/hexanes) to yield acetate **22** as a clear, colorless oil with minor impurities (1.54 g, 4.34 mmol, 11% yield); $^1$H NMR (400 MHz, $C_6D_6$) δ 3.87 (s, 2H), 1.73 (s, 3H), 0.27 (s, 3H), 0.19 (s, 9H), 0.18 (s, 9H); $^{13}$C NMR (100 MHz, $C_6D_6$) δ 170.6, 56.3, 20.4, 0.9, 0.9, 0.8, –1.5; HRMS (MM:FI+) *m*/*z* calc'd for $C_{10}H_{26}O_6Si_4$ $[M]^+$ 354.08064, found 354.08203.

To a flame-dried, 50-mL two-necked round bottom flask equipped with a Teflon-coated magnetic stirring bar, a central Liebig condenser, and a rubber septum were added acetate **22** (886.6 mg, 2.50 mmol, 1.0 equiv) and THF (8.3 mL). The resulting clear, colorless solution was cooled in an ice bath for 10 min, and $NaBH_4$ (227.0 mg, 6.00 mmol, 2.4 equiv) was added in a single portion. To a separate, flame-dried 10-mL round bottom flask were added $I_2$ (634.5 mg, 2.50 mmol, 1.0 equiv) and THF (4.2 mL). The $I_2$ solution was mixed by swirling before being transferred to the rapidly stirring $NaBH_4$ suspension over 1 h via syringe pump addition. After complete addition, the flask was removed from the cooling bath, and the reaction was warmed to reflux (75 ºC oil bath temperature). After 2 h, GC/MS analysis indicated consumption of acetate **22**. The reaction was cooled to 23 ºC and immersed in an ice bath. The reaction was then carefully quenched with the dropwise addition of methanol (2 mL) over 15 min. The quenched reaction mixture was then transferred to a separatory funnel containing deionized water (15 mL) with EtOAc (15 mL). The layers were partitioned, and the aqueous layer was extracted twice with EtOAc (5 mL). The combined organics were dried over $Na_2SO_4$, filtered through a cotton plug, and concentrated to yield a clear, colorless oil. The crude product was purified by flash column chromatography (2 to 12% EtOAc/hexanes gradient) to yield carbinol **13** as a white, semi-crystalline solid (239.6 mg, 0.949 mmol, 38 % yield); $^1$H NMR (400 MHz, $C_6D_6$) δ 3.22 (s, 2H), 0.26 (s, 3H), 0.22 (s, 6H), 0.21 (s, 3H), 0.19 (s, 9H); $^{13}$C NMR (100 MHz, $C_6D_6$) δ 54.7, 1.0, 0.9, 0.9, –2.1; HRMS (MM:FI+) *m*/*z* calc'd for $C_8H_{25}O_5Si_4$ $[M+H]^+$ 313.07791, found 313.07854.

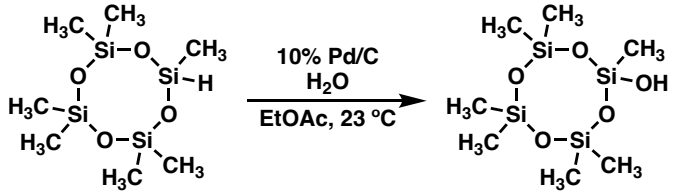


***23*** ***14***

Silanol **14**

To a 40-mL scintillation vial equipped with a Teflon-coated stirring bar were added Pd/C (2.7 mg, 2.5 mmol, 0.05 mol%), EtOAc (5.0 mL), and deionized water (270 μL, 15.0 mmol, 3.0 equiv). The vial was then capped with a septum cap which was vented to atmosphere with an 18-G needle. The black suspension was stirred rapidly at 23 ºC, and silane **23** was added dropwise over 15 min. *Caution: addition of silane **23** results in rapid evolution of hydrogen gas*. The black suspension was vigorously stirred at 23 ºC for 1 h, after which time gas evolution had ceased and GC/MS analysis indicated consumption of the silane. The reaction mixture was filtered through a 6 x 4 cm pad of neutral alumina using EtOAc (50 mL). The filtrate was concentrated to a clear, colorless oil which was purified by flash column chromatography (hexanes to 30% EtOAc/hexanes) to yield silanol **14** as a clear, colorless oil (868.6 mg, 2.91 mmol, 58% yield); $^{1}$H NMR (500 MHz, $C_6D_6$) δ 1.93 (s, 1H), 0.25 (s, 6H), 0.23 (s, 3H), 0.21 (s, 3H), 0.20 (d, $J$ = 1.1 Hz, 9H); $^{13}$C NMR (100 MHz, $C_6D_6$) δ 1.0, 0.9, 0.8, –3.0; (MM:FI+) *m*/*z* calc'd for $C_7H_{23}O_5Si_4$ $[M+H]^+$ 299.06225, found 299.06337.

## A.6 NMR Spectra

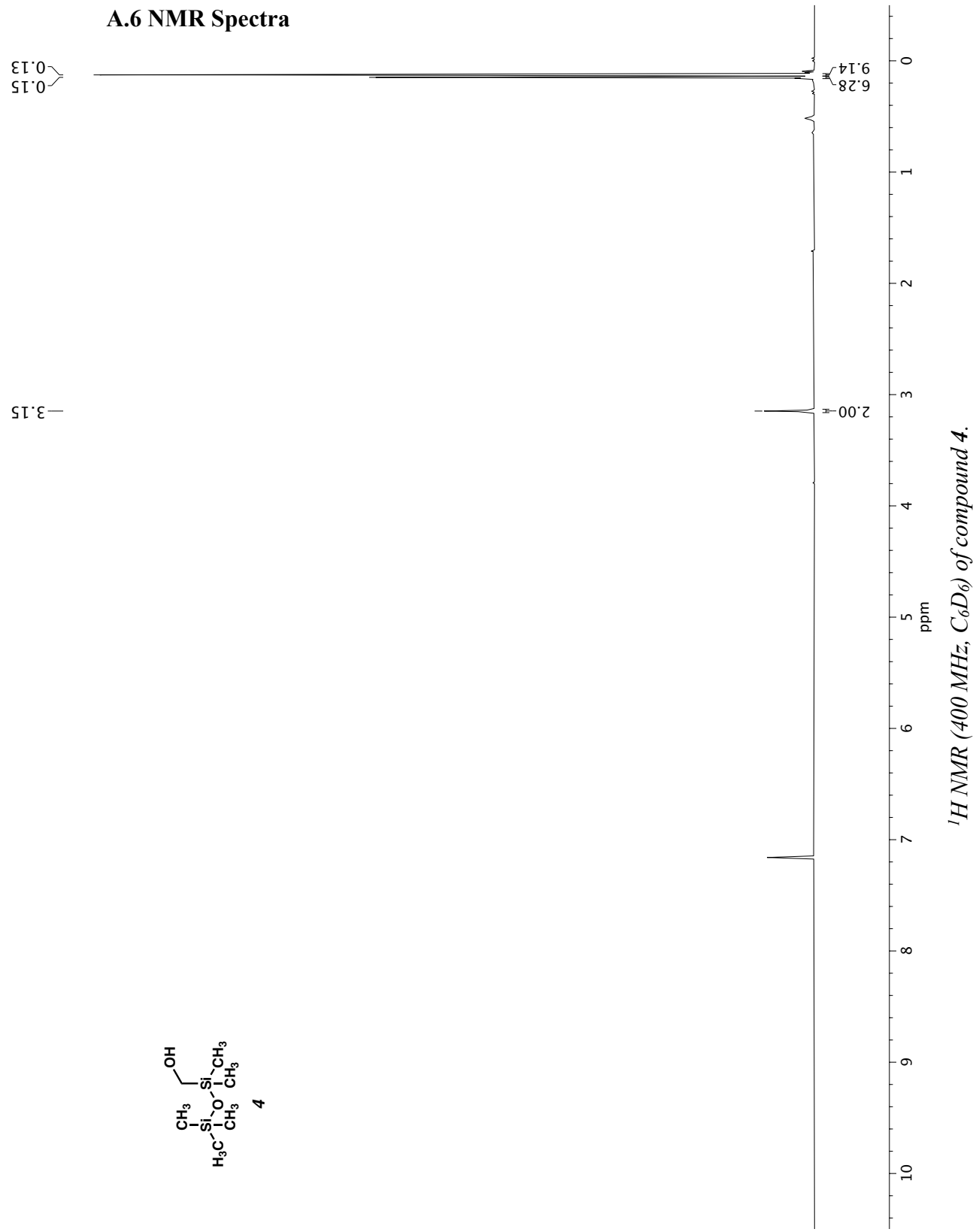


*$^1$H NMR (400 MHz, $C_6D_6$) of compound **4**.*

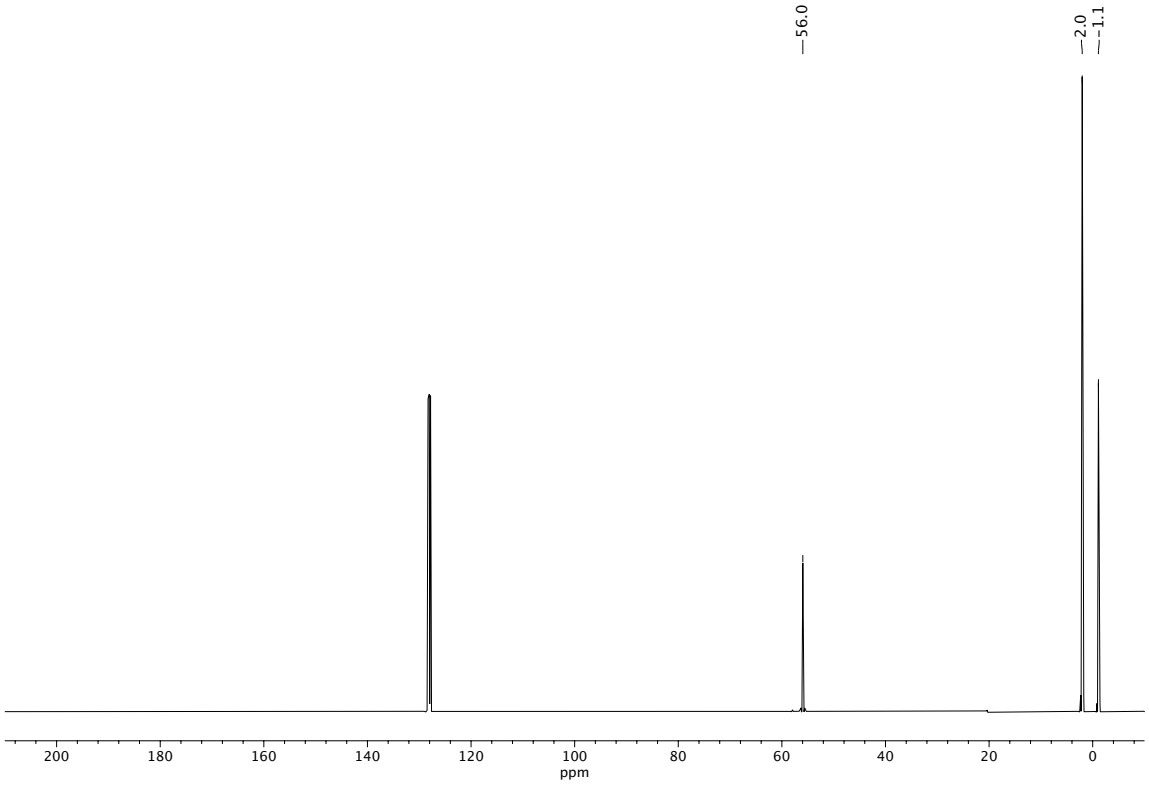


*$^{13}C$ NMR (100 MHz, $C_6D_6$) of compound **4**.*

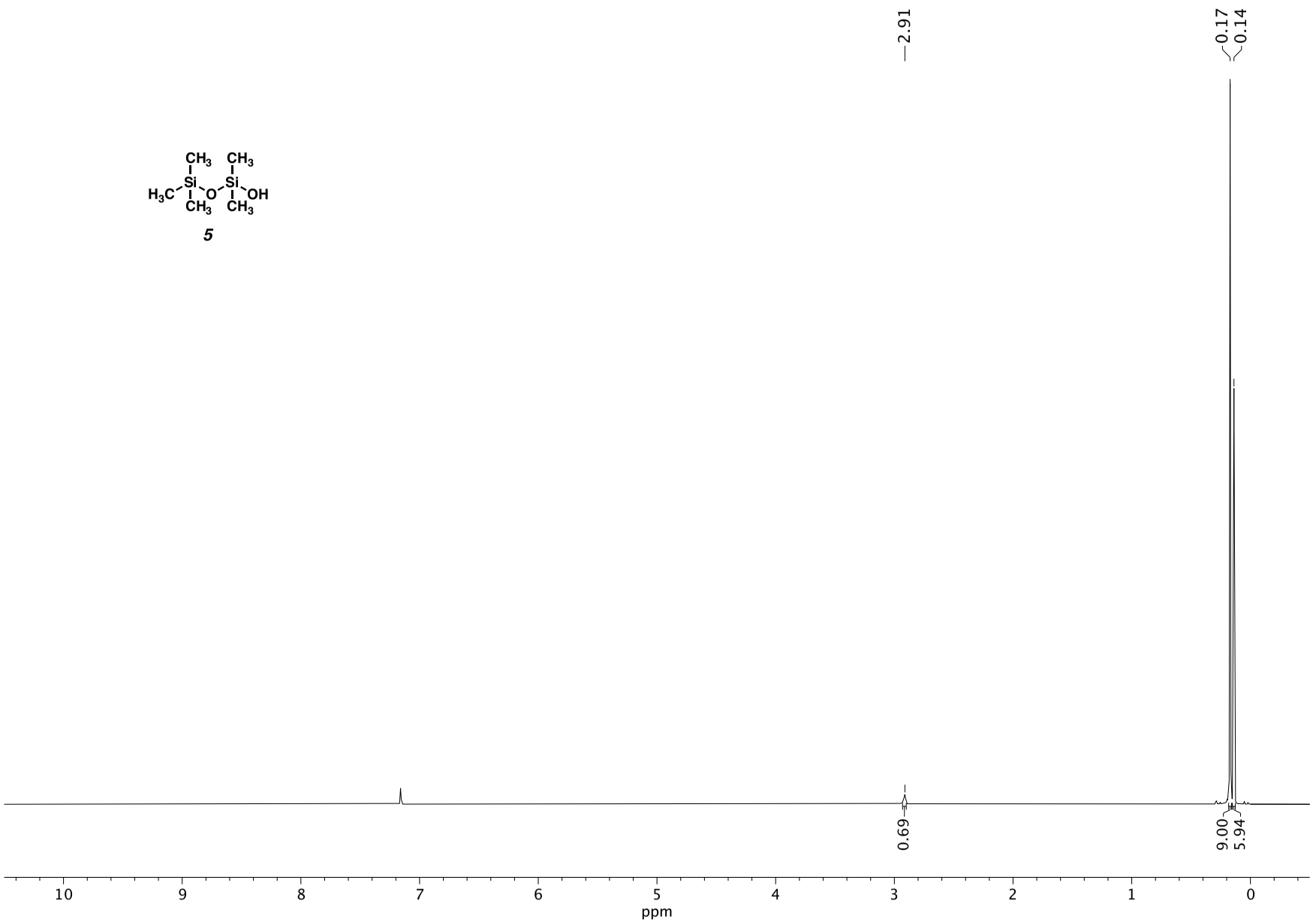


*5*

*$^{1}H$ NMR (400 MHz, $C_6D_6$) of compound **5**.*

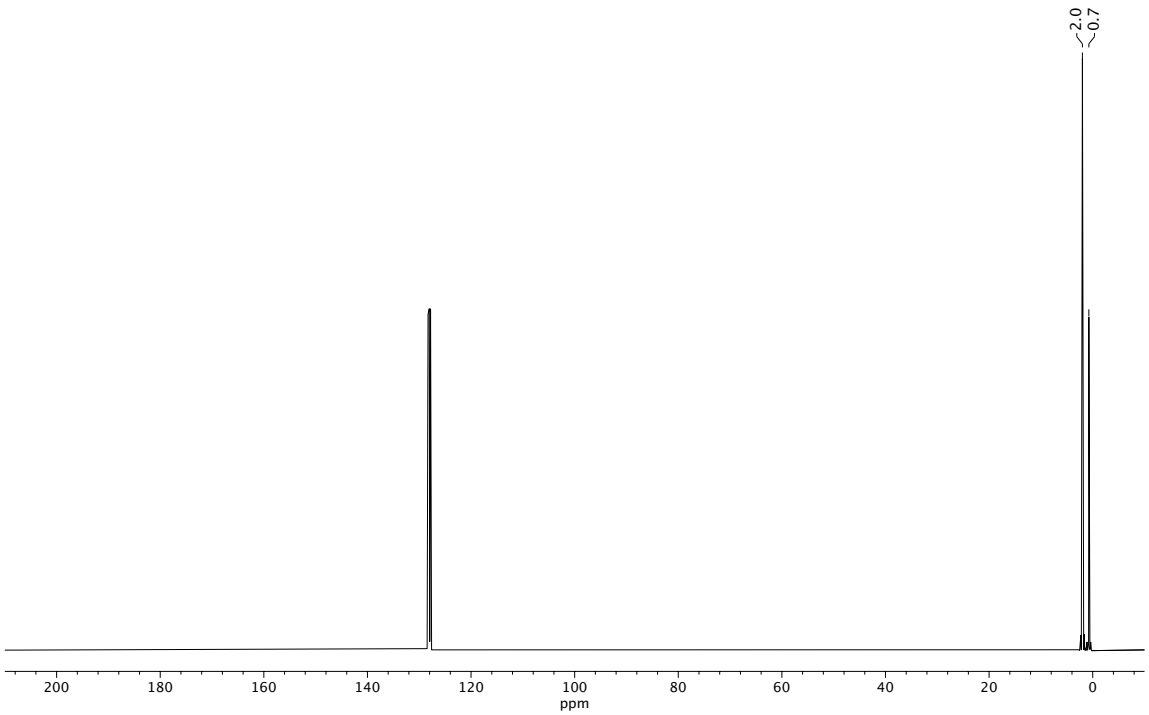


*$^{13}C$ NMR (100 MHz, $C_6D_6$) of compound **5**.*

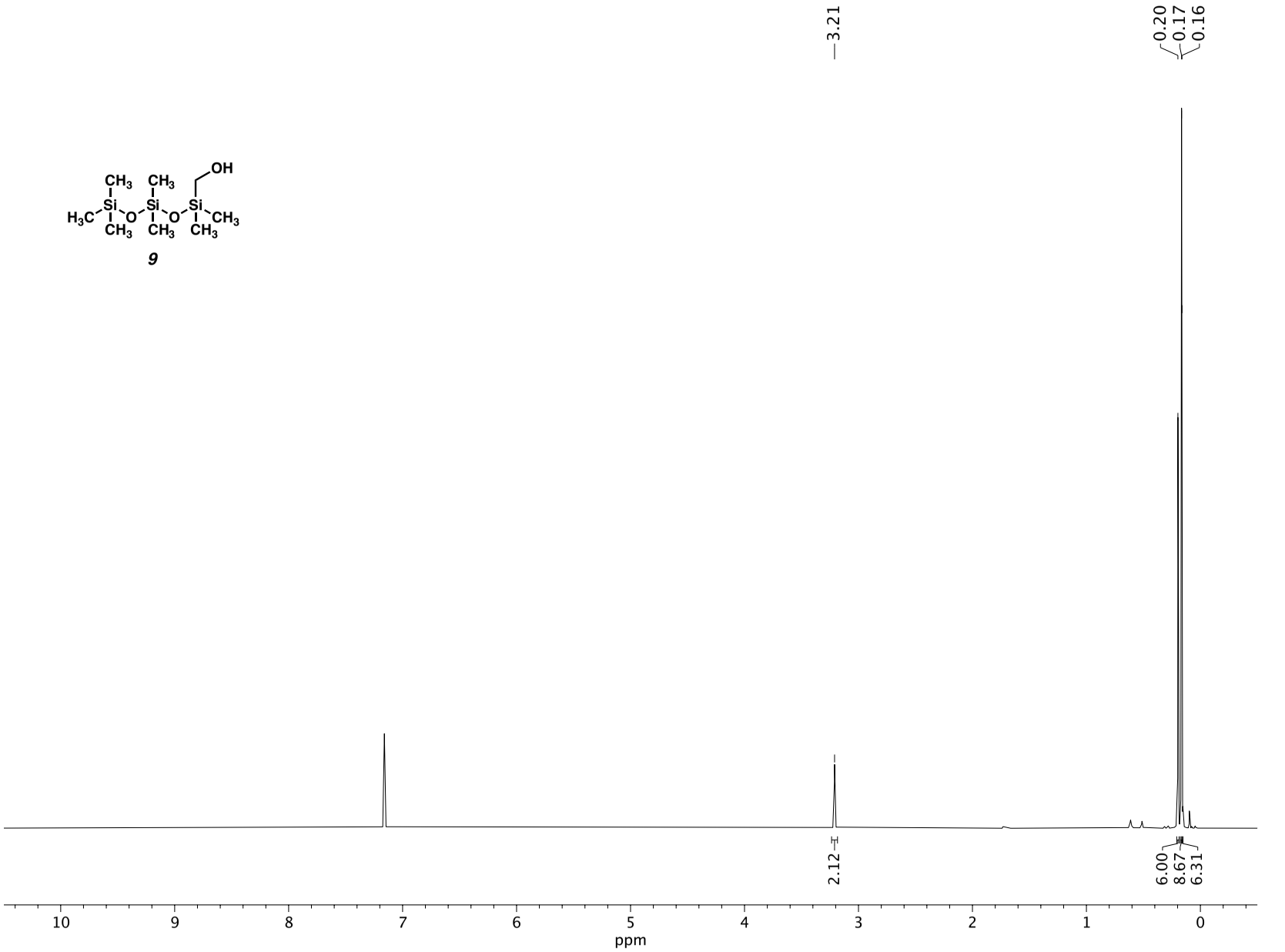


*$^{1}H$ NMR (500 MHz, $C_6D_6$) of compound **9**.*

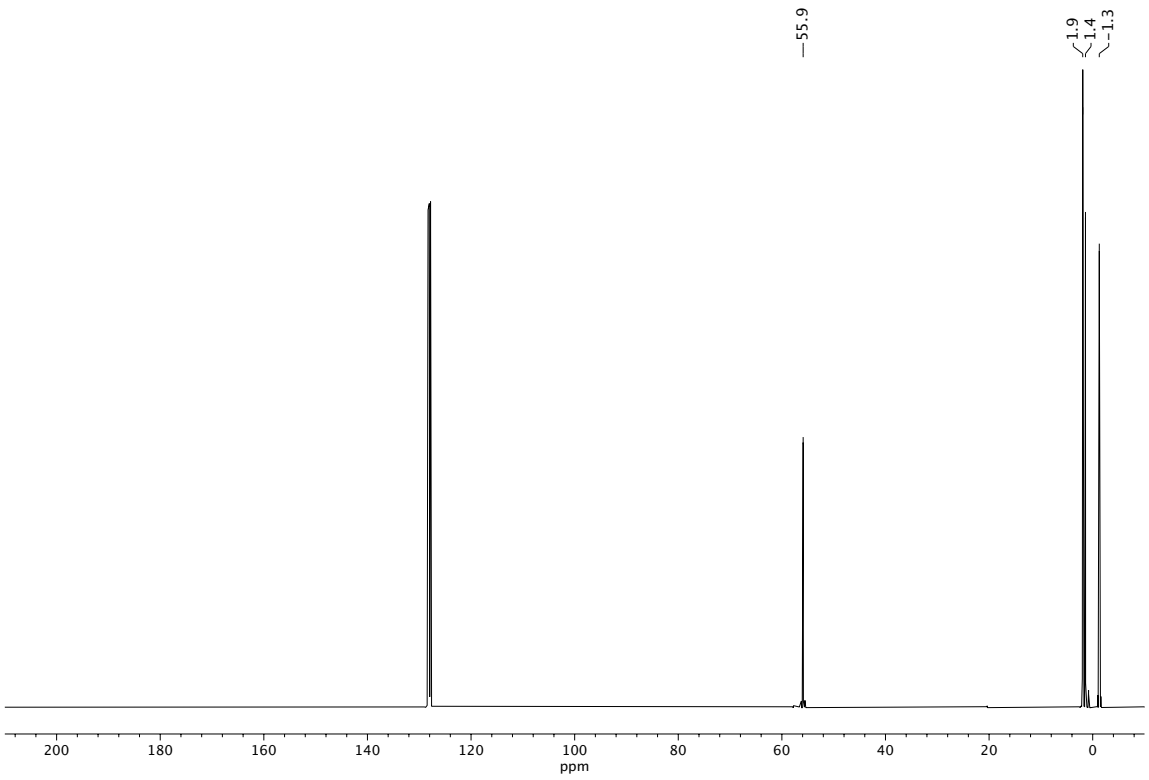


*$^{13}C$ NMR (100 MHz, $C_6D_6$) of compound **9**.*

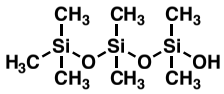


***10***




*$^{1}$H NMR (400 MHz, $C_6D_6$) of compound **10***

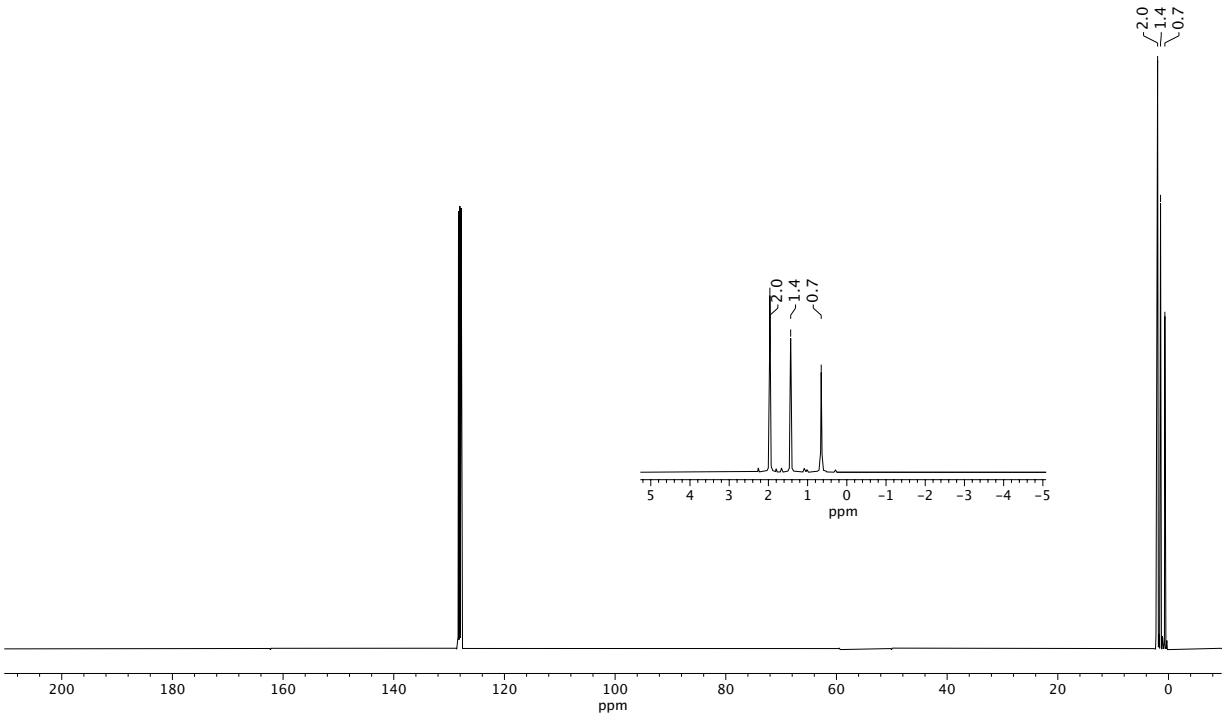


*$^{13}C$ NMR (100 MHz, $C_6D_6$) of compound **10**.*

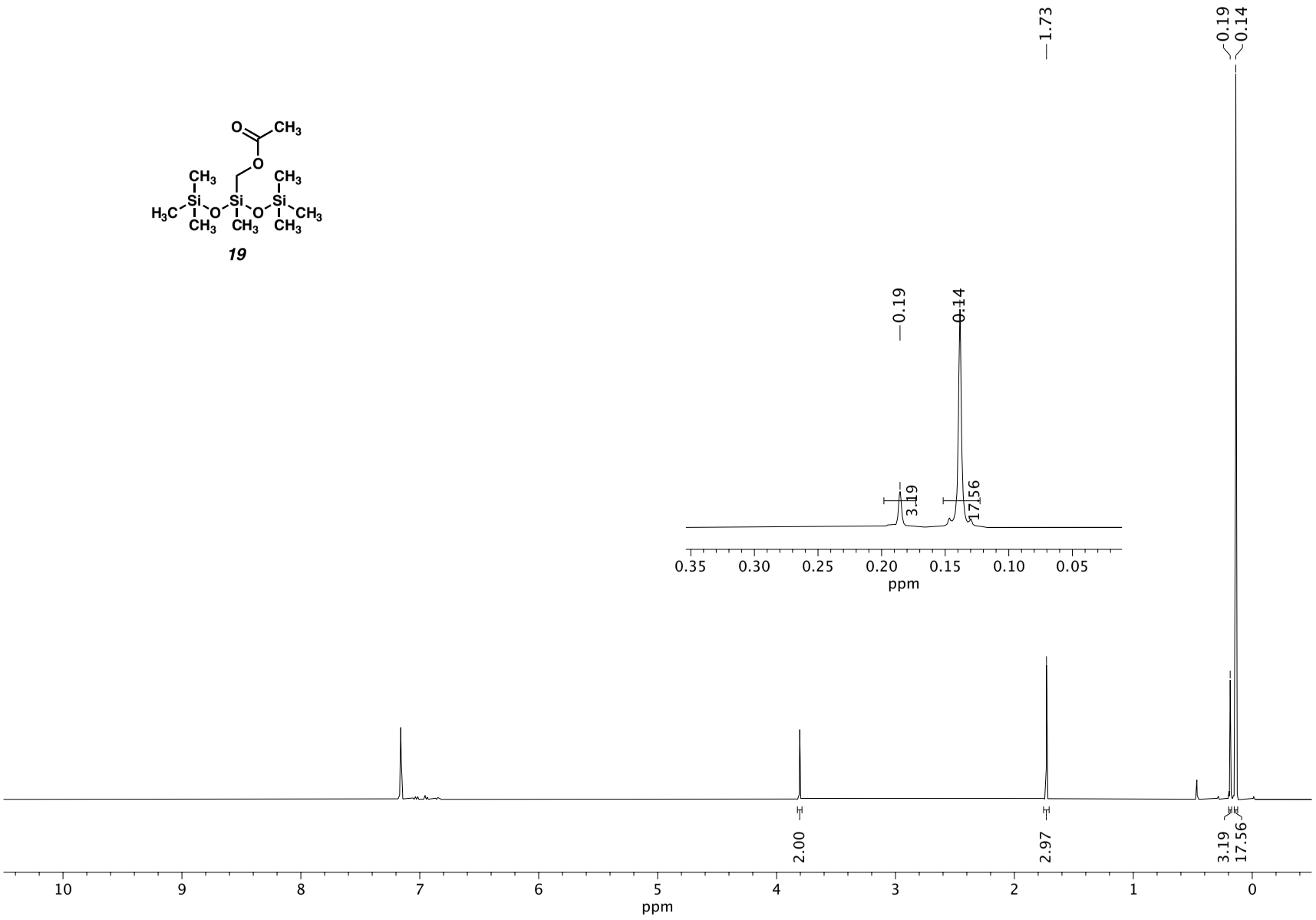


***19***

*$^1$H NMR (400 MHz, $C_6D_6$) of compound **19**.*

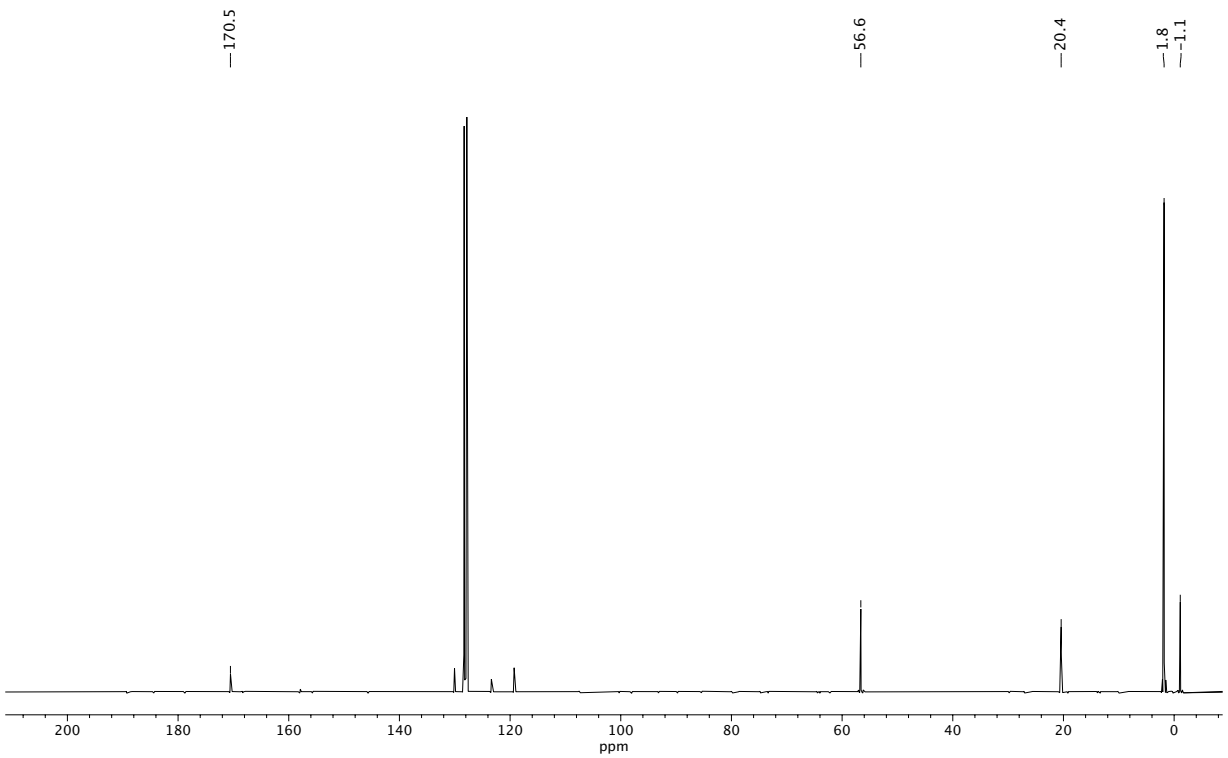


*$^{13}C$ NMR (100 MHz, $C_6D_6$) of compound **19**.*

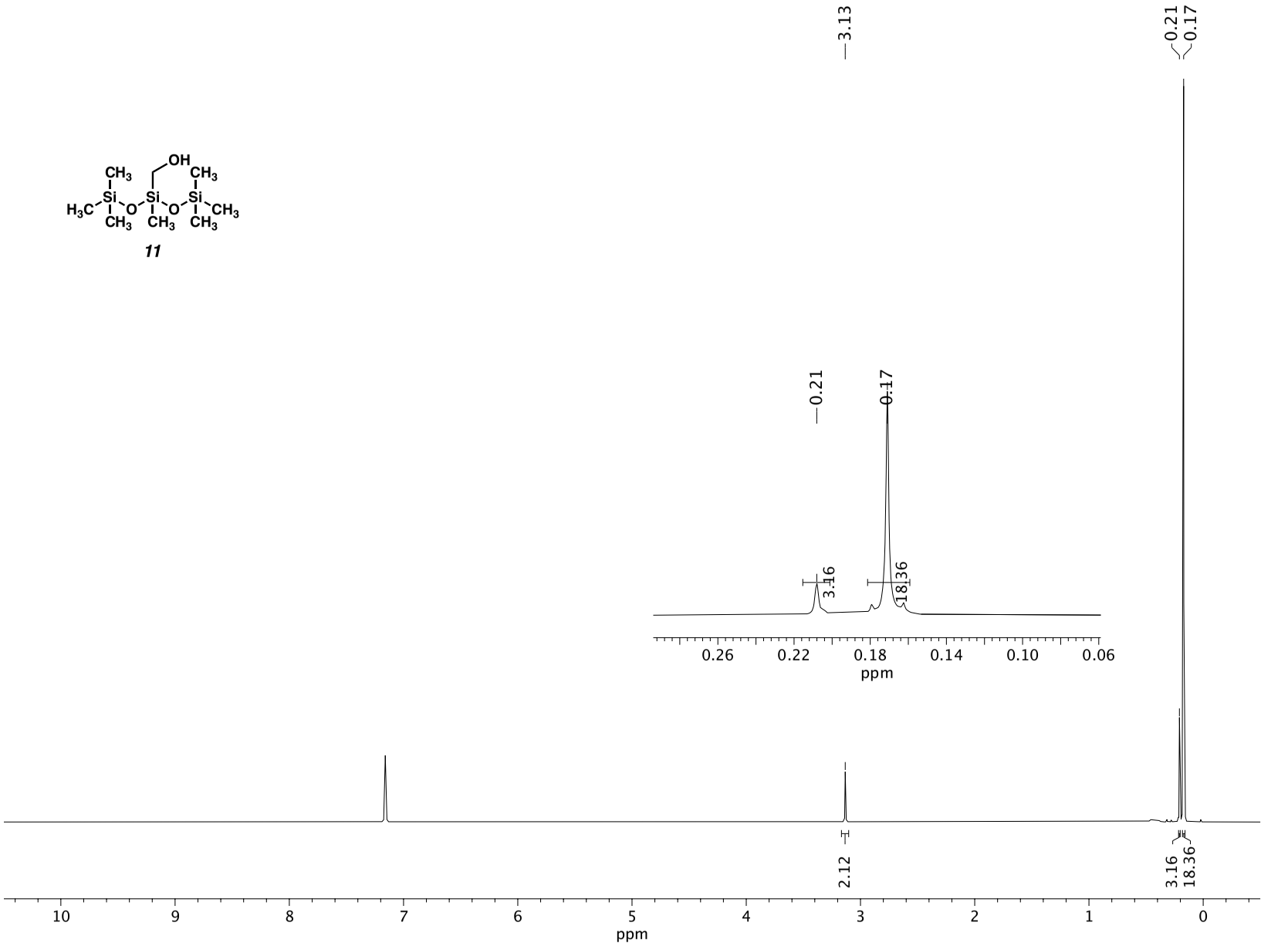


*$^{1}$H NMR (400 MHz, $C_6D_6$) of compound **11**.*

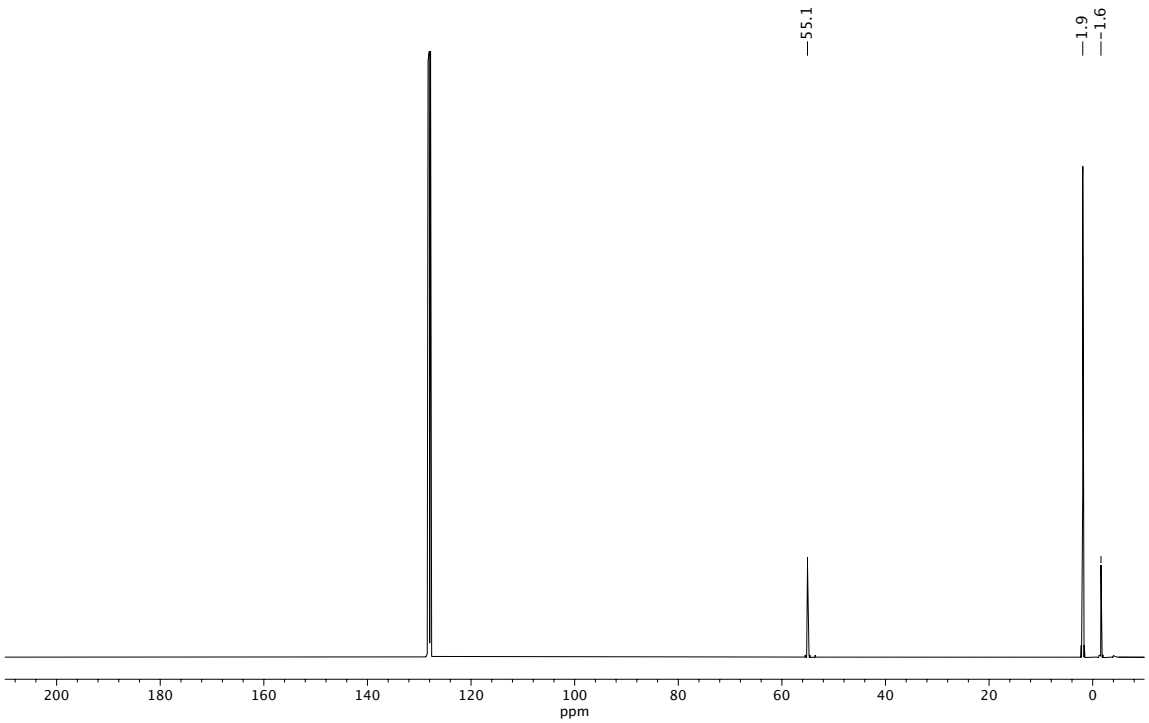


*$^{13}C$ NMR (100 MHz, $C_6D_6$) of compound **11**.*

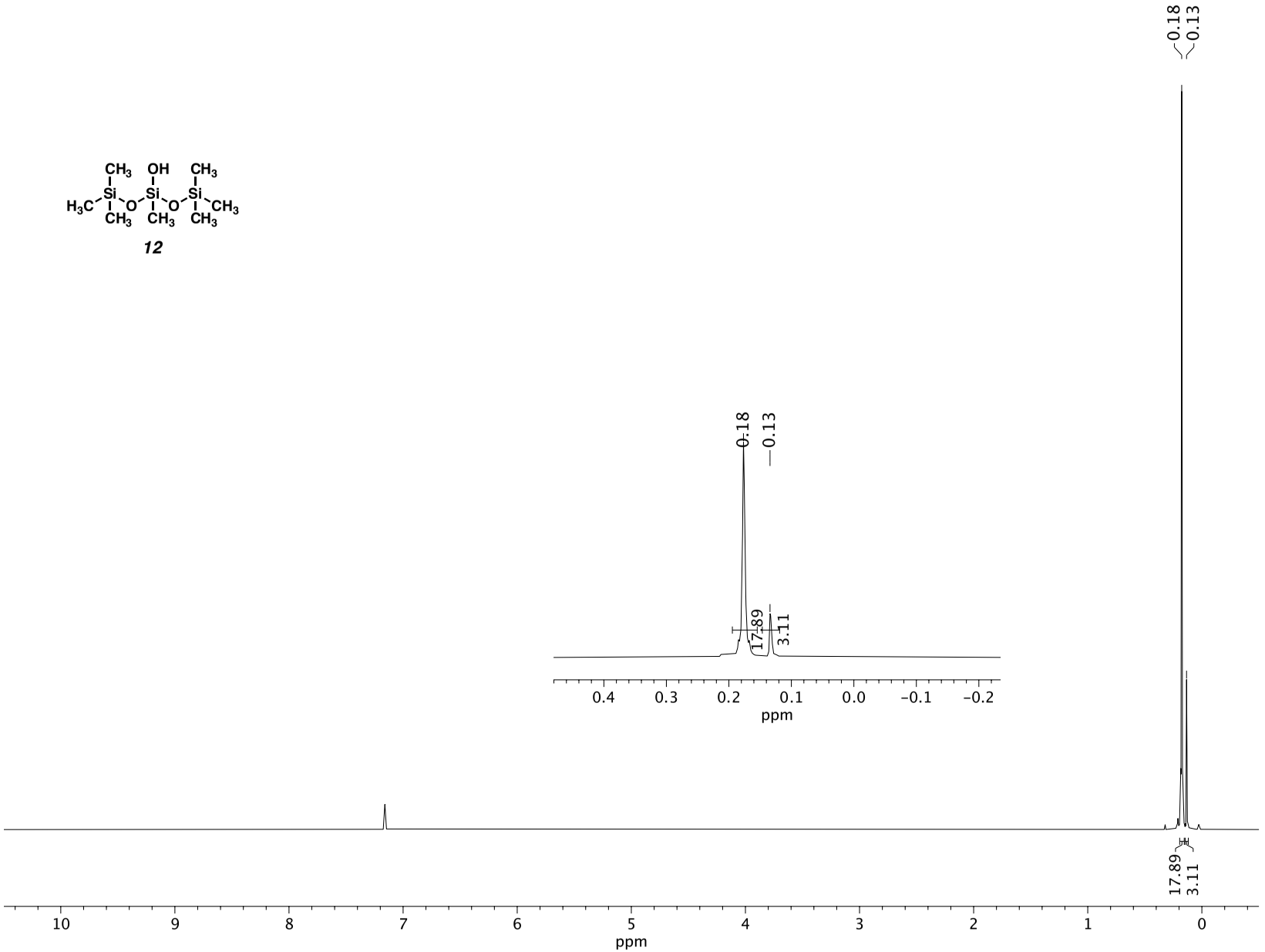


*$^{1}$H NMR (400 MHz, $C_6D_6$) of compound **12**.*

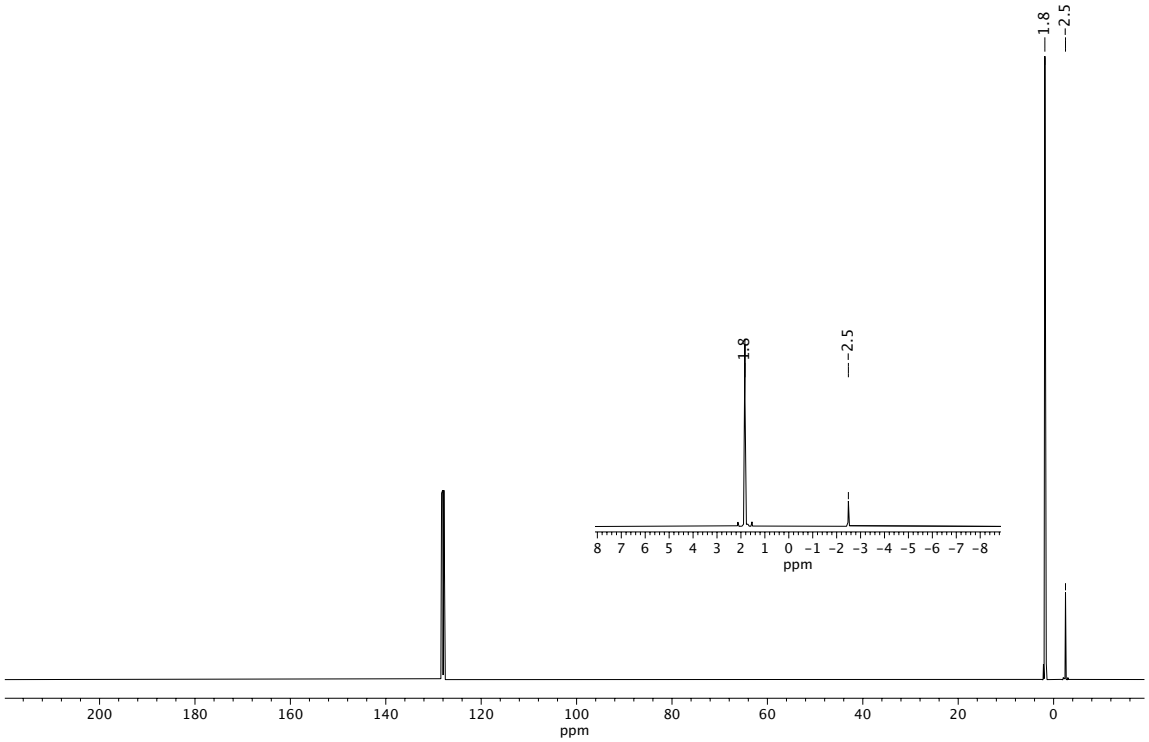


*$^{13}C$ NMR (100 MHz, $C_6D_6$) of compound **12**.*

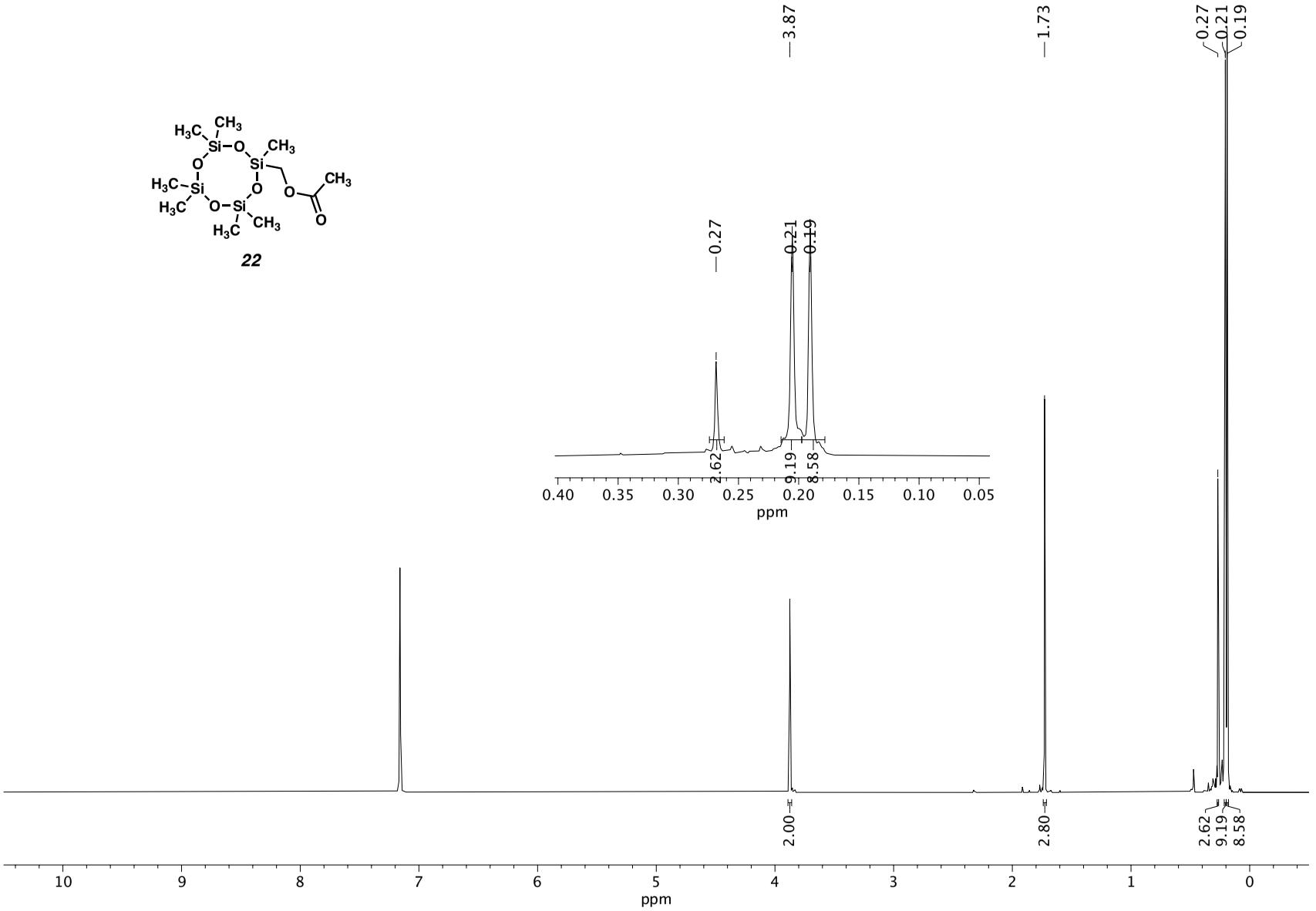


*$^{1}H$ NMR (500 MHz, $C_6D_6$) of compound **22**.*

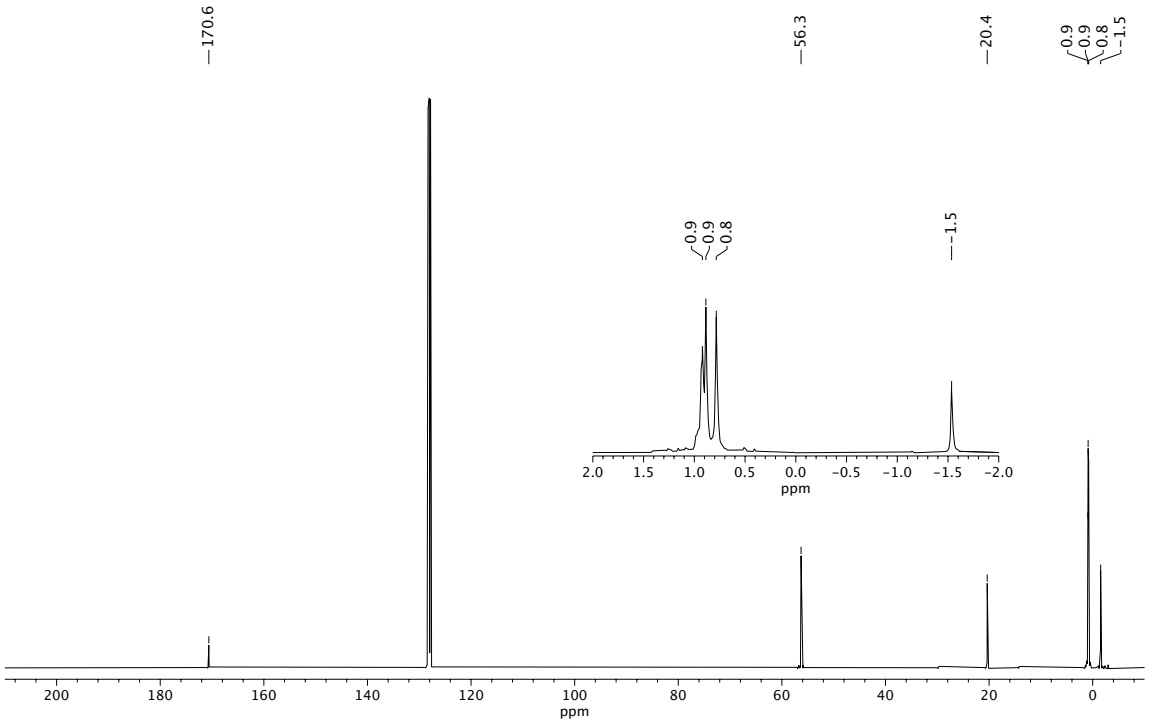


*$^{13}C$ NMR (100 MHz, $C_6D_6$) of compound **22**.*

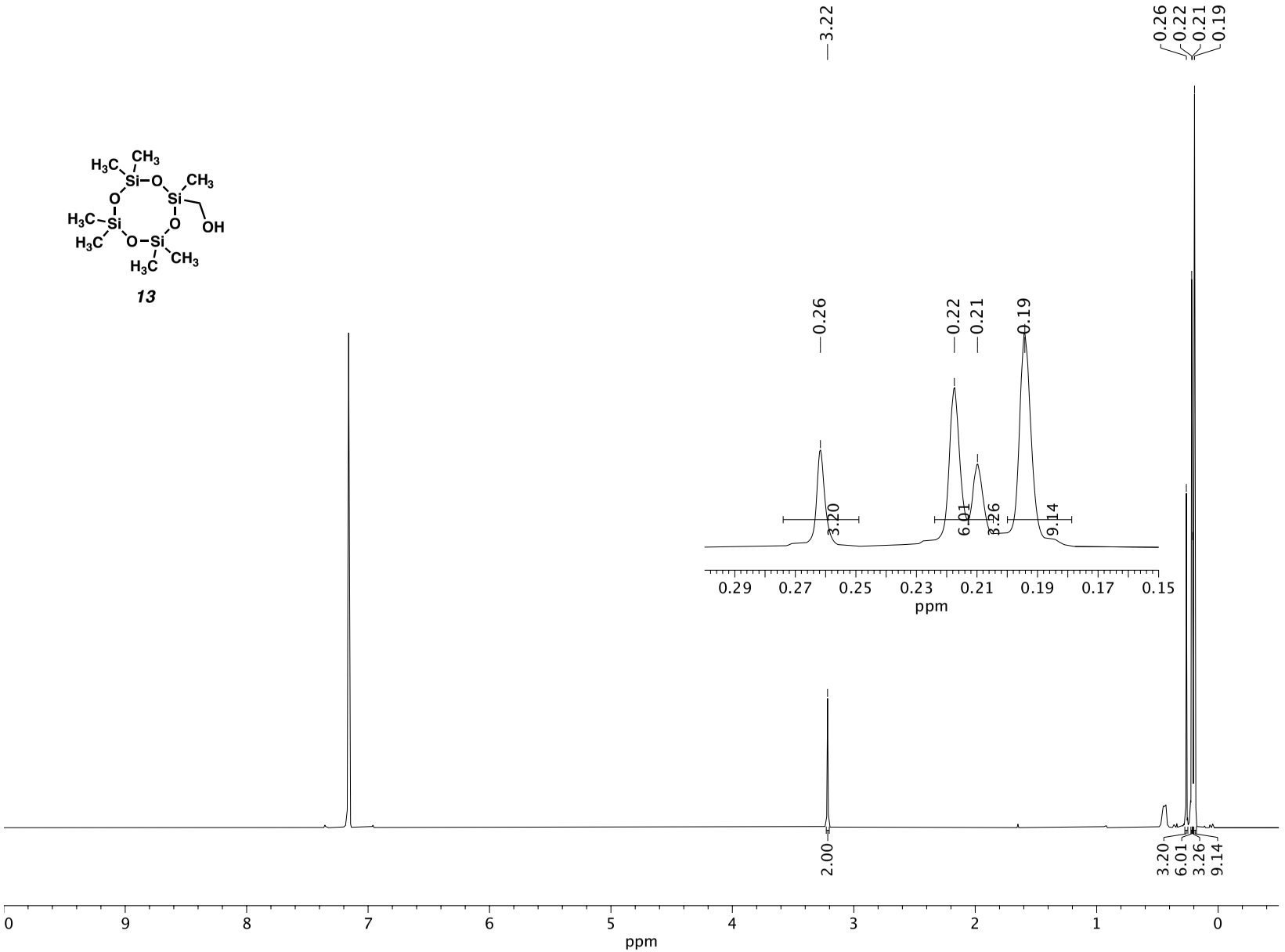


*$^{1}H$ NMR (400 MHz, $C_6D_6$) of compound **13**.*

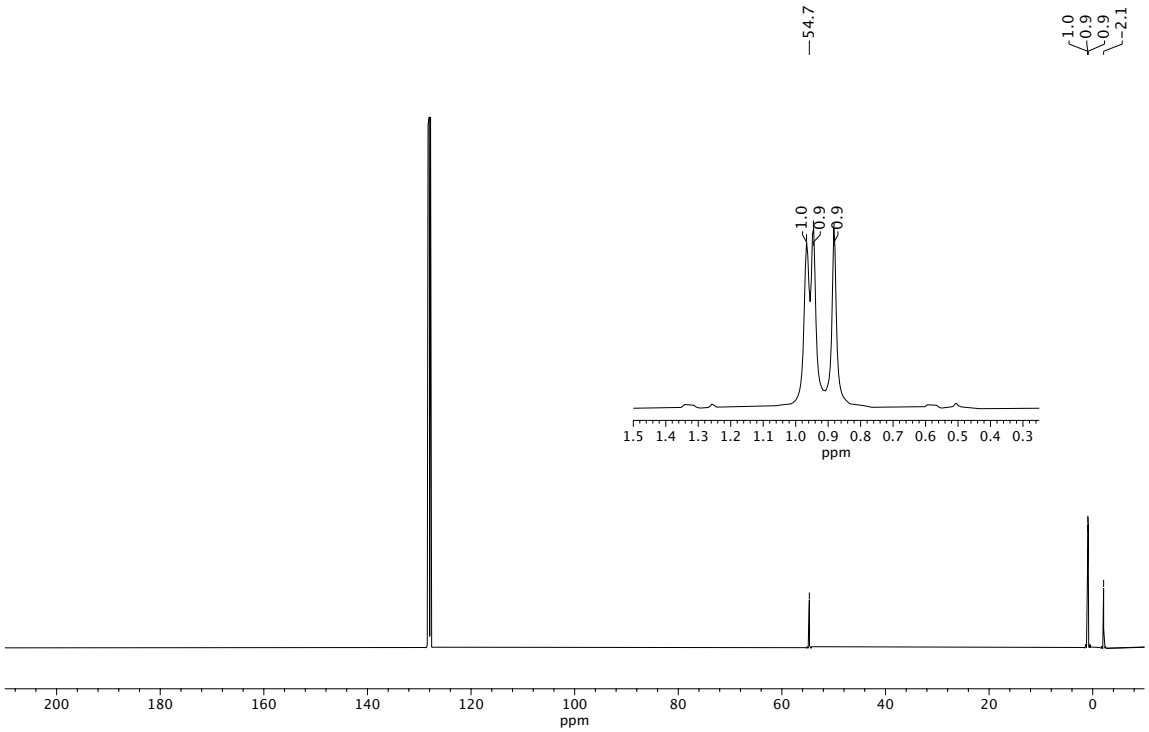


*$^{13}C$ NMR (100 MHz, $C_6D_6$) of compound **13**.*

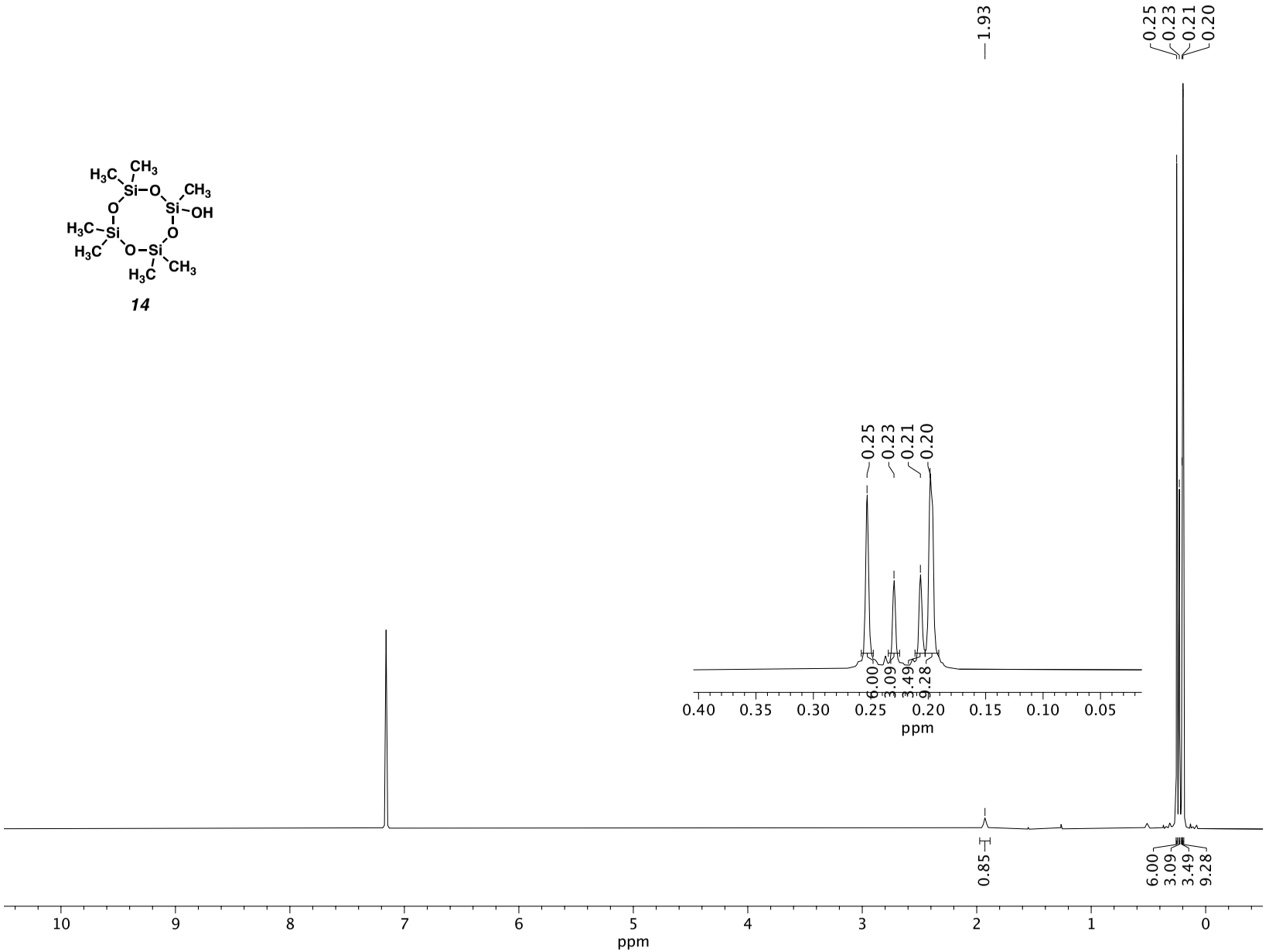


***14***

*$^{1}H$ NMR (500 MHz, $C_6D_6$) of compound **14**.*

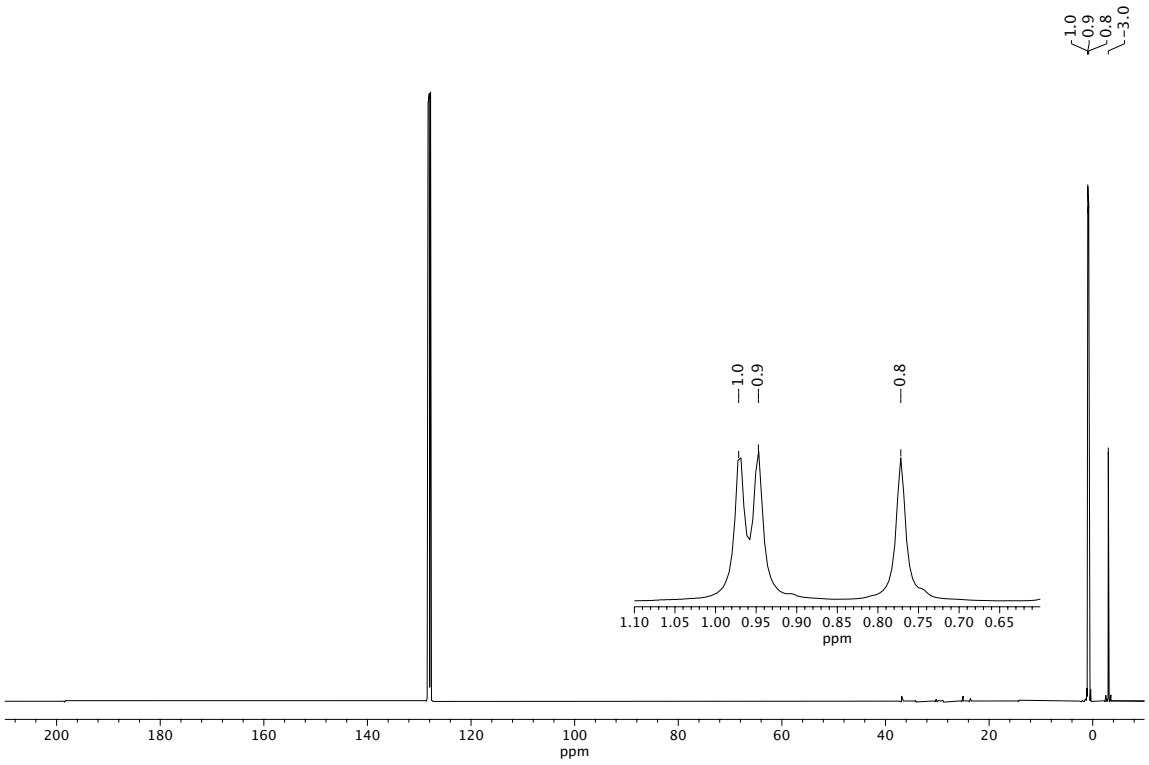


*$^{13}C$ NMR (100 MHz, $C_6D_6$) of compound **14**.*

## A.7 Bibliography for Appendix A


1. D. G. Gibson, L. Young, R.-Y. Chuang, J. C. Venter, C. A. Hutchison, H. O. Smith, Enzymatic assembly of DNA molecules up to several hundred kilobases. *Nat. Methods*. **6**, 343–345 (2009).

2. S. Kille, C. G. Acevedo-Rocha, L. P. Parra, Z.-G. Zhang, D. J. Opperman, M. T. Reetz, J. P. Acevedo, Reducing codon redundancy and screening effort of combinatorial protein libraries created by saturation mutagenesis. *ACS Synth. Biol.* **2**, 83–92 (2013).

3. H. Zhao, L. Giver, Z. Shao, J. A. Affholter, F. H. Arnold, Molecular evolution by staggered extension process (StEP) in vitro recombination. *Nat. Biotechnol.* **16**, 258–261 (1998).

4. H. Zhao, W. Zha, In vitro "sexual" evolution through the PCR-based staggered extension process (StEP). *Nat. Prot.* **1**, 1865–1871 (2006).

5. C. E. Boville, D. K. Romney, P. J. Almhjell, M. Sieben, F. H. Arnold, Improved synthesis of 4-cyanotryptophan and other tryptophan analogues in aqueous solvent using variants of TrpB from *Thermotoga maritima*. *J. Org. Chem.* **83**, 7447–7452 (2018).

6. F. W. Studier, Protein production by auto-induction in high-density shaking cultures. *Protein Expr. Purif.* **41**, 207–234 (2005).

7. F. P. Guengerich, M. V. Martin, C. D. Sohl, Q. Cheng, Measurement of cytochrome P450 and NADPH–cytochrome P450 reductase. *Nat. Prot.* **4**, 1245–1251 (2009).

8. C. R. Otey, "High-Throughput Carbon Monoxide Binding Assay for Cytochromes P450" in *Directed Enzyme Evolution: Screening and Selection Methods*, F. H. Arnold, G. Georgiou, Eds. (Humana Press, 2003), pp. 137–139.

9. S. A. Erhardt, F. Hoffmann, J. O. Daiß, J. Stohrer, E. Herdtweck, B. Rieger, Synthesis of 2,2,5,5-tetrasubstituted 1,4-dioxa-2,5-disilacyclohexanes via organotin(IV)-catalyzed transesterification of (acetoxymethyl)alkoxysilanes. *Chem. Eur. J.* **19**, 4818–4825 (2013).

10. M. Reiter, A. Kronast, S. Kissling, B. Rieger, In situ generated ABA block copolymers from $CO_2$, cyclohexene oxide, and poly(dimethylsiloxane)s. *ACS Macro Lett.* **5**, 419–423 (2016).